



UNIwersytet
Warszawski



Year: 2023

A-polynomials, symmetries and permutohedra for quivers and knots

Carrillo, Helder Larraguivel

Posted at The Institutional Repository of the University of Warsaw
ReIn UW: <https://repozytorium.uw.edu.pl/handle/item/4448>
Unique UUID of the publication: 6f79011c-7c9a-45ce-b952-aa63d444841f

Faculty of Physics
University of Warsaw
Institute of Theoretical Physics

A-polynomials, symmetries and permutohedra for quivers and knots

Hélder David Larraguível Carrillo

A thesis presented for the degree of
Doctor of Philosophy



Supervisor: Prof. Piotr Sułkowski

June 14, 2022

Dedication

I would like to dedicate this thesis to all the wonderful people who joined me in my journey throughout my Ph.D. It was a wild ride and I could not have done it without the love and support of my wife, Justyna Maćkowska, who stood by me all the way. She is the only one who witnessed most of the frustration and joy that went into these pages. For her, I am sure this thesis will have a very special and unique significance. Thank you for traveling with me, my love.

My mother, Claudia Carrillo, was another great source of motivation to whom I dedicate this manuscript. From competing with me to see who finishes first their PhD, to numerous video calls and text messages where she encouraged me to keep going. Now that she has resumed her Ph.D. thesis, it will be my pleasure to kindly repay her time and attention. See you on the other side!

I cannot leave aside the contribution of my father, Fausto Larraguível, to whom I also dedicate this work; thank you for inspiring me to question the world around me and to discover it through my own eyes. A turning point in my life was when he took me on a visit to the faculty of physics at the University of Guadalajara during my last year of high school. Little did we know that he had just taken me across the event horizon of a life as a physicist.

Thank you also to my family both in Mexico and Poland for clearing me up and asking me one of the hardest questions, "*What is your thesis about?*" I really take pleasure in explaining my research, and it has been a great exercise to articulate it in words that even I could understand. I will never forget their reactions to my answers.

I will also never forget all the people who seemed to feed on my soul when asking me, "*Have you finish your thesis?*". As if that was not a hard enough blow to my ego, they would then further inquiry, "*When are you going to finish?*" or "*How much is left?*". Thus, I made a list of those people who seemed to have the same interest as a founding agency that financed my research would have in my thesis. To please them, I will make sure that they receive a copy of my thesis for them to relish.

Now that the tables have turned, I will gladly and with the same determination ask all of you, "*Have you read my thesis?*", "*When are you going to read my thesis?*", "*Why have you not finish reading it, it is less than 120 pages?*" and my favorite "*How can it take you more time for you to read it than for me to write it?*". Do not even think about faking you read it, because I will immediately question you, "*Can you explain to me what this equation means?*", or "*Could you reproduce the derivation of this result?*". You have been fairly warned. You wanted it, have at it!

Acknowledgements

I am always grateful to my supervisor Piotr Sułkowski, whose advice shaped and developed me as a researcher. Thank you for introducing me to such captivating topics in mathematical physics that became the body of my thesis. I highly value every meeting, discussion, scientific trip, and joke; I hope they are accurately reflected as the fruits of my Ph.D. research.

I have also profited greatly from the time I spent together with my colleagues at the University of Warsaw and collaborators. This thesis is the result of all the coffee and beer we have shared over the years. I would especially like to thank Jakub Jankowski, Piotr Kucharski, and Dmitry Noshchenko, whom I see more as close friends than collaborators. Until this day, working with them has been a delightful experience, almost as rewarding as playing games together. This one is for you!

Last but not least, I cannot thank enough Miłosz Panfil for being almost like a second supervisor to me; and Shi Cheng, whose insights in string theory were enormously useful while preparing this manuscript. Additionally, I own a lot to Luiza Wiślicz, Olga Mazur and Monika Dzieścielska, no one likes to do bureaucratic duties, but thanks to their patience and kindness, I actually spend a lovely time chatting with them while handling paper work.

During the first half of my Ph.D., I was supported by my supervisor's ERC Starting Grant no. 335739 "Quantum fields and knot homologies" funded by the European Research Council under the Seventh Framework Program of the European Union. The second half of my PhD was financed thanks to my supervisor's TEAM grant, a program of the Foundation for Polish Science cofinanced by the European Union under the European Regional Development Fund no. POIR.04.04.00-00-5C55/17-00.

Contents

1	Introduction	8
1.1	Motivation	8
1.2	Outline	11
2	Background material	12
2.1	Supersymmetric gauge theories in 3d	12
2.1.1	Supersymmetric multiplets	13
2.1.2	Topological and global symmetries	15
2.1.3	The Super Lagrangian	16
2.1.4	Effective couplings and moduli space of SUSY vacua	17
2.1.5	Vortex partition function	18
2.1.6	Index and BPS particles	19
2.1.7	Quiver representation theory	20
2.1.8	Classical limit	22
2.2	Chern-Simons theory in 3d	23
2.2.1	Knot theory	26
2.2.2	From quantum to classical A-polynomials	30
2.2.3	Deforming the A-polynomial	32
2.3	Knots-quivers correspondence	33
2.3.1	Non-Abelian Chern-Simons and the deformed conifold	34
2.3.2	Geometric transition	37
3	Knot symmetries and permutohedra	40
3.1	On the uniqueness of the knots-quivers correspondence	40
3.1.1	Unliking	41
3.2	Local equivalence of quivers	42
3.2.1	Constraints on equivalent quivers	42
3.2.2	Local equivalence theorem	47
3.2.3	Proof of the local equivalence theorem	49
3.3	Global structure and permutohedra graphs	50
3.3.1	General solution of constraints for one transposition	51
3.3.2	General solution of constraints for two or more transposition	56
3.3.3	Permutohedra – what they are and why they arise	63
3.4	Equivalent quivers for knots	65
3.4.1	Trefoil knot, 3_1	65
3.4.2	Figure-eight knot, 4_1	67
3.4.3	Cinquefoil knot, 5_1	69
3.4.4	5_2 knot	71

3.4.5	7 ₁ knot	75
3.4.6	6 ₁ knot	77
3.4.7	6 ₂ , 6 ₃ , 7 ₃ knots	80
4	Quiver A-polynomials	85
4.1	Quantum derivation and definition	85
4.1.1	Properties of the quiver A-polynomial	88
4.2	Examples of explicit quiver A-polynomials	89
4.2.1	One node quiver	89
4.2.2	Homogeneous quiver	90
4.3	Genus zero two-node quivers	90
4.3.1	Diagonal $\begin{bmatrix} a & 0 \\ 0 & 1 \end{bmatrix}$	91
4.3.2	Diagonal $\begin{bmatrix} a & 0 \\ 0 & 1 \end{bmatrix}$	91
4.3.3	Reciprocal $\begin{bmatrix} a & 0 \\ 0 & 1-a \end{bmatrix}$	92
4.3.4	Diagonal $\begin{bmatrix} a & 0 \\ 0 & a \end{bmatrix}$	93
4.4	Higher genus quiver A-polynomials	96
5	Conclusions	98
A	Local symmetry graph algorithm	100
A.1	Find all pairings	100
A.2	First generation of equivalent quivers	101
A.3	From the second to the last generation of equivalent quivers	103
A.4	The algorithm	104
	References	109

List of Figures

2.1	The explicit graph of the quiver Q . By convention we ignore orientation of self loops, eg. $x_1 \rightarrow x_1$	21
2.2	Torus knot diagrams $T_{2,2p+1}$ for $p = 1, 2, 3$, or $3_1, 5_1, 7_1$	27
2.3	Twist knot diagrams $TK_{2,2 p +2}$ for $p = -1, -2, -3$, or $4_1, 6_1, 8_1$	27
2.4	Twist knot diagrams $TK_{2,2 p +1}$ for $p = 1, 2, 3$, or $3_1, 5_2, 7_2$	27
2.5	Three different types of crossings.	28
2.6	8_{19} (left) 9_{42} (right).	35
2.7	Schematic illustration of the geometric transition. Source [83]	38
3.1	The set of generators of the uncolored HOMFLY-PT homology for 4_1 knot and the parallelogram corresponding to the pairing $\lambda_2\lambda_5 = \lambda_3\lambda_4$	48
3.2	The set of generators of the S^2 -colored HOMFLY-PT homology for 4_1 knot (the labels $x_i x_j$ are consistent with the labels in figure 3.1).	48
3.3	The constraint $C_{12} + C_{15} = C_{13} + C_{14}$ as a parallelogram rule. There are cancellations when equating the sums of the q - and a -degrees of $x_1 x_2, x_1 x_5$ and $x_1 x_3, x_1 x_4$, since $\lambda_2\lambda_5 = \lambda_3\lambda_4$ implies $q_2 + q_5 = q_3 + q_4$ and $a_2 + a_5 = a_3 + a_4$	49
3.4	Planar realizations of permutohedra Π_n of orders 1,2,3,4. One quadrangular face of Π_4 is represented by an external region. Three-dimensional representation of permutohedron Π_4 is shown in figure 3.6.	64
3.5	Permutohedron Π_3 . Each vertex represents a particular permutation of 3 elements. Two vertices are connected by an edge if corresponding permutations differ by a flip of immediate neighbors. There are 3 types of flips, $(1\ 2)$, $(2\ 3)$ and $(1\ 3)$, which are represented by different colors in the figure.	64
3.6	Permutohedron Π_4 . Its vertices are labeled by permutations of elements $\{1, 2, 3, 4\}$, and different colors of edges correspond to different types of transpositions $(i\ j)$ (for $1 \leq i < j \leq 4$). Vertices connected by an edge differ by one transposition of neighboring elements.	65
3.7	Homology diagram and a quiver matrix for 3_1 knot. The labels 0, 2 and 3 are t -degrees of generators, while λ_i arise in specialization of quiver generating parameters. For 3_1 knot the quiver is unique, so the permutohedra graph consists of one vertex (shown in red).	66

3.8	Homological diagram for 4_1 knot, with labels λ_i assigned to various nodes (top). In the bottom the two equivalent quivers are shown, which differ by a transposition of elements $C_{2,5}$ and $C_{3,4}$ of the quiver matrix (shown in yellow, together with their symmetric companions). The positions of these elements are encoded in combinations $\lambda_2\lambda_5$ and $\lambda_3\lambda_4$, which are equal to each other (satisfy the center of mass condition).	68
3.9	Two copies of the homological diagram for 5_1 knot are shown on top. On each copy we denoted a parallelogram that encodes a symmetry, i.e. a transposition of two matrix elements that yields an equivalent quiver. In total there are 3 equivalent quivers, shown in bottom, which correspond to 3 vertices of the permutohedra graph. The permutohedra graph is made of two Π_2 that share a common vertex (in red).	70
3.10	Homology diagram for 5_2 knot; labels λ_i are consistent with (3.4.30).	72
3.11	The permutohedra graph for 5_2 knot consists of three Π_3 (shown schematically in bottom together with the formulas they correspond to) glued along common edges. The edges in this graph correspond to 6 types of transpositions arising from various quadruples of homology generators, which are also shown in various colors on the homological diagrams.	74
3.12	Homology diagram for 7_1 knot; labels λ_i are consistent with (3.4.33).	75
3.13	The permutohedra graph for 7_1 knot consists of two Π_3 and two Π_2 appropriately glued. Altogether it has 13 vertices representing equivalent quivers, and 8 symmetries corresponding to various quadruples of homology generators (and represented by different colors of the edges in the graph).	77
3.14	The permutohedra graph for 6_1 knot has 141 vertices that represent equivalent quivers (left). Excluding symmetries that involve λ_1 reduces the whole graph to a cube-like shape (right). Each face of this cube is one Π_4 (a bit squashed), and neighboring Π_4 's are glued along a square, which is a common face to both Π_4 's. The red vertex represents the quiver (3.4.41) (or its reordered form (3.4.43)).	78
3.15	Homology diagram for 6_1 knot; labels λ_i are consistent with (3.4.41).	78
3.16	Planar projection of a part of the permutohedra graph for 6_1 knot. In homological diagrams (on left and right) it is indicated how some of its symmetries, corresponding to edges of the graph, arise from quadruples of homology generators. The positions of two two permutohedra Π_4 mentioned in the text are indicated schematically in the bottom.	81
3.17	Homology diagram and local symmetries for 6_2 knot, each picture marked with * corresponds to two symmetries, due to double-valued nodes λ_5 and λ_6 .	82
3.18	Homology diagram and local symmetries for 6_3 knot.	83
3.19	Homology diagram and local symmetries for 7_3 knot.	84
A.1	Color legend of which entries are transposed on the quiver matrix.	101
A.2	A tree graph version of the symmetry graph of 5_2	103

Chapter 1

Introduction

1.1 Motivation

Quantum field theory (QFT) has been the basis for much of our understanding of modern physics. It explains the behavior of elementary particles all the way to the expansion of the Universe. It is the language in which many laws of Nature can be written. However, most of our understanding of QFT is derived from perturbative expansions or numerical analysis. This means that we still have much to explore if we want to understand the world of non-perturbative phenomena.

The pursuit of exact results for fully interacting QFT led to the development of supersymmetry, topological field theories, conformal field theories, integrable systems, and many more. This is because in these simpler or more symmetric setups, it is possible to obtain explicit formulas for the partition function and correlation functions. Having explicit formulas makes it easier to see new symmetries, which are not apparent from the Lagrangian. They also sometimes reveal hidden dualities between completely different theories.

The two examples of exactly solvable systems that we will be investigating are 3d $\mathcal{N} = 2$ *supersymmetric gauge theory* [1–4] and 3d *Chern-Simons (topological) theory* (CS) [5–7]. Although these theories are completely different, we will see that Wilson loops in Chern-Simons theory are dual to a 3d supersymmetric gauge theory for certain values of their couplings.

This duality was first discovered by Ooguri and Vafa [8] and was further developed by Labastida and Mariño [5] where they derived it in the context of *string theory* and *M-theory*. Essentially, they constructed two M-theory setups. In the first, its effective description is the Wilson loop in Chern-Simons theory, whereas the effective description of the second counts BPS particles in the 3d $\mathcal{N} = 2$ theory. The degeneracies of BPS states associated with Wilson loops in Chern-Simons theory are named Labastida-Mariño-Ooguri-Vafa (LMOV) invariants, after they conjectured that these numbers are always integers.

The above M-theory construction is very reminiscent of the *3d-3d correspondence* [9, 10]. This correspondence assigns a three-manifold to a 3d $\mathcal{N} = 2$ theory. Although both dualities involve the same 3d theory and remarkably similar string theory setups, they are distinct. For example, in the 3d-3d correspondence, we compute the Chern-Simons partition function on the knot complement¹, while in the LMOV

¹The knot complement is the three-manifold we construct by removing a tubular neighborhood (thickened knot) around the knot \mathcal{K} from the three-sphere, $S^3 \setminus T_{\mathcal{K}}^2$.

framework we calculate Wilson loops in Chern-Simons theory on the three-sphere. The interested reader may consult [11–14] for current research on those topics.

Thanks to Witten’s work [15], we know that Wilson loops in 3d Chern-Simons theory on the three-sphere are *knot invariants* for any gauge group and representation [16]. For instance, $SU(2)$ in the fundamental representation produces the famous Jones polynomial, whereas $SU(N)$ again in its fundamental representation yields the Hoste, Ocneanu, Millett, Freyd, Lickorish, Przytycki, and Traczyk (HOMFLY-PT) polynomial [17, 18]. The dependence on N is encoded in an additional parameter. This makes HOMFLY-PT a two-variable polynomial, which in the case $\mathcal{N} = 2$ reduces to the Jones polynomial. There is another polynomial invariant that encodes the previous two known as *superpolynomial* [19]. The superpolynomial is defined as *Poincaré characteristic of HOMFLY-PT homology*, or in more physical terms, as Wilson loops of (less rigorously defined) *refined Chern-Simons theory*.

There are two advantages of linking Chern-Simons theory to knot invariants.

First, because Chern-Simons is a gauge theory, we can study Wilson loops for various representations. In other words, if we choose symmetric representations of $SU(N)$, we are able to construct an infinite sequence of knot invariants labeled by the highest weight states (Young tableaux). Given that representations in gauge theory are referred to as colors, these infinite families of knot invariants are called *colored Jones*, *HOMFLY-PT* or *superpolynomials*, respectively.

The second advantage is that we can study the large color limit of the theory. The leading contribution of the large color asymptotic expansion is encoded in an algebraic curve named *A-polynomial*. The A-polynomial controls the entire spectrum of classical BPS states and plays an analogous role to the Seiberg-Witten curve for the 4d $\mathcal{N} = 2$ theory [20, 21].

Nevertheless, the A-polynomial is much more than just an ordinary algebraic curve. It can be reinterpreted as a classical Hamiltonian system that can be quantized [22]. The result of this quantization is the *quantum A-polynomial*. That is, a linear operator that produces a Schroedinger-like equation (recursion relation) for the sequence of colored knot invariants [23, 24]. Mathematically, the A-polynomial, for $\mathcal{N} = 2$, is defined as an $SL_2(\mathbb{C})$ characteristic variety of the knot complement [25]. Analogously to the previous knot polynomials, the A-polynomial can also be generalized to the $SU(N)$ case with an extra parameter encoding the N dependence [26]. From there, we may further generalize it to the *super-A-polynomial* [27]. A very important knot invariant is also encoded in the A-polynomial, namely the *hyperbolic volume of the knot complement*. This is at the heart of the long-sought-after *volume conjecture*, which states that the hyperbolic volume of a knot is the leading term in the asymptotic expansion of colored Jones polynomials [28, 29].

A great leap forward in our understanding of the relation between Chern-Simons theory and 3d $\mathcal{N} = 2$ theory occurred recently after noticing that colored knot invariants are special cases of a family of q -series named *quiver series* [30, 31]. These q -series arise naturally in the field of *quiver representation theory* [32–35]. A *quiver* is simply a directed graph whose nodes represent vector spaces and the arrows represent the morphisms between them. This field aims to study and enumerate distinct classes of isomorphisms in certain families of vector spaces. These enumerative invariants are called *motivic Donaldson-Thomas invariants*. They were conjectured by Kontsevich and Soibelman [36], and later proven by Efimov [37], to be positive integers.

The above relation is called *knots-quivers correspondence*, and it allowed for the first time to prove the integrality of the LMOV invariants for various infinite families of knots [31]. Plus, it yields new explicit formulas for colored superpolynomials, together with a rigorous constructive definition of colored superpolynomials. In addition, it was further discovered that quivers can be directly related to the 3d $\mathcal{N} = 2$ theory in more generality than knots [38–41]. Meanwhile, we stress that only certain quivers can be associated with knots and for specific values of the matter parameters.

The main goal of this thesis is two-fold.

First, in the context of knots-quivers correspondence, we show that, in general, there exists a large family of quivers that can be associated to the same knot [42]. We then find symmetry transformations that relate the equivalent quivers. Physically, this corresponds to a large web of dualities between different parameters of the 3d $\mathcal{N} = 2$ theory. To illustrate the rich combinatorial structure of the equivalent quivers, we represent them using a *colored graph*, which we call *colored symmetry graph*. The nodes of the symmetry graph are equivalent quivers and the edges stand for transformations relating equivalent quivers. Finally, we explain how colored symmetry graphs can be constructed from a purely combinatorial object named *permutohedra*, that is why we also refer to them as *permutohedra graphs*. Permutohedra are geometric representations of the permutation group in the form of a convex polytope [43]. This brings a surprising new combinatorial feature to knots and BPS particles.

Second, given the crucial role the A-polynomial plays in knot theory, we extend the concept from knots to the more universal case of quivers, and we introduce objects that we call *quiver A-polynomials* [44]. To do so, we derive a set of recursion relations for the coefficients of the quiver series and express them in terms of a set of linear operators in several variables². We demonstrate that it is possible to reduce the set of linear operators to a single linear operator that we refer to as the *quiver quantum A-polynomial*. The reason being that in the case where the quiver is associated to a knot, after a change of variables, it reduces to the quantum A-polynomial of a knot. We then obtain the *classical quiver A-polynomial* from the quantum one as the leading contribution of the asymptotic expansion of the quiver generating function.³

We expect this thesis to be a valuable contribution to the growing body of literature on knot theory, quiver representation theory, and the community of exact results. We also would like this to serve as a comprehensive review and introduction to the topic together with state-of-the-art results.

The results of this thesis are also presented in⁴:

- J. Jankowski, P. Kucharski, H. Larraguivel, D. Noshchenko and P. Sułkowski. *Permutohedra for knots and quivers*. Phys.Rev.D 104 (2021) 086017.
- H. Larraguivel, D. Noshchenko, M. Panfil and P. Sułkowski, *Nahm sums, quiver A-polynomials and topological recursion*. J. High Energy Phys. 2007, 151 (2020).

²These are analogous to the Schwinger-Dyson equations for the partition function [45].

³In [44] we also explored the inverse procedure of starting from the classical quiver A-polynomial and derive the quantum one using topological recursion.

⁴These two references above are cited in the text as [42] and [44], respectively. During my bachelor degree I also coauthored a paper [46], which is unrelated to the content of this thesis.

1.2 Outline

The organization of the thesis is as follows.

In **chapter 2** we review the necessary concepts and background that we will use throughout the thesis. We begin by presenting the 3d $\mathcal{N} = 2$ gauge theory Lagrangian and explaining how it reduces to a q -series. Then, the analogous q -series can be seen as a generating function for Wilson loops in 3d Chern-Simons theory. Next, for the mathematical background, we discuss in more detail how the quiver q -series naturally arises in quiver representation theory. We also carefully explain the appearance of knot invariants in 3d Chern-Simons theory.

We finish the first chapter by presenting the M-theory formulation of the duality between 3d $\mathcal{N} = 2$ gauge theory and 3d Chern-Simons theory, or *knots-quivers correspondence*.

In **chapter 3** we focus on the symmetries and dualities of the quiver partition function for quivers associated with knots via the knots-quivers correspondence. We present various examples in which we find a plethora of quivers that we can assign to each knot and explain the appearance of the permutohedra in detail. We give the physical interpretation as a monumental web of dualities between large families between distinct 3d $\mathcal{N} = 2$ SUSY gauge theory. We find a baffling number of equivalent quivers for various knots and we conjecture that it grows factorially with respect to the number of crossings of the knot diagram.

Later, in **chapter 4** we introduce the concept of a quiver A-polynomial, we derive the analogous of the Schwinger-Dyson equations for the quiver series and obtain the quantum and classical A-polynomials for various quivers. We also determine various classical quiver A-polynomials whose explicit quantum A-polynomials have yet to be found. Finally, we classify the quiver A-polynomials according to their genus.

In **chapter 5** we summarize our key results along with their main implications in the framework of the knots-quivers correspondence. Moreover, we discuss the challenges we find in each of our approaches and state the main challenges behind our conjectures. Finally, we comment on future research directions and list open questions related to our research.

Chapter 2

Background material

In this chapter, we will provide a quick overview of the physical and mathematical concepts this thesis builds upon. We begin by introducing the Lagrangian of 3d $\mathcal{N} = 2$ supersymmetric gauge theory. Next, we argue how the partition function for that theory reduces to a q -series. This particular q -series appears in the context of quiver representation theory, where it is referred to as the quiver generating series of the Donaldson-Thomas invariants. We do not expect the reader to be familiarized with quiver representation theory, so we give a brief explanation of what quiver representation theory is, and how the Donaldson-Thomas invariants are encoded in the quiver series.

Then we switch gears and present the relevant results we will be using from the 3d Chern-Simons theory. Having discussed those concepts, we will use them to introduce the colored HOMFLY-PT polynomials, which are a sequence of polynomial invariants of knots.

Finally, we will see that from topological string theory arises the conjecture that the partition function of 3d $\mathcal{N} = 2$ gauge theory is dual to the generating function of colored HOMFLY-PT polynomials. We will see how to interpret this duality as a geometric transition between strings propagating on the deformed conifold, and strings propagating on the resolved conifold.

2.1 Supersymmetric gauge theories in 3d

The first theories in our list are the 3d $\mathcal{N} = 2$ SUSY gauge theories. These are a marvelous source of exact results and insights into non-perturbative physics [47]. They enjoy a rich web of infrared dualities (e.g. level-rank duality, mirror symmetry, Aharony duality, particle-vortex duality [1, 47, 48]). They describe the low-energy physics of certain brane configurations in topological string theory [10]. They can be studied from the point of view of AdS_4/CFT_3 correspondence [49–51]. They have deep connections to quantum integrable systems and 2d CFTs and references therein [1]. Most importantly, for us, they are the 3d $\mathcal{N} = 2$ part of the 3d-3d correspondence. This builds a bridge from 3d $\mathcal{N} = 2$ gauge theories with topological quantum field theories and further distant areas of mathematics, such as topological invariants of 3d manifolds and modular forms. This at the same time relates their BPS spectra to Gromov-Witten invariants, Donaldson-Thomas invariants and lattice path counting [40, 41, 52].

For all the above reasons and more, we decided to kick off by reviewing the pe-

cular physical effects that occur in 3d gauge theories (topological charges, parity anomaly, particle-vortex duality, and infrared dualities)¹. Then, we will go one step further and present the SUSY version. We will review the field content of the supermultiplets, the algebra of supercharges and the SUSY transformations that leave the Lagrangian invariant. We will briefly comment on how SUSY localization ensures that the semiclassical approximation is exact. Finally, we will present the quiver series whose leading (classical) contribution in the asymptotic expansion (WKB) coincides with the SUSY theory. This leads to the conjecture that such quiver series is the full quantum partition function, not just in the classical limit.

Our review of 3d gauge theories will follow a logic similar to that presented in Tong's great lectures on gauge theory [7, Sec 8]. Regarding the SUSY theory, our derivation follows Closset and Kim's wonderful introductory notes on 3d $\mathcal{N} = 2$ gauge theories [1, Sec 2 & 4]. Lastly, for the reader who wishes to learn more about state-of-the-art research between 3d $\mathcal{N} = 2$ theories and quiver series, we strongly recommend the original papers of Ekhholm, Kucharski and Longhi [38, 39].

2.1.1 Supersymmetric multiplets

We begin by presenting the 3d $\mathcal{N} = 2$ theories on which we will work. We will introduce their supersymmetric multiplets and construct the explicit Lagrangian. We will encounter three main peculiarities when working with gauge theories in three dimensions compared to the others. These are the *Parity anomaly*, *topological symmetries* and the *particle vortex duality*. We will briefly explain their appearance and what they imply for our models. See [1, 7, 53] for a more detailed and pedagogical explanation.

We will only consider the 3d $\mathcal{N} = 2$ SUSY theories in $\mathbb{R}^2 \times S^1$. Our convention for the spinor matrices is as follows

$$(\gamma^\mu)_\alpha{}^\beta = \left\{ \sigma^3 = \begin{bmatrix} 1 & 0 \\ 0 & -1 \end{bmatrix}, -\sigma^1 = \begin{bmatrix} 0 & -1 \\ -1 & 0 \end{bmatrix}, -\sigma^2 = \begin{bmatrix} 0 & i \\ -i & 0 \end{bmatrix} \right\}, \quad (2.1.1)$$

where $\sigma^{1,2,3}$ are the Pauli matrices and $\alpha, \beta = \pm$ are the spinor indices, which we can raise or lower with $\epsilon^{\alpha\beta}$. We can easily see that they are a representation of the Clifford algebra $\{\gamma^\mu, \gamma^\nu\} = \delta^{\mu\nu}$ thanks to the property $\gamma^\mu \gamma^\nu = \delta^{\mu\nu} + i\epsilon^{\mu\nu\rho} \gamma_\rho$.

The careful reader will quickly notice that in 3d the gamma matrices (2.1.1) are actually half the size of the more familiar ones in 4d. In 4d, for massive free fermions, we have four particles, two particles with spins $\pm 1/2$ and two antiparticles with spins $\pm 1/2$. \mathcal{CPT} symmetry is preserved because we can interchange particles and antiparticles. Additionally, \mathcal{P} (parity) is also a symmetry because we can interchange (anti)particles with opposite spins.

On the other hand, for massive free fermions in 3d, we have half the number of particles, just a particle and antiparticle. So \mathcal{CPT} is a symmetry, but \mathcal{P} is broken. When coupled to an Abelian gauge field, this will lead to an anomaly, which in turn shifts one of the coupling constants of our theory.

Now that we have the spinor matrices, we can use them to write the SUSY algebra. We have four real supercharges Q_α and \bar{Q}_α , which form a representation of the $\mathcal{N} = 2$ SUSY algebras with the following anticommutation relations

$$\{Q_\alpha, \bar{Q}_\beta\} = 2\gamma_{\alpha\beta}^\mu P_\mu + 2i\epsilon_{\alpha\beta} Z, \quad \{Q_\alpha, Q_\beta\} = \{\bar{Q}_\alpha, \bar{Q}_\beta\} = 0, \quad (2.1.2)$$

¹All the theories we will be considering are Abelian gauge theories

where P_μ is the 3d momentum and Z is a real central charge.

For a $\mathcal{N} = 2$ gauge theory, there are two supermultiplets:

1. *Vector multiplet* \mathcal{V} which transforms under the adjoint representation.
2. *Chiral multiplet* Φ in a (possibly reducible) representation R of G_{Gauge} .

We will be concerned only with Abelian gauge theory; or, in other words, the gauge group is of the form

$$G_{Gauge} = \prod_{i=1}^m U(1)_{g,i}, \quad (2.1.3)$$

for some $m \in \mathbb{N}$.

This means that we have m vector multiplets \mathcal{V}^i with $i = 1, \dots, m$ in the Wess-Zumino gauge, which takes the form of

$$\mathcal{V}^i = (\sigma^i, A_\mu^i, \lambda^i, \bar{\lambda}^i, D^i), \quad (2.1.4)$$

where σ^i are real vector fields, A_μ^i are Abelian gauge fields, $\lambda^i, \bar{\lambda}^i$ are gaugini and D^i are auxiliary fields.

These fields transform under SUSY as

$$\delta\sigma^j = -\zeta^i \bar{\lambda}^j + \bar{\zeta}^j \lambda^j, \quad (2.1.5a)$$

$$\delta A_\mu^j = -i(\zeta^j \gamma_\mu \bar{\lambda}^j + \bar{\zeta}^j \gamma_\mu \lambda^j), \quad (2.1.5b)$$

$$\delta\lambda^j = i\zeta^j D^j - i\gamma^\mu \zeta^j \left(D_\mu^j \sigma^j + \frac{1}{2} \epsilon_{\mu\nu\rho} F^{\nu\rho,j} \right), \quad (2.1.5c)$$

$$\delta\bar{\lambda}^j = -i\bar{\zeta}^j D^j + i\gamma^\mu \bar{\zeta}^j \left(D_\mu^j \sigma^j + \frac{1}{2} \epsilon_{\mu\nu\rho} F^{\nu\rho,j} \right), \quad (2.1.5d)$$

$$\delta D^j = \zeta^j \gamma^\mu D_\mu^j \bar{\lambda}^j - \bar{\zeta}^j \gamma^\mu D_\mu^j \lambda^j, \quad (2.1.5e)$$

where we replaced the i superindex by j to avoid confusion with the imaginary unit i and j is not contracted. SUSY parameters ζ^j and $\bar{\zeta}^j$ are generic constant spinors in $\mathbb{R}^2 \times S^1$. In addition, $F_{\mu\nu}^j = \partial_\mu A_\nu^j - \partial_\nu A_\mu^j$ are the field strengths and $D_\mu^j = \partial_\mu^j - iA_\mu^j$ are the gauge covariant derivatives.

Next, the matter fields lying inside the chiral multiplet are

$$\Phi^i = (\phi^i, \psi^i, F^i), \quad (2.1.6)$$

where ϕ^i are complex scalar fields, ψ^i are Dirac spinors and F^i are auxiliary fields. These fields transform under SUSY as

$$\delta\phi^j = \sqrt{2}\zeta^j \psi^j, \quad (2.1.7a)$$

$$\delta\psi^j = \sqrt{2}\zeta^j F^j + \sqrt{2}i\sigma^j \bar{\zeta}^j \phi^j - \sqrt{2}i\gamma^\mu \bar{\zeta}^j D_\mu^j \phi^j, \quad (2.1.7b)$$

$$\delta F^j = -\sqrt{2}i\sigma^j \bar{\zeta}^j \psi^j + 2i\sigma^j \bar{\zeta}^j \lambda^j - \sqrt{2}i\bar{\zeta}^j \gamma^\mu D_\mu^j \psi^j. \quad (2.1.7c)$$

We also have the anti-chiral multiplet $\bar{\Phi}^i = (\bar{\phi}^i, \bar{\psi}^i, \bar{F}^i)$, which is the $\mathcal{CP}\mathcal{T}$ conjugate of Φ^i . $\bar{\Phi}^i$ takes values in the conjugate representation \bar{R} and its SUSY transformations are analogous to (2.1.7).

Finally, the SUSY transformations of Φ and $\bar{\Phi}$ imply the SUSY algebra

$$\delta_{\zeta^j}^2 = \delta_{\bar{\zeta}^j}^2 = 0, \quad \{\delta_{\zeta^j}, \delta_{\bar{\zeta}^j}\} = -2i\zeta^j \gamma^\mu \bar{\zeta}^j D_\mu^j - 2i\zeta^j \bar{\zeta}^j \sigma^j, \quad (2.1.8)$$

where we now see that the central charges are $Z^j = \sigma^j$.

2.1.2 Topological and global symmetries

In $d = 3 + 1$ Abelian gauge theories, we have two conserved currents. The first is the electric current, which is the result of gauge invariance and acts on Wilson lines. The second one is the magnetic current (formed out of the dual-field strength), which is a result of the Bianchi identity on the dual-field strength and it acts on 't Hooft lines. These two are examples of *generalised symmetries*, also known as *higher form symmetries* and the operators they act on are *non-local*².

In $d = 2 + 1$ EM we can construct analogous symmetries. We have the conserved current for the dual field strength

$$J_{Top}^\mu = \frac{1}{4\pi} \epsilon^{\mu\nu\rho} F_{\nu\rho}, \quad Q_{Top} = \int_{R^2} d^2x J_{Top}^0 = \frac{1}{2\pi} \int d^2x B, \quad (2.1.9)$$

which again is conserved thanks to the Bianchi identity. The normalization factor $1/4\pi$ is such that the charge Q_{Top} takes integer values. This charge is associated with a topological symmetry $U(1)_{Top}$. This symmetry acts on *monopole operators*, which is different from the 4d case, because these are actually local operators [7, sec 8].

The gauge theories we are considering have continuous global symmetries. It is of advantage to promote the global symmetries to local ones by introducing *external fields* (background fields)³, see [54, Chap 16] for an extensive treatment of the topic.

$$G_{Gauge} = \prod_{i=1}^m U(1)_{g,i}. \quad (2.1.10)$$

As we shall see, the presence of Abelian symmetries in 3d theories is different from that in other dimensions. This is because in the classical case they will give rise to the mass parameters m_E called *real mass*. In the quantum case, these real masses will lead to anomalies which, in turn, induce effective couplings.

We can group the external fields into a single vector multiplet

$$\mathcal{V}_{(E)}^i = (\sigma_{(E)}^i, A_{\mu(E)}^i, \lambda_{(E)}^i, \bar{\lambda}_{(E)}^i, D_{(E)}^i). \quad (2.1.11)$$

However, we do not want these external sources to break SUSY. Therefore, the condition that they are compatible with SUSY transformations imposes the following

$$\sigma_{(E)}^i = m_E^i, \quad A_{(E)}^i = \delta\lambda_{(E)}^i = \delta\bar{\lambda}_{(E)}^i = D_{(E)}^i = 0, \quad (2.1.12)$$

where $m_E^i \in \mathbb{R}$ are constants called real masses. The name masses is because, as we will see in the next subsection, when we vary the action w.r.t. external fields and substitute its equations back into the chiral Lagrangian (2.1.19), they effectively become masses $\sigma^i = m_E^i$ for the complex scalars ϕ and the spinors ψ

$$\mathcal{L}_m^i = \bar{\phi}^i (m_E^i)^2 \phi^i - i\bar{\psi}^i m_E^i \psi^i. \quad (2.1.13)$$

In our particular example, it happens that all global symmetries are also topological symmetries $U(1)_{t,i}$. However, this is not the case when we consider non-Abelian gauge fields, e.g., $G_{Gauge} = U(N)_g$. This is because the global symmetries still have a non-trivial center $U(1)_g \in U(N)_g$, but they do not lead to a topological symmetry. This is easily seen since the field strengths of a non-Abelian gauge field do not satisfy the Bianchi identity as in the Abelian case (2.1.9).

²They are non-local because they are defined on a curve $C \in \mathbb{R}^3$ rather than a point $x \in \mathbb{R}^3$.

³This has nothing to do with the auxiliary fields.

2.1.3 The Super Lagrangian

Without further ado, let us dive into the $3d \mathcal{N} = 2$ SUSY gauge theories on $\mathbb{R}^2 \times S^1$. The usual derivation of the Lagrangian for this theory is by dimensional reduction from a $4d \mathcal{N} = 1$ SUSY gauge theory [47, 48]. Here we will start directly from the Electromagnetism-Chern-Simons-matter Lagrangian in 3d without any superpotential. The Lagrangian in its most general form consists of three terms.

The $3d \mathcal{N} = 2$ SUSY Lagrangian can be written as

$$\mathcal{L}_{General} = \sum_{i=1}^m \left[\mathcal{L}_{EM}^i + \mathcal{L}_{CS}^i + \sum_{j \neq i} \mathcal{L}_{CS}^{i \neq j} + \mathcal{L}_{\Phi\bar{\Phi}}^i \right]. \quad (2.1.14)$$

First, the *SUSY Electromagnetic Lagrangian* terms are of the form

$$\mathcal{L}_{EM}^i = \frac{1}{e_{0,i}^2} \left[\frac{-1}{4} F_{\mu\nu}^i F^{\mu\nu,i} + \frac{1}{2} D_\mu^i \sigma^i D^{\mu i} \sigma^i - i \bar{\lambda}^i \gamma^\mu D_\mu^i \lambda^i - \frac{1}{2} D^i{}^2 \right], \quad (2.1.15)$$

compared to (2.2.1) we see the appearance of three additional terms that supersymmetrize it.

Next, we have *SUSY Abelian Chern-Simons Lagrangian*

$$\mathcal{L}_{CS}^i = \frac{k_i}{4\pi} \left[\epsilon^{\mu\nu\rho} A_\mu^i \partial_\nu A_\rho^i - 2D^i \sigma^i + 2i \bar{\lambda}^i \lambda^i \right], \quad (2.1.16)$$

where $k_i \in \mathbb{Z}$ are the Chern-Simons (couplings) levels. The first term in the brackets is known as the Abelian Chern-Simons Lagrangian. The remaining terms are there to preserve supersymmetry.

Now we introduce the interactions (mixing) between m distinct terms of the form

$$\mathcal{L}_{CS}^{j \neq l} = \frac{k_{jl}}{2\pi} \left(i \epsilon^{\mu\nu\rho} A_\mu^j \partial_\nu A_\rho^l - D^j \sigma^l - D^l \sigma^j + i \bar{\lambda}^j \lambda^l + i \bar{\lambda}^l \lambda^j \right), \quad (2.1.17)$$

where $k_{jl} \in \mathbb{Z}$ are the mixed Chern-Simons levels. The extra terms are needed to preserve supersymmetry as well.

A distinguished mixing term is between a gauge $U(1)_{g,i}$ with a global symmetry that appears as a background field. As we have already mentioned, in our example, those global symmetries are also topological symmetries $U(1)_{t,T_i}$ and so their mixing $k_{iT_i} = 1$ produces a special term in the Lagrangian known as the Fayet-Iliopoulos (FI) term

$$\mathcal{L}_{FI}^i = -\xi^i D^i, \quad \xi^i = \frac{1}{2\pi} m_E^{T_i}, \quad (2.1.18)$$

where $m^{(T_i)}$ is a real mass for the topological symmetry.

Lastly, for the matter fields we have the *Chiral Lagrangian*

$$\begin{aligned} \mathcal{L}_{\Phi\bar{\Phi}}^j = & D_\mu^j \bar{\phi}^j D^{\mu i} \phi^j - i \bar{\psi}^j \gamma^\mu D_\mu^j \psi^j - \bar{F}^j F^j + \bar{\phi}^j D^j \phi^j \\ & + \bar{\phi}^j \sigma^{j2} \phi^j - i \bar{\psi}^j \sigma^j \psi^j + \sqrt{2}i (\bar{\phi}^j \lambda^j \psi^j + \bar{\psi}^j \bar{\psi}^j \phi^j), \end{aligned} \quad (2.1.19)$$

where the real masses discussed in (2.1.13) are implicit in $\sigma_{(E)}^j = m_E^j$. Lastly, we point out that we will be working without a superpotential $W = 0$.

2.1.4 Effective couplings and moduli space of SUSY vacua

We start by integrating out the auxiliary fields F^i and D^i , use their equations of motion as Lagrange multipliers, and substitute their value back into the Lagrangian (2.1.14). Then, the resulting potential for the chiral and vector scalars ϕ^i and σ^i reduces to

$$U = \sum_{i=1}^m \left\{ e_{0,i}^2 \left[|\phi^i|^2 - \xi^i - \sum_{j=1}^m k_{ij} \sigma^j \right]^2 + m_E^2 |\phi|^2 \right\}, \quad (2.1.20)$$

where the moduli space of the SUSY vacua is determined by the condition $U = 0$ and is parametrized by ξ^i , k_{ij} and m_E^i . There are two main branches, the Higgs branch and the Coulomb branch. For the Higgs branch, we need $\sigma^i = 0$ and $U(\phi^i) = 0$. This branch usually has a broken gauge symmetry. Furthermore, this branch cannot exist for generic values of m_E^i .

Moving on to the Coulomb branch, where $\phi^i = 0$ and $U(\sigma^i) = 0$. Again, for generic FI and Chern-Simons couplings, this branch may not exist. Nevertheless, when this phase does exist, the gauge symmetries are generally unbroken, and the branch is parametrized by σ^i and the dual-photon/monopole operators.

To quantize our theory, we follow the standard convention for Chern-Simons contact terms for the R-Symmetry [1]. For a chiral multiplet Φ^i with charge $Q_i^{(j)} = \delta_{ij}$ under a $U(1)_{g,j}$ gauge field of R-charge r , we have

$$k_{ij} = \frac{-1}{2} \sum_{l=1}^m Q_i^{(l)} Q_j^{(l)}, \quad k_{iR} = \frac{-1}{2} Q_i^{(R)} (r-1), \quad k_{rr} = \frac{-1}{2} (r-1)^2, \quad (2.1.21)$$

where k_{ij} , k_{iR} and k_{RR} are the mixed $U(1)_i - U(1)_j$, mixed $U(1)_i - U(1)_R$ and pure $U(1)_R$ contact terms, respectively.

For the vector multiplet, we have $k_{RR} = 1/2$. Then, we compute the contact terms by summing all chiral and vector multiplets.

Next, we take the limit of heavy fermions $m_E^i \rightarrow \pm\infty$, which allows us to integrate out all fermions. This gives rise to the following effective action of the one-loop contribution

$$S_{eff} = \log \det (i\gamma^\mu D_\mu + m) \xrightarrow{m \rightarrow \pm\infty} \frac{i}{4\pi} \frac{\text{sign}(m)}{2} \int_{\mathbb{R}^2 \times S^1} d^3x \epsilon^{\mu\nu\rho} A_\mu \partial_\nu A_\rho. \quad (2.1.22)$$

The above is the so-called parity anomaly, which produces the following corrections to the Chern-Simons couplings

$$k_{ij}^{Effective} = k_{ij} + \frac{1}{2} \sum_{l=1}^m \text{sign}(m_E^l) Q_i^{(l)} Q_j^{(l)} = k_{ij} + \frac{1}{2} \delta_{ij}. \quad (2.1.23)$$

Analogously, there is another effective coupling arising from the background fields

$$k_{iR}^{Effective} = \frac{1}{2} Q_i^{(R)} \text{sign}(m_E^i) = \frac{1}{2} \delta_{iR} \text{sign}(m_E^i). \quad (2.1.24)$$

Finally, we can interpret all Chern-Simons contact terms as a renormalization of the FI parameters

$$\xi^{i,Effective} = \xi^i + \sum_{j=1}^m k_{ij}^{Eff} \sigma^j + \sum_{R=1}^m k_{iR}^{Eff} m_R. \quad (2.1.25)$$

Hence, the 1-loop contributions can be easily accounted for by replacing the UV parameters in (2.1.14) with the effective ones.

2.1.5 Vortex partition function

Given the fact that we are dealing with supersymmetric theories with explicit UV Lagrangian description (2.1.14) we are able to apply localization to compute their partition function. This technique is possible because the Hamiltonian is Q-exact. In other words, it can be expressed as the anti-commutator of SUSY charges $H = \{Q, \bar{Q}\}$, where $Q|0\rangle = 0$ by construction. This implies that the ground-state energy of SUSY theories is always zero, $H|0\rangle = 0$. Hence, any Q-closed observable will be identically zero

$$\langle Q(\Psi)\mathcal{O}\rangle = 0. \quad (2.1.26)$$

In the Lagrangian formalism, it translates to the Lagrangian being Q-exact as a form w.r.t. δ_{ζ^i} and $\delta_{\bar{\zeta}^i}$. This means that we are free to add any Q-exact terms to the Lagrangian and the v.e.v of any Q-closed observable should be invariant under such deformation

$$L + \tau L_{Q\text{-exact}} = L + \tau \delta_{\zeta} \delta_{\bar{\zeta}} J \implies \frac{d}{d\tau} \langle \mathcal{O} \rangle_{\tau} |_{\tau=0} = \frac{-i}{\hbar} \langle \delta_{\zeta^i} \delta_{\bar{\zeta}^i} J \mathcal{O} \rangle = 0, \quad (2.1.27)$$

where τ is an arbitrary parameter.

Thus, we can compute $\langle \mathcal{O} \rangle_{\tau}$ for any value of τ . In particular, we can take $\tau \rightarrow \infty$ and apply the saddle point expansion

$$\langle \mathcal{O} \rangle_{\tau \rightarrow \infty} = \int_{\mathcal{M}_{\text{Classical}}} d\phi_c \mathcal{O}(\phi_c) Z^{1\text{-loop}}(\phi_c) e^{-\beta S[\phi_c]}, \quad (2.1.28)$$

where $\mathcal{M}_{\text{Classical}} = \{\phi = \phi_c | \delta S[\phi] / \delta \phi = 0\}$ is the set of classical solutions to the Euler-Lagrange equations. The nice feature is that due to the fact that the observable is independent of τ the saddle-point expansion is exact. This means that the whole *partition function localizes to the semi-classical limit*.

It can be proven [1, sec 3] that the kinetic terms of the matter and vector multiplets are Q-exact

$$L_{Q\text{-exact}} = \frac{1}{e_{0,i}^2} \delta_{\zeta^i} \delta_{\bar{\zeta}^i} (\dots) + \frac{1}{g_i^2} \delta_{\zeta^i} \delta_{\bar{\zeta}^i} (\dots), \quad (2.1.29)$$

which means that we can take the weak coupling limit $e_{0,i}, g_i \rightarrow 0$ for the path integral.

The particle-like finite-energy classical solutions to the E-L equations in our set-up are *vortices*. They are charged under $U_t^j(1)$ and correspond to configurations of $\phi^j = \rho^j(r) e^{i\alpha^j(\theta)}$ winding asymptotically around \mathbb{R}^2 . They are analogous to the 4d string solutions and 2d instantons. They are called *topological solitons*. Hence the name, *vortex partition function*, Z_V^4 .

The partition function was first calculated in [2] using equivariant localization. Later it was also calculated using Higgs branch localization in [55]. We will not

⁴Technically, the 3d $Z_V^{\mathbb{R}^2 \times S^1}$ for $\mathcal{N} = 2$ is known as the *K-theoretic* vortex partition function [3, 11]. This because it can be considered as a K-theoretic lift of the 2d vortex partition function $Z_V^{\mathbb{R}^2}$ for $\mathcal{N} = (2, 2)$. This is from simple dimensional reduction $Z_V^{\mathbb{R}^2 \times S^1} \xrightarrow{\beta \rightarrow 0} Z_V^{\mathbb{R}^2}$ where β is the radius of S^1 .

reproduce the long computation of $Z_V^{\mathbb{R}^2 \times S^1}$ explicitly. Instead, we will present a conjectured general formula in terms of q -series proposed in [39, sec 5]

$$Z_V = \sum_{d_1, \dots, d_m=0}^{\infty} (-q)^{\sum_{i,j=1}^m C_{ij} d_i d_j} \frac{x_1^{d_1} \dots x_m^{d_m}}{(q^2)_{d_1} \dots (q^2)_{d_m}}, \quad (2.1.30)$$

where d_i are called the vortex numbers and they correspond to the vortex charges and we introduce the q -Pochhammers in the denominator

$$(x)_d = (x; q^2)_d = \prod_{k=0}^{d-1} (1 - xq^{2k}). \quad (2.1.31)$$

Then the identification of variables is of the form

$$C_{ij} = k_{ij}^{Effective} = k_{ij} + \frac{1}{2} \delta_{ij}, \quad \log x_i = \xi^{i, Effective}, \quad q = e^{\hbar}. \quad (2.1.32)$$

This is an essential result, and the q -series (2.1.30) will play a pivotal role in this thesis. As we shall see, the web of dualities will become apparent when we see that several knot invariants can also be brought to this form.

2.1.6 Index and BPS particles

Now that we have reached the summit with an explicit form for the vortex partition function (2.1.30), we can begin our descent and study all other quantities that follow from it. It was discovered in [3, 4, 11, 56] that both the partition function and the index for 3d $\mathcal{N} = 2$ theory on $S^2 \times S^1$ or on the squashed three-sphere $S_b^3 = \{(z_1, z_2) \in \mathbb{C} | b|z_1|^2 + b^{-1}|z_2|^2 = 1\}$, factorizes into a product of the vortex partition function (2.1.30) and the anti-vortex partition as

$$Z^{S_b^3} = Z_V(q) Z_{\text{anti-V}}(\tilde{q}), \quad q = e^{i\pi b^2}, \quad \tilde{q} = q^{1/b^4} = e^{i\pi b^{-2}}. \quad (2.1.33)$$

From this and other string theory arguments that we will present in section 2.3.2 we can interpret the vortex partition function as an index

$$Z_V = \text{Tr}(-1)^R e^{\beta H} q^{2J+R} \prod_{i=1}^m x_i^{f_i}, \quad (2.1.34)$$

where R is the charge of the R-symmetry $U_R(1)$ ⁵, q can be interpreted as the fugacity associated with rotations around \mathbb{R}^2 , J is the generator of those rotations and x_i are the fugacities associated with the topological symmetries $U_{t,i}(1)$.

The small difference between a partition function and an index lies only in the innocent insertion of the prefactor $(-1)^F$, where F counts the number of fermions in a given state [57]. This is combined with the fact that in SUSY theories all excited states $E > 0$ have degeneracy two, one state being bosonic and another fermionic.

⁵Where the relation between $(-1)^R$ and $(-1)^F$ is $q \rightarrow -q$.

This means that the index receives contributions only from the zero energy states $E = 0$. These states saturate the Bogomolnyi-Prasad-Sommerfield (BPS) bound⁶

$$m \geq |Z| \quad (2.1.35)$$

where m is the mass in the representation of the extended symmetry algebra and Z is the central charge.

To extract the degeneracy of the BPS spectrum, or count the number of BPS particles, we first introduce the q -exponential⁷, which for us will be the infinite q -Pochhammer symbol (2.1.31)

$$E_q(x) = \prod_{k=0}^{\infty} (1 - xq^{2k}) = \sum_{k=0}^{\infty} \frac{q^{\binom{k}{n}} x^k}{(q^2)_k} = \exp \left[\frac{-1}{1 - q^2} \sum_{k=1}^{\infty} \frac{x^k}{k [k]_{q^2}} \right], \quad (2.1.36)$$

where $[k]_{q^2} = (1 - q^{2k}) / (1 - q^2)$ is known as a q -number, since $[k]_{q^2} \rightarrow k$ when $q \rightarrow 1$.

Having the q -exponential, we can define the q -plethystic exponential as

$$EP_q[f(x)] = \exp \left[\frac{-1}{1 - q^2} \sum_{k=1}^{\infty} \frac{f(x^k)}{k [k]_{q^2}} \right] = \prod_{d=1}^{\infty} \prod_{k=0}^{\infty} (1 - x^d q^{2k})^{a_d}. \quad (2.1.37)$$

Lastly, we can rewrite (2.1.34) as

$$Z_V = \prod_{(d_1, \dots, d_m) \neq 0} \prod_{k=0}^{\infty} \prod_{j \in \mathbb{Z}} \left(1 - x_1^{d_1} \dots x_m^{d_m} q^{2k+j+1} \right)^{(-1)^{j+1} \Omega_{d_1, \dots, d_m; j}}, \quad (2.1.38)$$

where $\Omega_{d_1, \dots, d_m; j}$ counts the number of BPS particles with a given spin j and flavor charge d_i . In its current state, it is not clear from (2.1.38) that Ω should be a non-negative integer, besides the physical argument that we are counting BPS particles. Moreover, a priori we have no good argument why given a set of vortex numbers (d_1, \dots, d_m) we would have only finitely many particles with a given spin j . Nonetheless, this is not actually a conjecture, but a theorem. We will not go into the details of the proof, just explain how this q -series (2.1.30) appears naturally in a branch of mathematics called *quiver representation theory* that we will introduce in the next subsection.

2.1.7 Quiver representation theory

In the last couple of subsections, we have reduced the study of 3d $\mathcal{N} = 2$ theory to the study of certain q -series (2.1.30). These series are quite universal in the sense that they appear in several different contexts in physics and mathematics, from partition functions of 2d CFTs [58] to modular forms [59], knot invariants [31] Donaldson-Thomas theory [36].

For us, the working definition of a quiver is a directed graph Q formed from a set of m vertices Q_0 and a set of arrows between them Q_1 . For example, $Q = \{Q_0 = \{x_1, x_2, x_3\} \cup Q_1 = \{x_1 \rightarrow x_1, x_1 \rightarrow x_2, x_2 \rightarrow x_3, x_3 \rightarrow x_1\}\}$.

⁶The original bound was derived from classical field theory and used to obtain the classical vacuum solutions, but supersymmetry was not involved. It so happens that the same inequality arises in supersymmetric theories where it is related to short multiplets that preserve supersymmetry.

⁷This function it is also known as the quantum dilogarithm. This is because the dilogarithm is defined as $\text{Li}_2(x) = \sum_{k=1}^{\infty} x^k / k^2$ and some authors define the q -dilogarithm as $\text{Li}_{2,q}(x) = \sum_{k=1}^{\infty} x^k / (k [k]_q)$.

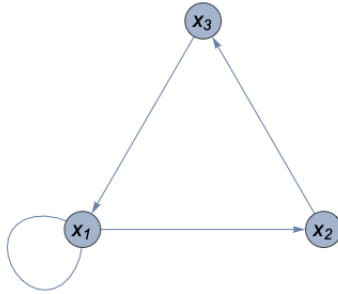


Figure 2.1: The explicit graph of the quiver Q . By convention we ignore orientation of self loops, eg. $x_1 \rightarrow x_1$.

Another way to encode the information of the graph of Q is by means of its *adjacency matrix* C . That is, an $m \times m$ matrix whose entries are defined as $C_{ij} = \{\# \text{ arrows } x_i \rightarrow x_j\}$. We will commonly refer to C as the quiver matrix. Moreover, we will be working only with symmetric quivers, those which have the same number of arrows from $x_i \rightarrow x_j$ as from $x_j \rightarrow x_i$. These obviously lead to symmetric quiver matrices $C_{ij} = C_{ji}$.

Now comes the relation to representation theory. We can associate with every quiver node x_i a vector space V_i over a field \mathbb{F} of dimension d_i . Likewise, we can associate to every quiver edge $x_i \rightarrow x_j$ a linear map $f_{ij} : V_i \rightarrow V_j$. We call the set of vector spaces V_i and maps f_{ij} a *quiver representation*.

As in many branches of mathematics, we are interested to describe the properties of quiver representations up to isomorphism. In this case, a morphism between quiver representations is a set of linear maps $g_{ii} : V_i \rightarrow W_i$, such that

$$f_{ij}(g_{ii}(V_i)) = g_{jj}(f_{ij}(V_i)), \quad (2.1.39)$$

and g_{ii} are invertible. All-in-all, this is a very complicated way to say that two quiver representations are equivalent if we can obtain one from the other via a change of basis in each vector space.

The natural question then arises as how many of these equivalence classes there are for a given dimension (d_1, \dots, d_m) ? As innocent as it might look, this is a very complicated question in general. In particular, because for standard fields $\mathbb{F} = \mathbb{R}, \mathbb{C}$ the group of isomorphisms, change of basis, of $\mathbb{R}^{d_i}, \mathbb{C}^{d_i}$ are $GL_{\mathbb{R}, \mathbb{C}}(d_i)$, respectively, which have an uncountable number of elements.

Therefore, a more sensible first attempt is to work with a finite field $\mathbb{F} = \mathbb{Z}_q$ for q prime. There, mathematicians established that the generating function for counting nonequivalent quiver representations for a symmetric quiver Q , with quiver matrix C is the q -series we obtained from the vortex partition function (2.1.30)

$$\boxed{P_C(x_1, \dots, x_m) \propto Z_V(x_1, \dots, x_m; k^{Eff}).} \quad (2.1.40)$$

Furthermore, the BPS particles exactly correspond to the number of nonequivalent quiver representations of C at dimension (d_1, \dots, d_m) . There in the context of quiver representation theory, $\Omega_{d_1, \dots, d_m; j}$ are known as *motivic Donaldson-Thomas invariants* (DT).

Finally, it were Knotsevich and Soibelman [36] who conjectured that for a given quiver representation there are finitely many equivalent classes. That translates to

the statement that for a given dimension vector (d_1, \dots, d_m) there are only finitely many values of j for which $\Omega_{d_1, \dots, d_m; j} \neq 0$. This crucial conjecture was later proven by Efimov [37] using all the power of Hall algebras.

To summarise, 3d \mathcal{N} theory is characterized via a set of effective Chern-Simons couplings $k_{ij}^{Eff} = C_{ij}$ which are in one-to-one correspondence with a symmetric quiver Q and BPS particles correspond to motivic DT invariants. The great advantage of this correspondence is the physical implication that there are only finitely many BPS particles of a given vortex number and spin.

2.1.8 Classical limit

Before moving to Chern-Simons theory and knot invariants, we bring our attention to the fact that the vortex partition function (2.1.40) has a singularity at $q = e^{\hbar} \xrightarrow{\hbar \rightarrow 0} 1$. This singularity arises from the q -Pochhammer in the denominator⁸. If we perform an asymptotic (WKB) expansion in powers of \hbar

$$\log P_C(x_1, \dots, x_m) \sim \sum_{k=-1}^{\infty} \hbar^k S_k(x_1, \dots, x_m), \quad (2.1.41)$$

where the leading (classical) term $S_{-1}(x_1, \dots, x_m)$ is computed from

$$\boxed{(-1)^{C_{ii}} x_i \prod_{j=1}^m z_j^{C_{ij}} + z_i = 1, \quad \log z_i = x_i \partial_{x_i} S_{-1}.} \quad (2.1.42)$$

The system of equations is known as *Nahm equations*⁹, since he derived them while studying 2d rational conformal field theories. In Nahms context though, he was considering $C_{ij} \in \mathbb{Q}$ and $x_i = q^{B_i}$, with $B_i \in \mathbb{Q}$.

This is a set of non-linear polynomial equations which in general have multiple solutions. Furthermore, a priori it is not even clear that a solution exists at all. Nevertheless, it was showed in [60] that these equations can be seen as a result of an optimization problem. Hence, by showing the function is convex, they were able to conclude that there is always a unique solution where $0 < z_i \leq 1$. They were considering the case where $x_i = 1$. However, this result generalizes straightforwardly to the x -dependent one. This because the x -dependent function is convex for $0 < x_i < \infty$.

It is also worth mentioning that there is always only one solution of these equations which is analytic at zero, with $z_i(x_1 = 0, \dots, x_m = 0) = 1$

$$z_i = \sum_{d_1, \dots, d_m=0}^{\infty} b_{d_1, \dots, d_m; i} x_1^{d_1} \dots x_m^{d_m} = \prod_{d_1, \dots, d_m=1}^{\infty} (1 - x_1^{d_1} \dots x_m^{d_m})^{-d_i \tilde{\Omega}_{d_1, \dots, d_m}}. \quad (2.1.43)$$

From its series expansion around $x_i = 0$ we can extract the *classical BPS particles*, or *numeric DT invariants*

$$\tilde{\Omega}_{d_1, \dots, d_m} = \sum_{j \in \mathbb{Z}} (-1)^j \Omega_{d_1, \dots, d_m; j}. \quad (2.1.44)$$

⁸Which in fact is singular at all roots of unity $q \rightarrow e^{i\pi k/l}$ for k, l coprime.

⁹Not to be confused with Nahm equations arising from monopole physics in gauge theories.

The condition $z_i(x_1 = 0, \dots, x_m = 0) = 1$ can be understood as a boundary condition arising from $P_C(x_1 = 0, \dots, x_m = 0) = 1$.

These set of equations appear in various contexts, Bethe ansatz of integrable spin chains, or in the case of the leading contribution of an ideal gas of particles with fractional spin statistics (fractons) [61, 62]. It was also conjectured that for the case where C_{ij} is associated with a knot, the equations (2.1.42) are related to the gluing equations for hyperbolic triangulations of the knot complement [59].

Another interesting appearance of those equations is their relation to algebraic K-theory. First, Zagier proved that for $m = 1$ there are only three values of $C = 0, 1/2, 1$ for which (2.1.40) becomes a modular form. Later, Nahm conjectured that the q -series becomes a modular form for certain C_{ij} and B_i such that the solution to his equations (2.1.42) is a torsion element of the Bloch group [63]. This conjecture was later proven by Garoufalidis [64]. However, it is not an if and only if statement, given that Vlashenko and Zwegers [60] were able to obtain modular forms for $m = 2$ whose z_i were not torsion elements of the Bloch group.

2.2 Chern-Simons theory in 3d

Chern-Simons theory plays a central role in the 3d $\mathcal{N} = 2$ theory, the SUSY theory contains a set of Chern-Simons couplings, so it is logical to start by properly introducing it.

A natural way to derive the Chern-Simons action from physical arguments, as presented in [65]. It is well known that in 4d electromagnetism (2.2.1)¹⁰ is the most general Abelian gauge invariant action. However, in 3d the situation is different, since it can be shown that the most general Abelian gauge invariant action is

$$S_{3dEM} = \int_{\mathbb{R}^{2,1}} d^3x \left(\frac{-1}{4e_0^2} F_{\mu\nu} F^{\mu\nu} + \frac{k}{4\pi} \epsilon^{\mu\nu\rho} A_\mu \partial_\nu A_\rho \right), \quad (2.2.1)$$

where the last term is known as the Abelian Chern-Simons term, k is a coupling constant and $\mu, \nu, \rho = 0, 1, 2$. Actually, this is not gauge invariant in full generality. After a gauge transformation, the action has an extra term which is a total derivative of the form

$$\frac{k}{4\pi} \int_{\mathbb{R}^{1,2}} d^3x \partial_\mu (\alpha \epsilon^{\mu\nu\rho} \partial_\nu A_\rho). \quad (2.2.2)$$

This means that the gauge invariance of Chern-Simons in general depends on the boundary conditions of A_μ on our manifold. In our case of interest, this term will vanish. For a more careful discussion, we encourage the reader to see Tong's lectures on gauge theory [7, Sec 8]. There he discusses what happens to (2.2.2) in the presence of magnetic flux, and how it imposes $k \in \mathbb{Z}$.

Surprisingly, the Chern-Simons term is not just gauge invariant but also invariant under arbitrary changes of coordinates. This is due to the fact that it is independent of the metric. This leads to the well-known topological invariance of Chern-Simons theory.

A natural generalization is to extend this result to non-Abelian gauge theories. Still we can go a bit further, we may ask, what is the most general non-Abelian

¹⁰Replacing $\mathbb{R}^{2,1} \rightarrow \mathbb{R}^{3,1}$ and $\mu, \nu = 0, 1, 2, 3$ in the action.

gauge theory in 3d that it is also metric independent? The answer turns out to be

$$S_{CS} = \frac{k}{4\pi} \int_M d^3x \text{Tr} \epsilon^{\mu\nu\rho} \left(A_\mu \partial_\nu A_\rho + i \frac{2}{3} A_\mu A_\nu A_\rho \right), \quad (2.2.3)$$

where $A_\mu = A_\mu^a T^a$ and T^a are Hermitian matrices generators of a compact simple Lie group G in the adjoint representation. Notice that now we are integrating over an arbitrary (real) compact oriented three-manifold M ; but from the (2.2.1) we started from $\mathbb{R}^{2,1}$ which is clearly a non-compact three-manifold, why the abrupt change? The argument is that, when we consider only the Chern-Simons term it is metric independent, so might as well consider \mathbb{R}^3 . Moreover, because this theory is well defined up to the point at infinity $\mathbb{R}^3 \cup \{\infty\}$ we may include it. This makes our three-manifold compact, $\mathbb{R}^3 \cup \{\infty\} \cong S^3$. From there, we might just take an arbitrary compact three-manifold.

As it stands, (2.2.3) is not fully gauge invariant. This because, as explained in [6, Chap 3], under a gauge transformation

$$A_\mu \rightarrow A_\mu^\Omega = \Omega^{-1} A_\mu \Omega - i \Omega^{-1} \partial_\mu \Omega, \quad (2.2.4)$$

with $\Omega \in SU(N)$ the action (2.2.3) is not invariant. Because it transforms as

$$S_{CS}[A_\mu^U] = S_{CS}[A_\mu] + 2\pi k \Gamma[\Omega], \quad (2.2.5)$$

where

$$\Gamma[\Omega] = \frac{1}{24\pi^2} \int_M d^3x \epsilon^{\mu\nu\rho} \text{Tr} (\Omega^{-1} \partial_\mu \Omega \Omega^{-1} \partial_\nu \Omega \Omega^{-1} \partial_\rho \Omega). \quad (2.2.6)$$

We can prove that this functional is invariant under smooth deformations of Ω . This implies that $\Gamma[\Omega]$ depends only on the homotopy class of Ω . When $G = SU(2)$ we know $\pi_3(SU(2)) \cong \mathbb{Z}$ and the value of $\Gamma[\Omega]$ is an integer¹¹. Classically, the term Γ does not affect the field equations of A_μ . Nevertheless, we want to quantize the theory using the path integral formalism.

$$Z(M) = \int [\mathcal{D}A_\mu] e^{i\hbar^{-1} S_{CS}[A_\mu]}. \quad (2.2.7)$$

There, $\Gamma[\Omega]$ will be an overall phase and in order to get rid of its contribution we need to impose that $k \in \mathbb{Z}$ ¹². In the case when $G = SU(N)$ the standard embedding of $SU(2)$ into $SU(N)$ suffice to conclude again that $k \in \mathbb{Z}$. That is why k is often referred to as the Chern-Simons level.

There is another subtlety we should discuss. The fact that the Chern-Simons action is metric independent is not enough to guarantee that the quantum theory will be topological. This because there might be anomalies coming from the measure \mathcal{A} that spoil the diffeomorphism invariance of the path integral (2.2.7). In the case of Chern-Simons, there is such an anomaly and it is called *framing anomaly* and makes (2.2.7) transform as

$$Z(M) \rightarrow \exp \left[\frac{\pi i c f}{12} \right] Z(M), \quad c = \frac{k d}{k + y}, \quad (2.2.8)$$

¹¹In fact, when $M = S^3$ we have $\Gamma[\Omega] = 1$.

¹²In the case of Chern-Simons we can absorb the \hbar^{-1} prefactor in the definition of k and we will omit it from now on.

where c is the central charge of the 2d Wess-Zumino-Witten theory with group G , f is the amount of framing, d is the dimension of G and y is the dual Coxeter number of G (where $G(N) = SU(N)$, then $y = N$) [5, Sec 2]. Atiyah then showed that framing is a choice of trivialization of the bundle $TM \oplus TM$. On top of that, he proved that different choices are parametrized by integers, implying that $f \in \mathbb{Z}$. Thus, the canonical choice is $f = 0$. From now on, we will always be working in canonical framing.

To summarize, Chern-Simons is a topological gauge theory. To preserve those symmetries in the quantum case

- (Non-Abelian) Gauge symmetry $\implies k \in \mathbb{Z}$.
- Diffeomorphism $\implies f \in \mathbb{Z}$ and canonically $f = 0$.

Now we pay attention to the observables of the theory. For these too, we demand that they preserve gauge and diffeomorphism invariance. Then the natural candidates are Wilson loop operators

$$W_R^C(A) = \text{Tr}_R U_C, \quad U_C = P \exp ie \oint_C A_\mu dx^\mu, \quad (2.2.9)$$

where e is the "charge" that we will set it equal to 1, U_C is the holonomy of A_μ around the oriented loop $C \subset M$ and P stands for the path-ordering, due to the non-Abelian nature of G . To compute the vacuum expectation value of (2.2.9) we insert it into the path integral

$$\langle W_R^C \rangle = \frac{1}{Z(M)} \int [\mathcal{D}A] W_R^C(A) e^{iS_{CS}} = P_R^K(a, q). \quad (2.2.10)$$

The amazing result is that when we choose $G = SU(N)$ (we will stick to this choice from now on) (2.2.10) can be written as a polynomial in the following variables

$$q = \exp\left(\frac{i\pi}{k+N}\right), \quad a = \exp\left(\frac{i\pi N}{k+N}\right), \quad (2.2.11)$$

where $P_R^K(a, q)$ is the colored HOMFLY-PT polynomial, colored ¹³ by the representation R . This because when (2.2.10) is in the fundamental representation, $P_\square^K(a, q)$ and the loop is a knot $C = \mathcal{K}$, then (up to different conventions of normalization) the resulting polynomial is the (uncolored) HOMFLY-PT polynomial of a knot [17, 18].

It is worth remembering that the representations R are labelled by their highest weight state, which in turn can be represented by a Young tableaux. In addition, we point out that just as the path integral has a framing anomaly, the knot invariants are uniquely defined (up to normalization by the unknot) and a choice of framing. Framing transformations act on colored HOMFLY-PT as an overall factor

$$P_R^K(a, q) \rightarrow a^{l(R)f} q^{\kappa_R f} P_R^K(a, q), \quad \kappa_R = l(R) + \sum_i (l_i^2(R) - 2il_i(R)), \quad (2.2.12)$$

where $l(R)$ is the number of boxes in the tableaux and $l_i(R)$ is the number of boxes in the i -th row.

¹³This is the standard name from gauge theories like QCD.

The fact that Chern-Simons is an exactly solvable theory means that we can compute the expectation values of Wilson loops (2.2.10) exactly. To perform that computation, we use the skein relations that will be introduced in the next subsection. In short, the skein relations provide an algorithmic method to compute (2.2.10) in a finite sequence of steps. Nevertheless, this sequence becomes increasingly harder and complex as one works with larger Young tableaux. Therefore, it is convenient to introduce a generating function which encodes the knot invariants for all values of the color. This is called the Ooguri-Vafa generating function [8]

$$\langle Z(U, V) \rangle = \left\langle \exp \left[\sum_{n=1}^{\infty} \frac{1}{n} \text{Tr} U^n \text{Tr} V^n \right] \right\rangle = \sum_R P_R^K(a, q) \text{Tr}_R V, \quad (2.2.13)$$

where $V = \exp \left[i \oint \tilde{A}_\mu dx^\mu \right] \in SU(\tilde{M})$ and it can be considered as an external source. To get the last equality we have used the Frobenius formula for characters of irreducible representations plus the fact that $\det U = \det V = 1$. Lastly, (2.2.13) makes sense when we consider $N \rightarrow \infty$ while keeping \tilde{M} finite but large.

We will be working with symmetric representations $R = S^r$ of $SU(N)$, which depend only on $r \in \mathbb{N}$, then (2.2.13) reduces to

$$P^K(x, a, q) = \sum_{r=0}^{\infty} \frac{x^r}{(q^2)_r} P_r^K(a, q), \quad (2.2.14)$$

where we set $\text{Tr}_r V \rightarrow x^r$ for $x \in \mathbb{C}$ and $(q^2)_r = (q^2; q^2)_r = \prod_{k=1}^r (1 - q^{2k})$ is the q -Pochhammer (a choice of normalization). Lastly, the first term $P_0^K(a, q) = 1$.

We can not emphasise enough the importance of the above generating function (2.2.14). Since, the knots-quivers correspondence is written as an identity between (2.1.40) and (2.2.14).

Before we go any further, we will explain in the next subsection how exactly are Wilson loops in Chern-Simons theory related to knot invariants.

2.2.1 Knot theory

Since Chern-Simons is a topological field theory, it is natural that its observables will be related to topological invariants of three-manifolds. In the case of knot theory, our three-manifold will be the three-sphere, $M = S^3$. Our observables, Wilson loops, may be any closed path (embedding) $\mathcal{K} : S^1 \rightarrow S^3$ up to homotopies. What do we mean by homotopies? In essence, smooth deformations of the loop S^1 without cutting it or taking it outside S^3 ¹⁴.

This is the mathematical definition of a knot \mathcal{K} . For us physicists, the most important fact is that all physical information of the observable depends only on the topology of the knot and can be written in terms of knot invariants.

There are three important families of knots we will be constantly referring to through out this work, the first is the *torus knots* $T_{m,l}$ this are a family of knots that can be embedded in the surface of a torus without self intersection. The parameters (m, l) are coprime integer numbers which count the number of times the knot is

¹⁴Of course, the proper mathematical definition are the three Reidemeister moves that relate equivalent knots [66].

wrapped around the meridian and the longitudinal axis of the torus. There is a natural one-parameter family of coprime pairs given by $(2, 2p + 1)$, with $p \in \mathbb{N}$. We show the first three elements of this family in figure 2.2.

The next two important one-parameter families of knots are called twist knots. They are easily obtained by repeatedly twisting a loop and then linking together its opposite ends. The first one $TK_{2,2|p|+2}$ for $-p \in \mathbb{N}$ whose first three elements are shown in figure 2.3¹⁵. The sign of p stands for the orientation of the twist. Then, the second family of twist knots is $TK_{2,2|p|+1}$ for $p \in \mathbb{N}$. We display the first three elements in figure 2.4.

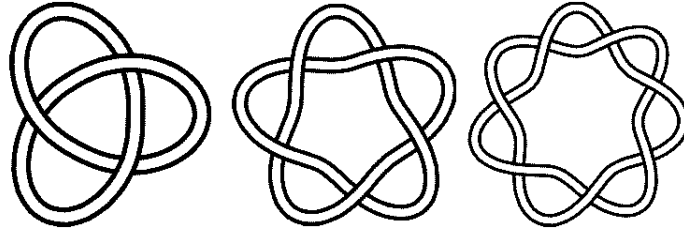


Figure 2.2: Torus knot diagrams $T_{2,2p+1}$ for $p = 1, 2, 3$, or $3_1, 5_1, 7_1$.

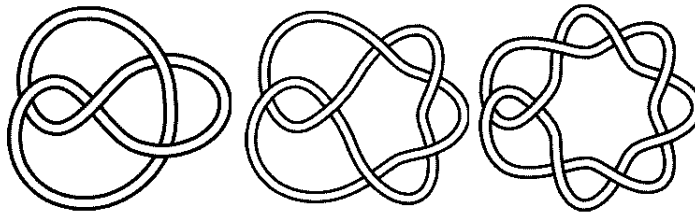


Figure 2.3: Twist knot diagrams $TK_{2,2|p|+2}$ for $p = -1, -2, -3$, or $4_1, 6_1, 8_1$.

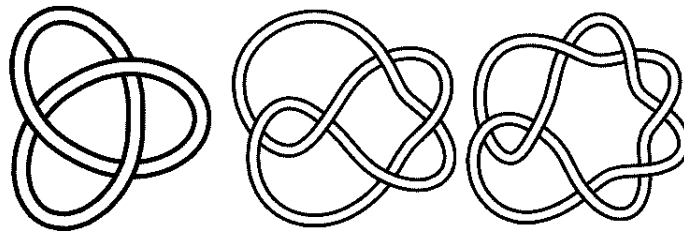


Figure 2.4: Twist knot diagrams $TK_{2,2|p|+1}$ for $p = 1, 2, 3$, or $3_1, 5_2, 7_2$.

There are several knot (homotopy) invariants which are used to distinguish, classify and study knots. The ones we will be using thought out in this thesis are *knot polynomials*. These are one, two or three variable polynomials which are uniquely assigned to each knot. Then, if two knots are equivalent they must have the same knot polynomial. However, the converse is not true and there are examples, like *mutant knots* which have the same knot polynomial, spite being different knots.

The knot polynomials we will be working with are *colored super polynomials*. But to build our way up to them, lets start with a set of simpler polynomials. The *Jones polynomial*, named after Fields medallist Vaughan Jones [16]. To compute

¹⁵All knot images are taken from the [Knot Atlas](#)

them from the knot diagram, first we should assign an orientation to it. With it we can implement the following two rules:

$$\text{Rule 1} \quad J(\bigcirc) = 1, \quad \text{or} \quad J(\bigcirc) = q + q^{-1}, \quad (2.2.15)$$

which is a normalization convention to which value we assign to the unknot 0_1 . The first choice is called the *reduced normalization* while the second goes by the name of *unreduced normalization*. The next rule is

$$\text{Rule 2} \quad q^2 J(L_+) - q^{-2} J(L_-) = (q - q^{-1}) J(L_0), \quad (2.2.16)$$

the famous *skein relation*. Here $L_{+,-,0}$ are as in figure 2.5. The skein means that we can resolve any crossing in our knot diagram, say L_+ and relate it to two other knot diagrams, one with L_- and other with no crossing or L_0 . This means that we can resolve one by one each crossing in our knot diagram, relate them to knots or links with fewer crossings. Eventually ending up with just a bunch of unknots.

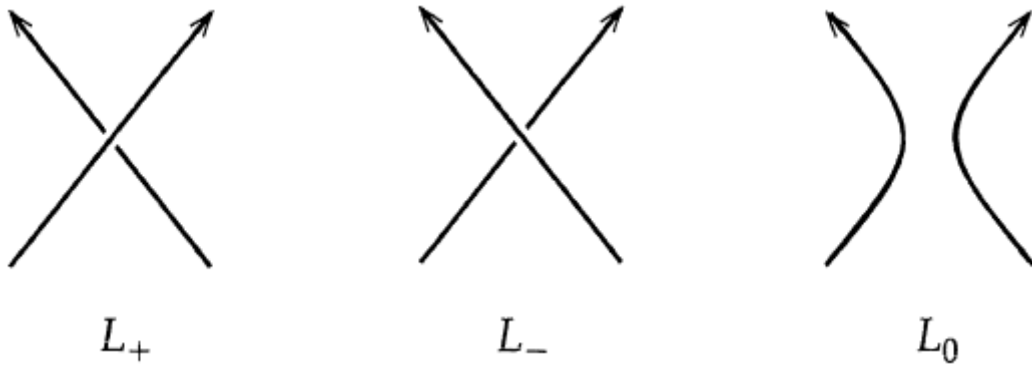


Figure 2.5: Three different types of crossings.

Four months after Jones announced his new knot polynomial, the HOMFLY-PT polynomial was announced

$$a P_{\square}(L_+) - a^{-1} P_{\square}(L_-) = (q - q^{-1}) P_{\square}(L_0), \quad (2.2.17)$$

with their respective normalization conditions

$$P_{\square}(\bigcirc) = 1, \quad \text{or} \quad P_{\square}(\bigcirc) = (a - a^{-1}) / (q - q^{-1}). \quad (2.2.18)$$

In the end, we can easily see that both skein relations (2.2.16) and (2.2.17) are homogeneous with respect to a rescaling of the polynomials. Thus, making normalizations just conventions. Still, for the rest of this work we will present our results in the reduced normalization. Also, from the HOMFLY-PT polynomial we can recover the Jones polynomial when $a = q^2$ ¹⁶.

There is an easy way to relate the uncolored HOMFLY-PT polynomial to the expectation value of the Wilson line operator (2.2.19), namely the following identity

$$W_{\square}^{\mathcal{K}} = P_{\square}^{\mathcal{K}}(a, q). \quad (2.2.19)$$

¹⁶There are several different conventions for these polynomials. For example, some authors replace $q \rightarrow q^{1/2}$, so we should keep it in mind when comparing with other formulas.

This means that Wilson loops in Chern-Simons theory also satisfy the skein relations (2.2.17) in their fundamental representation $R = \square$. In fact, there are analogous linear relations for the whole sequence of colored HOMFLY-PT, meaning for each R . We will not discuss them here, but refer the reader to Witten's original paper [15] or a more pedagogical and introductory review [28] in terms of R -matrices and braid groups.

Before moving on, it is crucial to discuss a powerful generalization of the Jones and HOMFLY-PT polynomials, the so called *Khovanov homology* [67–70]. This generalization is also commonly referred to *categorification* of the Jones polynomial. In very practical terms, the Jones polynomial of a knot often has minus signs in front of various coefficients. This is no surprise since the skein relation (2.2.16) includes them already. However, Khovanov noticed that there is a unique way to promote a Jones polynomial of a knot into a two-variable polynomial (q, t) with only positive coefficients

$$P^{\mathcal{K}}(q, t) = \sum_{i,j} q^i t^j \dim H_{i,j}(\mathcal{K}), \quad (2.2.20)$$

but most importantly, such that $J^{\mathcal{K}}(q, t)$ can be seen as the *Poincaré polynomial* of a chain complex and $t = -1$ reduces to the Jones polynomial.

This terminology is more familiar in the case of Riemann surfaces of genus g , Σ_g . It is well known that we can fully classify any Σ_g based on their *homology groups* $H_i(\Sigma_g)$, e.g. $H_0(\Sigma_g) = \mathbb{Z}$, $H_1(\Sigma_g) = \mathbb{Z}^{2g}$ and $H_2(\Sigma_g) = \mathbb{Z}$. Then, the Poincaré polynomial is

$$P^{\Sigma_g}(t) = t^0 \text{rank } H_1 + t^1 \text{rank } H_1 + t^2 \text{rank } H_2 = 1 + 2gt + t^2 \quad (2.2.21)$$

$$P^{\Sigma_g}(t = -1) = 2 - 2g = \chi(\Sigma_g) \quad (2.2.22)$$

where $\chi(\Sigma_g)$ is the Euler characteristic of Σ_g .

There are several *axioms* homologies of manifolds need to satisfy which are encoded as properties in the Poincaré polynomial. Khovanov noticed a systematic way to deduce those properties from a knot diagram using a *resolution cube*. We will not give more details about this procedure, simply mention that from this perspective Jones polynomial can be thought as the graded (one-variable polynomial) Euler characteristic of the knot.

As one would expect, there is an analogous categorification of the HOMFLY-PT polynomial. Whose formal definition is a mouthful of category theory [68], so our working definition will be a triply graded homology whose Poincaré polynomial is of the form

$$P_{\square}^{\mathcal{K}}(a, q, t) = \sum_{i,j,k} a^i q^j t^k \dim H_{i,j,k}(\mathcal{K}) = \sum_{i \in \mathcal{G}(\mathcal{K})} a^{a_i} q^{q_i} t^{t_i} \dim H_{a_i, q_i, t_i}(\mathcal{K}), \quad (2.2.23)$$

and its graded Euler characteristic $t = -1$ reduces to the HOMFLY-PT polynomial. On the r.h.s. $\mathcal{G}(\mathcal{K})$ is the set of non-vanishing coefficients, $\dim H_{a_i, q_i, t_i}(\mathcal{K}) \neq 0$ and we refer to the exponents (a_i, q_i, t_i) as the *generators of the knot homology*. We will refer to it as the *uncolored super polynomial*.

Last but not least, the colored super polynomial is not generally defined. However, in [19] they were able to compute it for a large class of knots. They accomplished it thanks to the constraints that the axioms of a homology imposed on the colored super polynomial. They also showed that in the case $t = -1$ it reduces to the colored HOMFLY-PT polynomial from (2.2.10).

2.2.2 From quantum to classical A-polynomials

There is yet another important knot, polynomial invariant, which naturally arises from colored Jones, HOMFLY-PT and super polynomials. Because the colored knot super polynomials are not independent from one another, we can derive recursion relations to compute the hold sequence of them based on the first few terms. As we did before, lets start with the Jones polynomial to illustrate the point.

Take the Jones polynomial colored by symmetric representations S^r of the group $SU(N)$, where r is the number of boxes, denoted by $J_r(q)$ ¹⁷. The theorem of Garoufalidis and Lê [24], states that there exists a linear operator $\widehat{A}(\widehat{M}, \widehat{L}, q)$ which is a polynomial in \widehat{M} , \widehat{L} and q such that

$$\widehat{A}(\widehat{M}, \widehat{L}, q) \cdot J_r(q) = \sum_{i,j,k} q^i \widehat{M}^j \widehat{L}^k \cdot J_r(q) = 0, \quad (2.2.24)$$

where \widehat{M} and \widehat{L} are linear operators with the following properties

$$\widehat{M}J_r(q) = q^r J_r(q), \quad \widehat{L}J_r(q) = J_{r+1}(q). \quad (2.2.25)$$

From the above properties, it is straight forward to deduce that \widehat{M} and \widehat{L} satisfy the following commutation relation $\widehat{M}\widehat{L} = q\widehat{L}\widehat{M}$.

Mathematically, this means that the colored Jones polynomial $J_r(q)$ is a *q-holonomic sequence* and the quantum A polynomial is the *q-shift linear operator* annihilating it¹⁸. What does that mean? The term *holonomic* comes from differential equations. A function $f(x)$ is said to be holonomic if there is a linear differential operator (ODE) of the form

$$\sum_i p_i(x) D_x^i f(x) = 0, \quad (2.2.26)$$

where D_x^i means the i -th derivative w.r.t x and $p_i(x)$ are polynomials.

An equivalent definition [71, Def 9.2.1] or [72, Chap 7] of a *holonomic sequence*. We say that $s(n)$ is a holonomic sequence, if there exists a linear shift operator such that

$$\sum_i p_i(n) s(n+i) = 0, \quad n \geq 0, \quad (2.2.27)$$

where again $p_i(n)$ are polynomials. We hope this clarifies the connection between holonomic functions/sequences and the colored Jones polynomial. All functions and sequences in this thesis are (q -)holonomic, so we will discuss their properties in more detail in chapter 4 where they form the basis of our results.

Moving on, (2.2.24) is sometimes called a Schroedinger-like equation, or more often *quantum curve* [27, 73, 74]. This because the linear operator \widehat{A} can be thought of as a quantum Hamiltonian which acts on the "wave function" $J_r(q)$ and annihilates it (sets it to zero). We might say that the eigenvalue is zero. Interestingly, just as an actual wave function we can perform a WKB expansion of (2.2.24) to study its asymptotics when $r \rightarrow \infty$ and $q \rightarrow 1$. To do that, we remind ourselves that from Chern-Simons the colored Jones polynomials arise from the identification of variables

¹⁷From now on we will omit the \mathcal{K} superscript since we know we are referring to knots.

¹⁸When it acts on the colored Jones polynomial it sets it to zero.

$q = \exp [i\pi/(k + N)]$ (see (2.2.11)). Then, we may perform the physicist favourite, the large N expansion. Or in our analogy with quantum mechanics $N \propto 1/\hbar$, with $q \xrightarrow{\hbar \rightarrow 0} 1$, that is

$$\log J_r(q) \xrightarrow{q \rightarrow 1} \sum_{k=-1}^{\infty} \hbar^k S_k(r), \quad (2.2.28)$$

where S_{-1} is the leading *classical term* and S_k with $k \geq 0$ are the quantum corrections. Using the form (2.2.28) and inserting it into (2.2.24) we obtain

$$\widehat{A}(\widehat{M}, \widehat{L}, q) \cdot J_r(q) = 0 \xrightarrow{q \rightarrow 1} A(m, l) = 0, \quad (2.2.29)$$

where $m, l \in \mathbb{C}^*$ and $A(m, l)$ is the *classical A polynomial* in m and l . The zero locus $A(m, l) = 0$ is a complex curve in $\mathbb{C}^* \times \mathbb{C}^*$. From one of the roots of $A(m, l)$ we can obtain the leading coefficient S_{-1} . In this way, we may think of the classical A-polynomial as a classical Hamiltonian just like in standard WKB analysis.

Actually, the classical A polynomial was introduced long before the quantum one. Originally, the classical A polynomial was defined directly from the topological data of the knot [25]. To see this, let's go back to our picture of the knot \mathcal{K} embedded in S^3 . Then, we can define the *tubular neighborhood* of the knot as the embedding $T^{\mathcal{K}} : \mathcal{K} \times D^2 \rightarrow S^3$, such that $f(x, 0) = x \forall x \in \mathbb{C}$ where D^2 is the two-dimensional disc. In practical terms, a tubular neighborhood is a solid torus whose core is \mathcal{K} .

We proceed to remove $T^{\mathcal{K}}$ from S^3 , the remaining manifold we call it the *knot complement* $S^3 \setminus T^{\mathcal{K}}$. Next we want to study its fundamental group $\pi_1(S^3 \setminus T^{\mathcal{K}})$, which in the case of the knot complement it is called the *knot group*. The only non-trivial cycles of $S^3 \setminus T^{\mathcal{K}}$ are those that wind up with the boundary $\partial(S^3 \setminus T^{\mathcal{K}})$. The knot group is usually a highly non-trivial group, a clever way to extract some information is to study its representations into a simpler and better understood $SL(2, \mathbb{C})$

$$\rho : \pi_1(\partial(S^3 \setminus T^{\mathcal{K}})) \rightarrow SL(2, \mathbb{C}). \quad (2.2.30)$$

We point out that, since the tubular neighborhood $T^{\mathcal{K}}$ has the topology of a solid torus T^2 , this implies that the topology of the boundary of the knot complement is also a torus $\partial(S^3 \setminus T^{\mathcal{K}}) \cong T^2$. It is well known that the generators of $\pi_1(T^2) = \mathbb{Z} \times \mathbb{Z}$ are the two basic cycles m along its meridian and l along its longitudinal. In the case of $\pi_1(\partial(S^3 \setminus T^{\mathcal{K}}))$ the cycle m is contractible in $S^3 \setminus T^{\mathcal{K}}$ while l is not. Due to the fact that m and l commute, that implies that $\rho(m)$ and $\rho(l)$ also commute. This implies that both can be simultaneously reduced to their Jordan form

$$\rho(m) = \begin{bmatrix} m & 1 \\ 0 & m^{-1} \end{bmatrix}, \quad \rho(l) = \begin{bmatrix} l & 1 \\ 0 & l^{-1} \end{bmatrix}, \quad (2.2.31)$$

where the bullet represents an irrelevant term in case the matrix is $\rho(m)$ or $\rho(l)$ is degenerate.

Thus, we have constructed the following map which assigns two complex variables to each representation of the knot group

$$\text{Hom}(\pi_1(M), SL(2, \mathbb{C}))/conj. \rightarrow (\mathbb{C}^* \times \mathbb{C}^*)/\mathbb{Z}_2 \quad (2.2.32)$$

$$\rho \mapsto (m, l), \quad (2.2.33)$$

where m and l are the eigenvalues of $\rho(m)$ and $\rho(l)$. The image of this map is the zero locus of the A polynomial of \mathcal{K} , $A(m, l) = 0$ ¹⁹. Lastly, the modulo \mathbb{Z}_2 arises from the identification $(m, l) \sim (m^{-1}, l^{-1})$, which in turn implies the property that A polynomials are *palindromic*

$$A(m^{-1}, l^{-1}) = m^\mu l^\lambda A(m, l), \quad (2.2.34)$$

for some $\mu, \lambda \in \mathbb{Z}$.

Our derivation of the A polynomial closely follows that of [75]. There the authors also elucidate an elegant interpretation of the A polynomial directly from Chern-Simons theory on a three-manifold M such that $\partial M = \Sigma_g$. Here we just present the general idea in a nutshell and encourage the interested reader to the previous reference.

The *moduli space of solutions* (symplectic phase space) to the E-L equations of the Chern-Simons action (2.2.3)

$$\epsilon^{\mu\nu\rho} (\partial_\mu A_\nu + A_\mu A_\nu) = 0, \quad (2.2.35)$$

are the flat gauge connections on M , with gauge group G , $\mathcal{M}_{flat}(M, G)$. In $\mathcal{M}_{flat}(M, G)$ there is a natural reduction to $\mathcal{M}_{flat}(\Sigma_g, G)$ by restricting to the boundary $\partial M = \Sigma_g$. There we can find that the space $\mathcal{L}_{flat} \subset \mathcal{M}_{flat}(\Sigma_g, G)$ of flat connections on Σ_G that extend to M forms a *Lagrangian submanifold*. That is given, the Atiyah-Bott symplectic form [76]

$$\omega = \frac{1}{4\pi^2} \int_{\Sigma_g} \text{Tr} \delta A \wedge \delta A, \quad (2.2.36)$$

where δ denotes the exterior derivative on \mathcal{M} and δA is a 1-form on Σ along with \mathcal{M} , then

$$\omega|_{\mathcal{L} \subset \mathcal{M}} = 0. \quad (2.2.37)$$

The Lagrangian submanifold \mathcal{L}_{flat} can be thought as a constraint on the classical phase space $\mathcal{M}_{flat}(M, G)$ ²⁰

$$\tilde{A} = 0. \quad (2.2.38)$$

In particular, when $M = S^3/T^\mathcal{K}$ and $G = SL(2, \mathbb{C})$ the above equation yields the classical A polynomial as in (2.2.29).

2.2.3 Deforming the A-polynomial

Just as the Jones polynomial can be generalized to the HOMFLY-PT polynomial, or to the Khovanov polynomial and superpolynomial, there are corresponding generalizations to the A polynomial. First generalization of the quantum A polynomial for colored HOMFLY-PT colored under symmetric representations was proven in [77]. Namely,

$$\hat{A}(\hat{M}, \hat{L}, a, q) \cdot P_r(a, q) = 0, \quad (2.2.39)$$

where the operators act analogously as in the colored Jones (2.2.25), with the added fact that now \hat{A} is also a polynomial in a . However, the explicit form for such a

¹⁹It is defined up to an overall constant which does not affect its zero locus.

²⁰The tilde in (2.2.38) is just to distinguish it from A the gauge connection.

quantum A polynomial were already performed in [78, 79] three years earlier. There they exploited Zeilberger's algorithm for q -holonomic sequences.

In spite of not having a rigorous mathematical definition, from the insights of topological string theory and its relation to knot homologies, the authors conjecture the existence of a *quantum/classical super A polynomial* [27]. Which basically the t -deformation of (2.2.39).

Finally, the actual form of the A polynomial we will be working is its *dual*. By dual we mean the quantum A polynomial of the generating function (2.2.14)

$$\boxed{P^{-1}(x, a, q) \widehat{A}_{dual}(\widehat{x}, \widehat{y}, a, q) \cdot P(x, a, q) = 0 \xrightarrow{q \rightarrow 1} A_{dual}(x, y, a, t) = 0,} \quad (2.2.40)$$

where \widehat{x} and \widehat{y} satisfy the commutation relation $\widehat{y}\widehat{x} = q\widehat{x}\widehat{y}$. Were we can easily translate from the quantum super A polynomial by finding how \widehat{M} and \widehat{L} relate to \widehat{x} and \widehat{y}

$$\sum_{r=0}^{\infty} \frac{x^r}{(q^2)_r} \widehat{M} \cdot P_r = \sum_{r=0}^{\infty} \frac{(qx)^r}{(q^2)_r} P_r = \widehat{y} \cdot \sum_{r=0}^{\infty} \frac{x^r}{(q^2)_r} P_r, \quad (2.2.41)$$

and

$$\sum_{r=0}^{\infty} \frac{x^r}{(q^2)_r} \widehat{L} \cdot P_r = \sum_{s=1}^{\infty} \frac{x^{s-1}}{(q^2)_{s-1}} P_s = \widehat{x}^{-1}(1 - \widehat{y}^2) \cdot \sum_{r=0}^{\infty} \frac{x^r}{(q^2)_r} P_r, \quad (2.2.42)$$

where we have defined $s = r + 1$ and we used $(q^2)_r = (1 - q^{2r})(q^2)_{r-1}$.

Thus the dual quantum/classical super A polynomial is related to the super A polynomial as

$$\boxed{\sum_{r=0}^{\infty} \frac{x^r}{(q^2)_r} \widehat{A}(\widehat{M}, \widehat{L}, a, q) \cdot P_r(x, a, q) = \widehat{A}(\widehat{y}, \widehat{x}^{-1}(1 - \widehat{y}^2), a, q) \cdot P(x, a, q),} \quad (2.2.43)$$

keeping in mind that because \widehat{x} and \widehat{y} when we normal order them there will be several q -prefactors due to their commutation relations.

2.3 Knots-quivers correspondence

Finally, we are in a position to address one of the main topics of this thesis, the *knots-quivers correspondence*. It is a modern topic of active research and which has attracted attention both from physicists and mathematicians interested in topological string theory and knot theory. It has yielded a few quite non-trivial results such as the explicit q -series conjectured for the vortex partition function (2.1.40), a proof of the integrality of LMOV invariants for several infinite families of knots [31] and the interpretation of BPS/DT invariants as counting holomorphic discs on Calabi-Yau threefolds [38].

The simple statement of the correspondence is the equality between the quiver generating series (2.1.30) and the generating series of colored superpolynomials (2.2.14) upon certain identification of variables

$$\boxed{P_C(x_1 = a^{a_1} q^{q_1 - C_{1,1}} (-t)^{t_1} x, \dots, x_m = a^{a_m} q^{q_m - C_{m,m}} (-t)^{t_m} x) = P^K(x, a, q, t),} \quad (2.3.1)$$

for an appropriate choice of quiver matrix C_{ij} , along with the specialization $x_i = a^{a_i} q^{q_i - C_{ii}} (-t)^{t_i} x$ and $t_i = C_{ii}$. This identification of variables is called *knot change of variables*. As a short hand notation, we will use

$$\boxed{x_i = \lambda_i x, \quad \lambda_i = a^{a_i} q^{q_i - C_{ii}} (-t)^{t_i}.} \quad (2.3.2)$$

To make it clearer for the reader, in chapter 3 we will present various examples of how to derive a quiver starting from the generating series of colored HOMFLY-PT polynomials (2.2.14) ²¹.

Moreover, in chapter 3, we will also show that the choice of quiver matrix C_{ij} is not unique. We will then study the symmetry transformations relating a large family of C_{ij} that lead to the same $P_{\mathcal{K}}$.

The state-of-the-art of the knot-quivers correspondence is that it has been proven to hold for all *arborescent knots*, also named 2-tangles²² [80, 81]. They accomplished it by constructing a quiver out of algebraic tangles.

The reason why this correspondence has been proven only for arborescent knots so far is because the colored superpolynomials of arborescent knots enjoy two important properties. The first one is the *exponential growth hypothesis*

$$P_{S^r}^{\mathcal{K}}(a, q = 1, t) = [P_{\square}^{\mathcal{K}}(a, q = 1, t)]^r, \quad (2.3.3)$$

which means that the (a_i, t_i) homology generators for the colored superpolynomials are completely defined by the uncolored polynomial. This is a crucial property that allows to compute the superpolynomials for a large class of knots, in spite not having a precise definition of HOMFLY-PT homology.

The second property is that arborescent knots are *thin knots* [82]. The thinness or thickness of a knot, is defined in terms of the δ -grading

$$\delta_i = 2a_i + q_i - t_i, \quad (2.3.4)$$

where (a_i, q_i, t_i) are the homological degrees (2.2.23). A knot that satisfies $\delta_i = \delta = \text{const.}$ is said to be thin, if not it is thick.

Of the 165 prime knots with up to ten crossings, only 12 are thick, see [82, (49)] for a complete list. The only thick two knots with less than ten crossings are 8_{19} and 9_{42} , which are depicted in figure 2.6. The knots-quivers correspondence is still unproven for thick knots and is at the forefront of ongoing research.²³ Next we will explain the string theory origin of this duality.

2.3.1 Non-Abelian Chern-Simons and the deformed conifold

Back in the 70's 't Hooft had proposed that the Feynman diagram expansion of non-Abelian gauge theories could be rewritten in terms of a string theory amplitude. The way to realize this is by writing the free energy genus expansion

$$F(g, N) = \sum_{g=0}^{\infty} \sum_{h=1}^{\infty} F_{g,h} g_s^{2g+h-2} N^{-h}, \quad (2.3.5)$$

²¹There is also a version of the knots-quivers correspondence with a more general change of variables than (2.3.2). Namely, $x_i = \lambda_i x^{n_i}$, for $n_i \in \mathbb{N}$. The interested reader may consult [38]

²²We do not explain the concept of a tangle since it is not needed for this thesis.

²³While typing this thesis, we became aware of unpublished computations by M. Stosić, where he claims to obtain an explicit quiver matrix C for the knot 8_{19} .

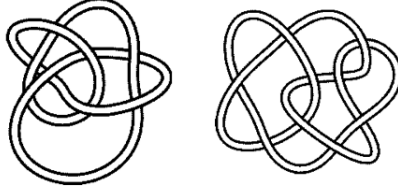


Figure 2.6: 8_{19} (left) 9_{42} (right).

where g is the coupling constant of the gauge group and N is the rank of the gauge group, which in our case it will be $SU(N)$.

However, we can think of (2.3.5) as an open string theory amplitude, where we sum over all topologies of the string worldsheet $\Sigma_{g,h}$. Then, g_s is interpreted as a string coupling constant and N^h are the Chan-Paton factors associated with the boundary of the open string. Finally, $F_{g,h}$ are the string theory amplitudes on $\Sigma_{g,h}$.

This leads to the idea that we can start with a topological string theory (UV) and its low energy (IR) limit, after compactification, the resulting effective theory is simply a non-Abelian gauge theory. We will construct our Chern-Simons theory following the pedagogical line of thought of Mariño [5, Sec 8], for the original derivation see [8].

Let us start from the following string configuration, we have a eleven-dimensional space

$$\begin{aligned}
 \text{space-time : } & S^1 \times \mathbb{R}^4 \times (CY_3 = T^*S^3) \\
 & \cup \\
 N \text{ M5-branes wrapping : } & S^1 \times \mathbb{R}^2 \times S^3 \\
 M \text{ M5'-branes (probes) wrapping : } & S^1 \times \mathbb{R}^2 \times L_{\mathcal{K}},
 \end{aligned} \tag{2.3.6}$$

where $L_{\mathcal{K}}$ is the knot conormal (which we will define in a moment), by probe we mean that they are non-dynamical objects (background geometry), T^*S^3 is also known as the *deformed conifold*. We can easily define the deformed conifold in terms of its embedding coordinates in $(\eta_1, \eta_2, \eta_3, \eta_4) \in \mathbb{C}^4$

$$\sum_{i=1}^4 \eta_i^2 = r, \tag{2.3.7}$$

where $r \in \mathbb{R}^*$. By rewriting the complex variables in terms of real ones $\eta_j = x_j + iy_j$ we obtain the two equations for the real coordinates

$$\sum_{i=1}^4 (x_i - y_i) = r, \quad \sum_{i=1}^4 x_i y_i = 0, \tag{2.3.8}$$

where the first equation defines S^3 of radius \sqrt{r} upon setting $y_i = 0$ and the second equation defines the coordinates of the cotangent bundle at the point x_i . This leads to the topology of T^*S^3 . It is a symplectic manifold w.r.t. the canonical symplectic form

$$\omega(q, p) = \sum_{i=1}^3 dq_i \wedge dp_i, \tag{2.3.9}$$

where $q_i \in S^3$ is a coordinate patch and p_i are coordinates on the cotangent bundle around q_i . Next, we can construct a complex structure which is compatible with

the symplectic form, thus promoting it to a Kähler manifold. Lastly, because the Ricci curvature of both exactly cancel each other this manifold ends up being a Calabi-Yau three-fold, CY_3 .

To proceed, we need to find a Lagrangian submanifold of T^*S^3 that gives boundary conditions for the ends of the string. A Lagrangian submanifold is a half-dimensional submanifold on which the canonical symplectic form (2.3.9) vanishes identically.

The natural candidate for a Lagrangian submanifold in the presence of a knot is called the *knot conormal* $L_{\mathcal{K}}$. Lets parametrize the knot inside S^3 as a curve $q_i(s)$ with $s \in [0, 2\pi]$ and $q_i(0) = q_i(2\pi)$

$$L_{\mathcal{K}} = \left\{ (q(s), p) \in T^*S^3|_{\mathcal{K}} \left| \sum_{i=1}^3 p_i \frac{dq_i(s)}{ds} = 0 \right. \right\}. \quad (2.3.10)$$

The knot conormal $L_{\mathcal{K}}$ has a simple geometric interpretation, namely as a set of planes which are perpendicular to the tangent vector of the knot at every point. Hence, its topology is $S^1 \times \mathbb{R}^2$.

Given that we have two stacks of branes, this configuration allows for three types of strings which can end on these branes:

1. Strings with both ends on the N M5-branes are described by a $A \in su(N)$ Chern-Simons theory on S^3 .
2. Strings with both ends on the M M5'-branes, which are described by a $\tilde{A} \in su(M)$ Chern-Simons action on $L_{\mathcal{K}}$.
3. Strings with one end on an N M5-brane and another end on an M M5'-brane $\mathcal{A}(q(s)) = \phi(q(s)) + \chi\xi(q(s))$.

where ϕ is a scalar field in its bifundamental representation (N, \bar{M}) and χ is a Grassman field. The fact that they are evaluated only at the knot \mathcal{K} is because the third type of strings have to be constant and with endpoints at different branes N and M . The only possibility for the strings to satisfy both conditions is if they lie on the intersection $S^3 \cap L_{\mathcal{K}} = \mathcal{K}$. In other words, the third type of strings lie along the knot itself.

The action for the strings that stretch across branes is

$$S_{scalar} = \oint_{\mathcal{K}} \text{Tr} \left(\bar{\phi} d\phi + \bar{\phi} A \phi - \phi \tilde{A} \bar{\phi} \right), \quad (2.3.11)$$

where, after integrating out ϕ and $\bar{\phi}$ we obtain the functional determinant

$$S_{scalar}^{eff} = -\log \det \left(\frac{d}{ds} + \sum_{i=1}^3 (A_i - \tilde{A}_i) \frac{dq_i(s)}{ds} \right) = \sum_{n=1}^{\infty} \frac{1}{n} \text{Tr} U^n \text{Tr} V^{-n}, \quad (2.3.12)$$

where U and V are the holonomies of A and \tilde{A} around the knot \mathcal{K} , as in (2.2.9). Lo and behold, out of the M probe branes we obtained the Ooguri-Vafa operator (2.2.13), where the \tilde{A} can be seen as an external source for the action

$$S_{CS}(A) + S_{scalar}^{eff} = S_{CS}(A) + \sum_{n=1}^{\infty} \frac{1}{n} \text{Tr} U^n \text{Tr} V^{-n} \implies F_{TopString}(V) = F_{CS}(V). \quad (2.3.13)$$

This is a way to find an topological open string theory interpretation of Chern-Simons theory. In the upcoming subsection, we will find a dual closed string amplitude on the resolved conifold that leads to the interpretation of knot invariants (2.2.13) as Gromov-Witten invariants, or BPS states of a 3d $\mathcal{N} = 2$ theory (2.1.34). There is where the quiver takes a geometric interpretation [38].

2.3.2 Geometric transition

Based on the genus expansion (2.3.5) we can formally resum the series by introducing the 't Hooft parameter $t = g_s N$ and obtain

$$F(g_s, t) = \sum_{g=0}^{\infty} g_s^{2g-2} F_g(t), \quad F_g(t) = \sum_{n=1}^{\infty} F_{g,h} t^h, \quad (2.3.14)$$

where $F(g_s, t)$ can now be interpreted as a closed topological string amplitude. This is known as the *open/closed string duality*. To find explicitly the closed string theory dual is a non-trivial task, which is performed on a case-by-case basis. The most famous example of this open/closed duality is AdS/CFT. It is worth mentioning that we are actually constructing a more general version of the open/closed duality. This because the open/closed duality interpretation holds for the pure Chern-Simons theory, without knots or probe branes.

Having clarified that, on the open string side we have D-branes where the ends of the string are attached. These D-branes do not appear on the closed string side after resummation. However, the effect of the D-branes is to deform the background geometry, and so the resummation can be understood as a *geometric transition*.

The geometric transition occurs when we shrink S^3 to zero, $r = 0$ in (2.3.8). This produces the *conifold singularity*. There are two standard methods to avoid a singularity, one is to deform the complex parameters, which leads to the deformed conifold. An alternative method is to perform a blow-up to resolve the singularity, which leads to the *resolved conifold*.

The resolved conifold can be defined by the algebraic equation

$$|z_1|^2 + |z_4|^2 - |z_2|^2 - |z_3|^2 = a, \quad (2.3.15)$$

where if we take $z_2 = z_3 = 0$ on the above, then we can think of z_1, z_4 as coordinates on the base \mathbb{P}^1 . This also leads to consider z_2, z_3 as coordinates of the fibers. In other words, $X = \mathcal{O}(-1) \times \mathcal{O}(-1) \rightarrow \mathbb{P}^1$.

To deduce the appearance of the resolved conifold from the conifold singularity, (2.3.7) with $r = 0$, we can perform the change of variables $2\eta_1 = x + y$, $2i\eta_2 = x - y$, $2i\eta_3 = u + v$ and $2\eta_4 = v - u$ to obtain

$$xy = uv. \quad (2.3.16)$$

Here we can notice that a general solution of the above equation is

$$x = \lambda v, \quad u = \lambda y, \quad (2.3.17)$$

with λ the inhomogenous coordinate in \mathbb{P}^1 . Then, we can reinterpret (v, y) and (x, u) as the north and south coordinates charts for the bundle $\mathcal{O}(-1) \times \mathcal{O}(-1)$ on \mathbb{P}^1 . We can further change variables $x = z_1 z_3$, $y = z_2 z_4$, $u = z_1 z_2$ and $v = z_3 z_4$.

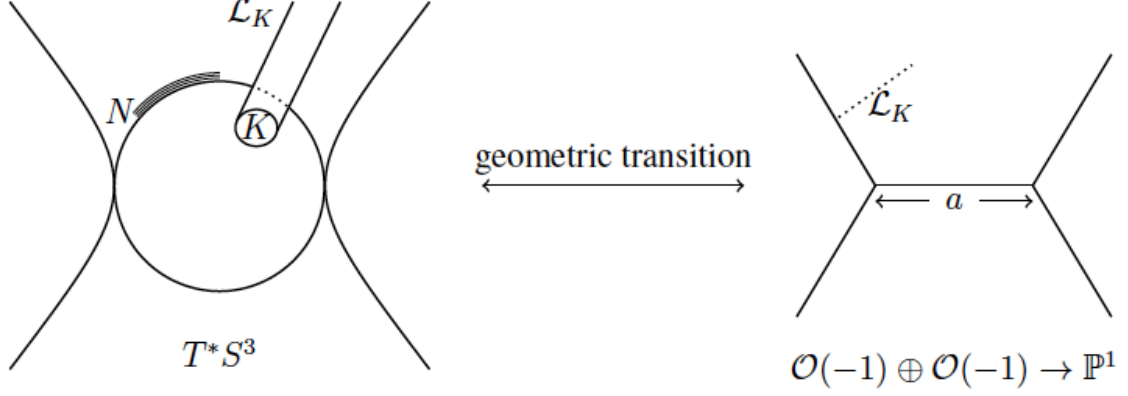


Figure 2.7: Schematic illustration of the geometric transition. Source [83]

Substituting them in (2.3.17) we get $\lambda = z_1/z_4$, which in deed is the inhomogenous coordinate for $|z_1|^2 + |z_4|^2 = a$. Thus, we deduced the *conifold transition*, from the deformed conifold to the resolved one, as seen in figure 2.7.

In our case, the N M5-branes wrapping S^3 turn into the flux supported on \mathbb{P}^1 and their volume is encoded in the Kähler parameter a . Whereas, the M M5-branes that serve as a probe, are still present and wrapping a Lagrangian submanifold $C_{\mathcal{K}}$ of X associated with the knot. The open strings that end on the M M5'-branes, turn into M2-branes intersecting the M M5'-branes. The table 2.1 summarises the whole M theory setup.

Geometry	Geometric transition	
	Deformed conifold	Resolved conifold
Space-time	$S^1 \times \mathbb{R}^4 \times T^*S^3$	$S^1 \times \mathbb{R}^4 \times X$
N M5-branes	$S^1 \times \mathbb{R}^2 \times S^3$	$S^1 \times \mathbb{R}^2 \times \mathbb{P}^1$
M M5-branes	$S^1 \times \mathbb{R}^2 \times L_{\mathcal{K}}$	$S^1 \times \mathbb{R}^2 \times L_{\mathcal{K}}$
M2-branes	Disc with boundary on $M \cap N$	Disc with boundary on $L_{\mathcal{K}}$
Low-energy theory	Chern-Simons on S^3	3d $\mathcal{N} = 2$ SUSY
Observables	Knot invariants	BPS particles (quivers)

Table 2.1: M-theory setup

Finally, the BPS states arise from the M2-branes wrapping a 2-cycle $\beta \in H(X, L_{\mathcal{K}})$ and ending on the M5'-branes. Since, the M2-branes are light, in the effective theory they can be approximated as point particles propagating on $\mathbb{R}^2 \times S^1$. The BPS states are labeled by two 3d spins $(2j, 2i) \in \mathbb{Z}^2$ and a representation R of the gauge group $SU(M)$.

All-in-all, the string theory amplitudes take the form

$$F = \sum_{g=0}^{\infty} \sum_{h=1}^{\infty} F_{g,h} g_s^{2g+h-2} = \sum_{n=1}^{\infty} \frac{1}{n} \frac{N_{R,i,j} a^{ni} q^{nj}}{q - q^{-1}} \text{Tr}_R V^n = \log \sum_R P_R^{\mathcal{K}}(a, q) \text{Tr}_R V, \quad (2.3.18)$$

where $q = e^{g_s}$, a is the radius of \mathbb{P}^1 in the resolved conifold and $N_{R,i,j}$ is the number of BPS particles with spins (i, j) . This are also referred to as the Labastida-

Mariño-Ooguri-Vafa invariants. The r.h.s of the above equation is the Ooguri-Vafa generating function for colored HOMFLY-PT polynomials (2.2.13).

In summary, Chern-Simons in S^3 (on the deformed conifold side) produces knot invariants, whereas from 3d $\mathcal{N} = 2$ theory (on the resolved conifold side) yields the quiver description. This is the M-theory origin of the knots-quivers correspondence.

We expect this review has been clear and enlightening for the reader and that it sets the stage for where our results will be presented. We will provide explicit examples of the knots-quivers correspondence, quiver A-polynomials and so on. We hope this enables the reader to fully appreciate the broad scope of dualities our results contribute to.

Chapter 3

Knot symmetries and permutohedra

The aim of this chapter is to carefully study the relation between knots and quivers and its implications for 3d $\mathcal{N} = 2$ theory. We begin by explaining how quiver series are invariant under an operation called unlinking. In a few words, this operation erases an arrow between nodes of the quiver, in exchange for adding an extra node. This operation will allow us to prove the local equivalence theorem. The main implication of this theorem is that, under certain conditions, there could be multiple distinct quivers yielding the same quiver series. All these quivers will be considered equivalent, and are related under a transposition of off-diagonal elements of their respective quiver matrices.

We will show, that the quivers associated to knots satisfy the conditions of the local equivalence theorem. Then, we will explore the set of all equivalent quivers that can be assign to the same knot. We can also interpret this as a web of dualities between different couplings of the 3d $\mathcal{N} = 2$ SUSY gauge theory.

As we will see, the number of equivalent quivers grows pretty rapidly even for simple knots. So, we represent the set of equivalent quivers as a graph, where every equivalent quiver is a node, and edges are transpositions relating them. As it turns out, these graphs can be built out of simpler graphs known as permutohedra. We will carefully explain what a permutohedron is and why they arise in the set of equivalent quivers.

We will summarise our results in table 3.1, where we list the number of equivalent quivers associated to a given knot. Then, we conjecture that such equivalent classes of quivers exist for any knot. These results are also published in [42].

3.1 On the uniqueness of the knots-quivers correspondence

As we argue in section 2.3, we can associate a quiver to a knot, based on the equality of their generating functions (2.3.1). It was noticed already in the initial knots-quivers correspondence paper [31] that for certain knots, two or more quiver matrices, of the same size, could be assigned to the same knot. Moreover, they found that we can always enlarge the quiver matrix with two extra rows and columns with appropriately chosen entries, which yields the same quiver series.

Furthermore, in [39] the authors discovered yet another operation which allows to increase the size of the quiver matrix and still have the same quiver series (2.1.40).

They named this operation *unlinking*, since it erases one arrow between quiver nodes. We will discuss unlinking more carefully, in 3.1.1. For now, it suffices to mention that unlinking allows to add an extra row and column to the quiver matrix. The entries of these extra row and column are fixed by the values of the starting quiver matrix. In fact, this operation is defined for any quiver, so in particular applies to those associated to knots.

Lastly, for most quivers and in particular those associated with knots, we can perform the operation of unlinking an infinite number of times. This means that we can associate an infinite number of distinct quivers to the same knot. This naturally leads to the following questions for quivers associated with knots:

1. Is there minimum size of a quiver associated to a given knot?
2. Is the quiver of minimum size unique? If not how many quivers of minimum size are there, are there finite or infinite?
3. If there are multiple quivers of minimum size, is there a transformation relating them?

In this chapter, we will provide the answer to these questions and present the amazing results they lead to. As we will see, apart from the unknot 0_1 and the trefoil 3_1 in 2.2, all examples of knots that we consider in the reduced normalization have a multiple quivers associated to the same knot ¹.

The answer to the first question is straightforward. Take the Poincare polynomial of a knot (2.2.23), $P_1^{\mathcal{K}}(a, q, t)$, and compare it with the first-order term of the quiver series (2.1.40)

$$\sum_{i \in \mathcal{G}(\mathcal{K})} \frac{a^{a_i} q^{q_i} t^{t_i} x}{(q^2)_1} \dim H_{a_i, q_i, t_i}(\mathcal{K}) = \sum_{i=1}^m (-q)^{C_{ii}} \frac{a^{a_i} q^{q_i - C_{ii}} (-t)^{C_{ii}} x}{(q^2)_1} \quad (3.1.1)$$

From the above equation, we can conclude that $m = \#(\mathcal{G}(\mathcal{K}))$. Thus, the minimum size of the quiver is the number of generators of the knot homology, or monomials of the Poincare polynomial. We will refer to the quivers Q of size $\#(\mathcal{G}(\mathcal{K}))$ as *minimal quivers*.

3.1.1 Unliking

Lets start from a symmetric quiver Q of size m with a quiver matrix C . We chose a pair of nodes $a, b \in Q$ which have at least one arrow between, $C_{ab} = C_{ba} \neq 0$. Then, we can add a new node n to the quiver $\tilde{Q} = Q \cup n$. The entries of the enlarged quiver matrix \tilde{C} are

$$\begin{aligned} \tilde{C}_{ab} &= C_{ab} - 1, & \tilde{C}_{nn} &= C_{aa} + 2C_{ab} + C_{bb} - 1, \\ \tilde{C}_{in} &= C_{ai} + C_{bi} - \delta_{ai} - \delta_{bi}, & \tilde{C}_{ij} &= C_{ij} \quad \text{for all other cases,} \end{aligned} \quad (3.1.2)$$

where δ_{ij} is the Kronecker delta.

¹In case of the unreduced normalization the trefoil knot 3_1 also has multiple quivers associated to it. We concentrate on the multiplicity of quivers for the reduced normalization, since in the unreduced normalization the question of the number of quivers associated to the same knot is much more involved and we leave for future research.

Then, it was proven in [39] that upon setting $x_n = q^{-1}x_ax_b$, the quiver generating series of Q and \tilde{Q} are the same

$$\boxed{P_C(x_1, \dots, x_m) = P_{\tilde{C}}(x_1, \dots, x_m, x_n = q^{-1}x_ax_b)}. \quad (3.1.3)$$

The simplest example of unlinking is

$$C = \begin{bmatrix} C_{aa} & C_{ab} \\ C_{ba} & C_{bb} \end{bmatrix} = \begin{bmatrix} 0 & 1 \\ 1 & 0 \end{bmatrix} \quad \longrightarrow \quad \tilde{C} = \begin{bmatrix} \tilde{C}_{aa} & \tilde{C}_{ab} & \tilde{C}_{an} \\ \tilde{C}_{ba} & \tilde{C}_{bb} & \tilde{C}_{bn} \\ \tilde{C}_{na} & \tilde{C}_{nb} & \tilde{C}_{nn} \end{bmatrix} = \begin{bmatrix} 0 & 0 & 0 \\ 0 & 0 & 0 \\ 0 & 0 & 1 \end{bmatrix}. \quad (3.1.4)$$

The origin of the name unlinking for this operation comes from its topological string theory interpretation. We may think of the BPS spectrum of 3d $\mathcal{N} = 2$ theory, as Gromov-Witten invariants for the open topological string. These geometric invariants count holomorphic curves inside a Calabi-Yau three-fold with boundary on the Lagrangian $L_{\mathcal{K}}$ (2.3.10).

In that context, each quiver node can be associated to a holomorphic curve and the quiver arrows to links between the curves. Hence, the quiver matrix C can be interpreted as the *linking matrix* of the holomorphic curves. Given that we can preform the unlinking operation C_{ab} times on the nodes a and b , this completely unlinks the two curves a and b . The deep physical meaning of this quite simple operation is a duality between two distinct values of the couplings of the 3d $\mathcal{N} = 2$ theory.

3.2 Local equivalence of quivers

In the previous subsection 3.1.1, we argued that it is possible to have two distinct quivers with the same quiver generating series (3.1.3). This general property of quiver generating series also applies to quivers associated with knots. Nevertheless, the quivers we obtain from unlinking (3.1.3) lead to larger quiver matrices. In other words, the quivers obtained from unlinking are not the minimal quivers we can associate to a knot.

Now we will focus our attention on finding distinct quivers of the same size, which produce the same quiver series (2.1.40). We will say that two distinct minimal quiver matrices C and C' are *equivalent*, if their quiver series (2.1.40) are equal after the knot change of variables (2.3.2)

$$P^{\mathcal{K}}(a, q, t, x) = P_C(x_1 = \lambda_1 x, \dots, x_m = \lambda_m x) = P_{C'}(x_1 = \lambda'_1 x, \dots, x_m = \lambda'_m x) \quad (3.2.1)$$

where $\lambda_i = \lambda'_i = a^{a_i} q^{q_i} t^{t_i}$ and $t_i = C_{ii} = C'_{ii}$.

Next, we will analyse the constraints the above definition imposes on the equivalent quiver matrix C' . We derive those constraints by expanding each side of (3.2.1) and comparing to each order in x . We will discuss the cases that lead to nontrivial equivalent quiver matrices.

3.2.1 Constrains on equivalent quivers

The above equation is a definition, but it is also an identity that the equivalent quiver needs to satisfy. Taking (3.2.1) as a starting point, we can actually deduce many properties of equivalent quivers.

First, we expand order-by-order in x both sides of (3.2.1). At $\mathcal{O}(x^0)$ and $\mathcal{O}(x^1)$ both sides of (3.2.1) are always equal. Then, at $\mathcal{O}(x^2)$ we have

$$\begin{aligned} \frac{P_2(a, q, t)x^2}{(1-q^2)(1-q^4)} &= \sum_{i=0}^m \frac{(-q)^{4C_{ii}}x^2\lambda_i^2}{(1-q^2)(1-q^4)} + \sum_{i \neq j} \frac{(-q)^{C_{ii}+2C_{ij}+C_{jj}}x^2\lambda_i\lambda_j}{(1-q^2)(1-q^2)} \\ &= \sum_{i=0}^m \frac{(-q)^{4C_{ii}}x^2\lambda_i^2}{(1-q^2)(1-q^4)} + \sum_{i \neq j} \frac{(-q)^{C_{ii}+2C'_{ij}+C_{jj}}x^2\lambda_i\lambda_j}{(1-q^2)(1-q^2)}. \end{aligned} \quad (3.2.2)$$

After cancelling identical terms, the previous equation reduces to

$$\sum_{i < j} \left(q^{2C_{ij}} - q^{2C'_{ij}} \right) (-q)^{C_{ii}+C_{jj}} \lambda_i \lambda_j = 0. \quad (3.2.3)$$

As we know, lambdas are monomials in a , q and t . Thus, we can think of the above as a polynomial in a and t , whose coefficients depend on q . If we assume $\lambda_i \lambda_j \neq \lambda_k \lambda_l$ for all i, j, k and l , the previous equation is satisfied only when $C'_{ij} = C_{ij}$. This is the trivial case, since it would lead to $C = C'$. To obtain a nontrivial solution, we can study the case when

$$\lambda_a \lambda_b = q^{2s} \lambda_c \lambda_d \implies \begin{cases} a_a + a_b = a_c + a_d \\ q_a + q_b = q_c + q_d + 2s, \\ t_a + t_b = t_c + t_d \end{cases} \quad (3.2.4)$$

where $s \in \mathbb{Z}$ and $1 \leq a, b, c, d \leq m$. Notice that in the case when the knot \mathcal{K} is a thin knot, the above equation together with (2.3.4) would imply $s = 0$. For the moment, we will not restrict ourselves to thin knots and will keep $s \neq 0$.

Then, let us assume that $C'_{ij} = C_{ij}$ holds for all i and j , except for $i, j = a, b, c, d$. This cancels all the terms of (3.2.3) except for

$$\lambda_a \lambda_b (-q)^{C_{aa}+C_{bb}} \left(q^{2C_{ab}} + q^{-2s+2C_{cd}} \right) = \lambda_a \lambda_b (-q)^{C_{aa}+C_{bb}} \left(q^{2C'_{ab}} + q^{-2s+2C'_{cd}} \right), \quad (3.2.5)$$

where we used $C_{aa} + C_{bb} = C_{cc} + C_{dd}$ that comes from the t -powers in (3.2.4). Again, the nontrivial solution is

$$C'_{ab} = C_{cd} - s, \quad C'_{cd} = C_{ab} + s. \quad (3.2.6)$$

A simple interpretation of the above result is, up to the second order, when $s = 0$, the equivalent quiver matrix C' is (3.2.6) is identical to C except for a transposition of its entries $C_{ab} \leftrightarrow C_{cd}$.

Moving on to the third order case $\mathcal{O}(x^3)$ of (3.2.1)

$$\begin{aligned} \frac{P_3(a, q, t)x^3}{(1-q^2)(1-q^4)(1-q^6)} &= \sum_{i=0}^m \frac{(-q)^{9C_{ii}}x^3\lambda_i^3}{(1-q^2)(1-q^4)(1-q^6)} + \sum_{i \neq j} \frac{(-q)^{4C_{ii}+4C_{ij}+C_{jj}}x^3\lambda_i^2\lambda_j}{(1-q^2)(1-q^4)(1-q^2)} \\ &\quad + \sum_{i \neq j \neq k} \frac{(-q)^{C_{ii}+2C_{ij}+C_{jj}+2C_{jk}+C_{kk}+2C_{ik}}x^3\lambda_i\lambda_j\lambda_k}{(1-q^2)(1-q^2)(1-q^2)}. \end{aligned} \quad (3.2.7)$$

We are only interested in terms containing $\lambda_a \lambda_b$ or $\lambda_c \lambda_d$, since the other ones will cancel each other out. They are given by

$$\begin{aligned} \frac{x^3 \lambda_a \lambda_b}{(1-q^2)(1-q^4)(1-q^6)} & \left[(-q)^{4C_{aa}+4C'_{ab}+C_{bb}} \lambda_a + (-q)^{4C_{bb}+4C'_{ab}+C_{aa}} \lambda_b \right. \\ & + (1+q^2)(-q)^{C_{aa}+2C'_{ab}+C_{bb}+2C_{bc}+C_{cc}+2C_{ac}} \lambda_c \\ & + (1+q^2)(-q)^{C_{aa}+2C'_{ab}+C_{bb}+2C_{bd}+C_{dd}+2C_{ad}} \lambda_d \\ & \left. + (1+q^2) \sum_{i \neq a,b,c,d} (-q)^{C_{aa}+2C'_{ab}+C_{bb}+2C_{bi}+C_{ii}+2C_{ai}} \lambda_i \right] \end{aligned} \quad (3.2.8)$$

and

$$\begin{aligned} \frac{x^3 \lambda_c \lambda_d}{(1-q^2)(1-q^4)(1-q^6)} & \left[(-q)^{4C_{cc}+4C'_{cd}+C_{dd}} \lambda_c + (-q)^{4C_{dd}+4C'_{cd}+C_{dd}} \lambda_d \right. \\ & + (1+q^2)(-q)^{C_{cc}+2C'_{cd}+C_{dd}+2C_{ad}+C_{aa}+2C_{ac}} \lambda_a \\ & + (1+q^2)(-q)^{C_{cc}+2C'_{cd}+C_{dd}+2C_{bd}+C_{bb}+2C_{bc}} \lambda_b \\ & \left. + (1+q^2) \sum_{i \neq a,b,c,d} (-q)^{C_{cc}+2C'_{cd}+C_{dd}+2C_{di}+C_{ii}+2C_{ci}} \lambda_i \right] \end{aligned} \quad (3.2.9)$$

for $P_{C'}$ and analogously for P_C .

Next, we match the selected terms from above on both sides of (3.2.1) to obtain

$$\begin{aligned} \lambda_a & \left[(-q)^{4C_{aa}+4C'_{ab}+C_{bb}+2s} + (1+q^2)(-q)^{C_{cc}+2C'_{cd}+C_{dd}+2C_{ad}+C_{aa}+2C_{ac}} \right] \\ & = \lambda_a \left[(-q)^{4C_{aa}+4C_{ab}+C_{bb}+2s} + (1+q^2)(-q)^{C_{cc}+2C_{cd}+C_{dd}+2C_{ad}+C_{aa}+2C_{ac}} \right], \end{aligned} \quad (3.2.10a)$$

$$\begin{aligned} \lambda_b & \left[(-q)^{4C_{bb}+4C'_{ab}+C_{aa}+2s} + (1+q^2)(-q)^{C_{cc}+2C'_{cd}+C_{dd}+2C_{bd}+C_{bb}+2C_{bc}} \right] \\ & = \lambda_b \left[(-q)^{4C_{bb}+4C_{ab}+C_{aa}+2s} + (1+q^2)(-q)^{C_{cc}+2C_{cd}+C_{dd}+2C_{bd}+C_{bb}+2C_{bc}} \right], \end{aligned} \quad (3.2.10b)$$

$$\begin{aligned} \lambda_c & \left[(-q)^{4C_{cc}+4C'_{cd}+C_{dd}} + (1+q^2)(-q)^{C_{aa}+2C'_{ab}+C_{bb}+2C_{bc}+C_{cc}+2C_{ac}+2s} \right] \\ & = \lambda_c \left[(-q)^{4C_{cc}+4C_{cd}+C_{dd}} + (1+q^2)(-q)^{C_{aa}+2C_{ab}+C_{bb}+2C_{bc}+C_{cc}+2C_{ac}+2s} \right], \end{aligned} \quad (3.2.10c)$$

$$\begin{aligned} \lambda_d & \left[(-q)^{4C_{dd}+4C'_{cd}+C_{cc}} + (1+q^2)(-q)^{C_{aa}+2C'_{ab}+C_{bb}+2C_{bd}+C_{dd}+2C_{ad}+2s} \right] \\ & = \lambda_d \left[(-q)^{4C_{dd}+4C_{cd}+C_{cc}} + (1+q^2)(-q)^{C_{aa}+2C_{ab}+C_{bb}+2C_{bd}+C_{dd}+2C_{ad}+2s} \right], \end{aligned} \quad (3.2.10d)$$

$$\begin{aligned} \lambda_i & \left[(-q)^{C_{aa}+2C'_{ab}+C_{bb}+2C_{bi}+C_{ii}+2C_{ai}+2s} + (-q)^{C_{cc}+2C'_{cd}+C_{dd}+2C_{di}+C_{ii}+2C_{ci}} \right] \\ & = \lambda_i \left[(-q)^{C_{aa}+2C_{ab}+C_{bb}+2C_{bi}+C_{ii}+2C_{ai}+2s} + (-q)^{C_{cc}+2C_{cd}+C_{dd}+2C_{di}+C_{ii}+2C_{ci}} \right]. \end{aligned} \quad (3.2.10e)$$

Starting from (3.2.10a) let us match the q -monomials in a way that yields a nontrivial solution. This leads to the following linear equations for C and C'

$$\begin{aligned} 4C_{aa} + 4C'_{ab} + C_{bb} + 2s & = C_{cc} + 2C_{cd} + C_{dd} + 2C_{ad} + C_{aa} + 2C_{ac} + 2, \\ C_{cc} + 2C'_{cd} + C_{dd} + 2C_{ad} + C_{aa} + 2C_{ac} & = 4C_{aa} + 4C_{ab} + C_{bb} + 2s, \\ C_{cc} + 2C'_{cd} + C_{dd} + 2C_{ad} + C_{aa} + 2C_{ac} + 2 & = C_{cc} + 2C_{cd} + C_{dd} + 2C_{ad} + C_{aa} + 2C_{ac}, \end{aligned} \quad (3.2.11a)$$

or

$$\begin{aligned}
4C_{aa} + 4C'_{ab} + C_{bb} + 2s &= C_{cc} + 2C_{cd} + C_{dd} + 2C_{ad} + C_{aa} + 2C_{ac}, \\
C_{cc} + 2C'_{cd} + C_{dd} + 2C_{ad} + C_{aa} + 2C_{ac} &= C_{cc} + 2C_{cd} + C_{dd} + 2C_{ad} + C_{aa} + 2C_{ac} + 2, \\
C_{cc} + 2C'_{cd} + C_{dd} + 2C_{ad} + C_{aa} + 2C_{ac} + 2 &= 4C_{aa} + 4C_{ab} + C_{bb} + 2s. \quad (3.2.11b)
\end{aligned}$$

Analogously for (3.2.10b), (3.2.10c) and (3.2.10d), together with $C_{aa} + C_{bb} = C_{cc} + C_{dd}$ and (3.2.6), yields the two nontrivial possible pairwise cancellations:

$$\begin{aligned}
C_{ab} + s &= C_{cd} - 1, & C_{ab} + s &= C_{cd} + 1, \\
C_{aa} + C_{cd} &= C_{ad} + C_{ac} + s + 1, & C_{aa} + C_{cd} &= C_{ad} + C_{ac} + s, \\
C_{bb} + C_{cd} &= C_{bd} + C_{bc} + s + 1, & \text{or} & C_{bb} + C_{cd} = C_{bd} + C_{bc} + s, \quad (3.2.12) \\
C_{ab} + C_{cc} + s &= C_{bc} + C_{ac}, & C_{ab} + C_{cc} + s &= C_{bc} + C_{ac} + 1, \\
C_{ab} + C_{dd} + s &= C_{bd} + C_{ad} & C_{ab} + C_{dd} + s &= C_{bd} + C_{ad} + 1.
\end{aligned}$$

Making use of (3.2.12) along with $C_{aa} + C_{bb} = C_{cc} + C_{dd}$, we conclude that $s = 0$. Substituting this result in (3.2.10a) and (3.2.10e), leads to a similar result after an analogous analysis. Altogether yields the following system of equations in its two equivalent forms:

$$C_{cd} = C_{ab} - 1, \quad C_{ci} + C_{di} = C_{ai} + C_{bi} - \delta_{ai} - \delta_{bi} \quad (3.2.13a)$$

$$\text{or} \quad C_{ab} = C_{cd} - 1, \quad C_{ai} + C_{bi} = C_{ci} + C_{di} - \delta_{ci} - \delta_{di}. \quad (3.2.13b)$$

These are the constraints that the quiver matrix C needs to satisfy in order to have equivalent quivers according to our definition (3.2.1). They have a simple interpretation as transposition $C_{ab} \leftrightarrow C_{cd}$, which leads to an equivalent quiver. However, we have not proved that this conditions are enough to guarantee the existence of an equivalent quiver. Neither we have verified that there are no new constraints arising from expanding (3.2.1) to higher orders. The fact that this conditions are sufficient is the main content of the local equivalence theorem 2.

What happens when lambdas are proportional to each other, rather than their product (3.2.4)? Continuing our investigation of possible nontrivial solutions to (3.2.3), let us try the different ansatz $\lambda_a = q^{2s_1} \lambda_c$, $\lambda_b = q^{2s_2} \lambda_d$. At second-order in x we encounter the term

$$q^{2C_{ab}} \lambda_a \lambda_b + q^{2C_{cd}} \lambda_c \lambda_d + q^{2C_{ad}} \lambda_a \lambda_d + q^{2C_{bc}} \lambda_b \lambda_c. \quad (3.2.14)$$

This term appears on both sides of (3.2.1) and so we would like to cancel the q -monomials pairwise. We can enumerate the possible cancellations:

1. $q^{2C_{ab}} \lambda_a \lambda_b = q^{2C'_{ab}} \lambda_a \lambda_b$ leads to the trivial situation $C_{ab} = C'_{ab}$.
2. $q^{2C_{ab}} \lambda_a \lambda_b = q^{2C'_{cd}} \lambda_c \lambda_d$ reduces to the situation we encountered before in (3.2.13b) and (3.2.13a).
3. $q^{2C_{ab}} \lambda_a \lambda_b = q^{2C'_{ad}} \lambda_a \lambda_d$ produces analogs equations as (3.2.10a) and (3.2.10e) imply $s = 0$ and $C_{bi} = C_{di}$ for $i \neq a, b, d$. In short, this implies that b and d are indistinguishable and the transposition $C_{ab} \leftrightarrow C_{ad}$ can be understood as a relabeling $b \leftrightarrow d$.
4. $q^{2C_{ab}} \lambda_a \lambda_b = q^{2C'_{bc}} \lambda_b \lambda_c$ as the previous case, it is a relabeling $a \leftrightarrow c$.

We argued so far that if a quiver matrix C satisfies (3.2.13) and $\lambda_a \lambda_b = \lambda_c \lambda_d$ we can transpose $C_{ab} \leftrightarrow C_{cd}$ to obtain an equivalent quiver C' . A well-known result is that the permutation group of n elements S_n can be generated by transpositions. Therefore, if we are able to compose transpositions, we may construct more complex permutations. This poses the question, if there exists more than one possible transposition, can we compose them to obtain a new equivalent quiver?

Suppose that a quiver matrix C admits the transposition $C_{ab} \leftrightarrow C_{cd}$ and $C_{cd} \leftrightarrow C_{ef}$. Next, assume we perform the transposition $C_{cd} \leftrightarrow C_{ef}$. Now we can not perform the transposition $C_{ab} \leftrightarrow C_{cd}$. This is because before the transposition $C_{cd} \leftrightarrow C_{ef}$, we had $C_{ac} + C_{bc} = C_{cc} + C_{cd}$ (if $C_{ab} < C_{cd}$) or $C_{ac} + C_{bc} = C_{cc} + C_{cd} - 1$ (if $C_{ab} > C_{cd}$), which is no longer satisfied after $C_{cd} \leftrightarrow C_{ef}$. An analogous argument applies when we perform the first $C_{ab} \leftrightarrow C_{cd}$.

As a consequence, we can not compose transpositions into larger permutations. Nevertheless, we have not yet excluded all nontrivial ways of matching terms in (3.2.2). For instance, there could be permutations producing an equivalent quiver that could be decomposed into transpositions that individually do modify the partition function. We do not expect such permutations to exist. Thus, we propose the following conjecture based on the evidence we discuss below:

Conjecture 1. *Consider a quiver matrix C corresponding to the knot K . If there exists another symmetric quiver matrix C' such that $C' \sim C$ in the sense of the definition (3.2.1), then either $C' = C$ or they are related by a sequence of disjoint transpositions, each exchanging nondiagonal elements*

$$C_{ab} \leftrightarrow C_{cd}, \quad C_{ba} \leftrightarrow C_{dc}, \quad (3.2.15)$$

for some pairwise different $1 \leq a, b, c, d, \leq m$, such that

$$\lambda_a \lambda_b = \lambda_c \lambda_d \quad (3.2.16a)$$

and

$$C_{ab} = C_{cd} - 1, \quad C_{ai} + C_{bi} = C_{ci} + C_{di} - \delta_{ci} - \delta_{di}, \quad 1 \leq i \leq m, \quad (3.2.16ba)$$

or

$$C_{cd} = C_{ab} - 1, \quad C_{ci} + C_{di} = C_{ai} + C_{bi} - \delta_{ai} - \delta_{bi}, \quad 1 \leq i \leq m. \quad (3.2.16bb)$$

In the case of thin knots, it is easy to see that all possible equivalent quivers are simply permutations of the off-diagonal entries of the quiver matrix. To see this, take the second-order expansion in x (3.2.2). To have cancellations we need that the products of lambdas be equal up to q^s prefactors $\lambda_a \lambda_b = q^{s_1} \lambda_c \lambda_d = q^{s_2} \lambda_e \lambda_f = \dots$. Using the thinness condition (2.3.4) we can conclude that $s_1 = s_2 = \dots = 0$. Additionally, the fact that $C'_{ij} \in \mathbb{Z}$ imposes that any equivalent quiver matrix C' is equal C except for permutations of off-diagonal elements.

Then, the conjecture reduces to find all possible lambdas that satisfy such constraints, which are finitely many. After that, simply perform all possible permutations and compare the resulting series. We carried out this analysis for 3_1 , 4_1 , and 5_1 knots and found that they agree with our conjecture 1.

For thin knots, we can provide another argument in favour of conjecture 1. We can exclude 3-cycles that may consist of transpositions that do not preserve the quiver series. Suppose that $\lambda_a\lambda_b = \lambda_c\lambda_d = \lambda_e\lambda_f$, and (3.2.2), and C' is a permutation of the three elements $(C_{ab} C_{cd} C_{ef})$ or $(C_{ab} C_{ef} C_{cd})$ with C_{ab}, C_{cd}, C_{ef} being all distinct. We can consider all possible ways the q -monomials may cancel out at cubic order in x (3.2.7). This yields 44^3 systems of 30 linear equations. Using a computer, we may verify that they do not have a nontrivial solution.

In the next section we formulate and prove the local equivalence theorem 2. Together, conjecture 1 and the local equivalence theorem imply that we find all possible equivalent quivers for the knots under study.

3.2.2 Local equivalence theorem

Theorem 2. *Consider a symmetric quiver matrix C , of size m , corresponding to the knot K and another symmetric quiver matrix C' , of the same size. Lets assume also that $\lambda'_i = \lambda_i$ for $1 \leq i \leq m$, where λ_i are the ones from the knot change of variables (2.3.2). If C and C' are related by a sequence of disjoint transpositions, each exchanging non-diagonal elements*

$$C_{ab} \leftrightarrow C_{cd}, \quad C_{ba} \leftrightarrow C_{dc}, \quad (3.2.3)$$

for some pairwise different $1 \leq a, b, c, d \leq m$, such that

$$\lambda_a\lambda_b = \lambda_c\lambda_d \quad (3.2.4a)$$

and

$$C_{ab} = C_{cd} - 1, \quad C_{ai} + C_{bi} = C_{ci} + C_{di} - \delta_{ci} - \delta_{di}, \quad 1 \leq i \leq m, \quad (3.2.4ba)$$

or

$$C_{cd} = C_{ab} - 1, \quad C_{ci} + C_{di} = C_{ai} + C_{bi} - \delta_{ai} - \delta_{bi}, \quad 1 \leq i \leq m, \quad (3.2.4bb)$$

then C and C' are equivalent in the sense of the definition (3.2.1).

In practice, for a given knot \mathcal{K} we find all possible quadruple of pairwise different $1 \leq a, b, c, d \leq m$ satisfying (3.2.4a). We refer to (3.2.4a) as the *center of mass condition* and a quadruple satisfying it we will call it a *pairing*. It is worth mentioning that not all pairings allow for transpositions (3.2.3) leading to an equivalent quiver, since they still need to further satisfy (3.2.4b). Pairings that do satisfy all constraints (3.2.4) from the theorem 2 are *symmetries*. A symmetry is either *trivial* when $C'_{ij} = C_{ij}$ or *nontrivial* when $C'_{ij} \neq C_{ij}$. Finally, we denote by $N_C(s)$ the number of equivalent quiver matrices to C , as a function of the number of symmetries s .

A convenient geometrical way to visualise symmetries is through the homological diagram of the knot. In terms of a, q and t the center of mass condition (3.2.4a) translates to the vector equation $\vec{v}_a + \vec{v}_b = \vec{v}_c + \vec{v}_d$, where $\vec{v}_i = (q_i, a_i)$ is a vector of homological degrees of the generator i . This is analogous to the center of mass condition from classical mechanics for a system of four equal mass particles $\{a, b\}$ and $\{c, d\}$ and hence the name. Geometrically, it can be drawn as a parallelogram with diagonals ab and cd , see figure 3.1.

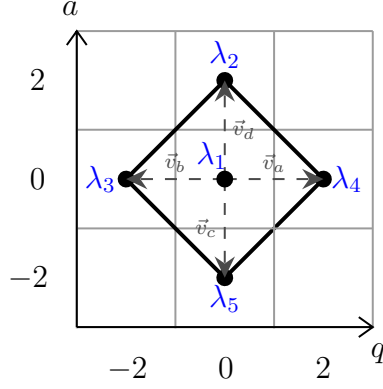


Figure 3.1: The set of generators of the uncolored HOMFLY-PT homology for 4_1 knot and the parallelogram corresponding to the pairing $\lambda_2\lambda_5 = \lambda_3\lambda_4$

The third-order constraints (3.2.4b) have an analogous representation in terms of generators of the S^r -colored HOMFLY-PT homology for $r = 2$. This is because the off-diagonal elements of the quiver matrix enter the quiver series starting from the quadratic term (3.2.2)

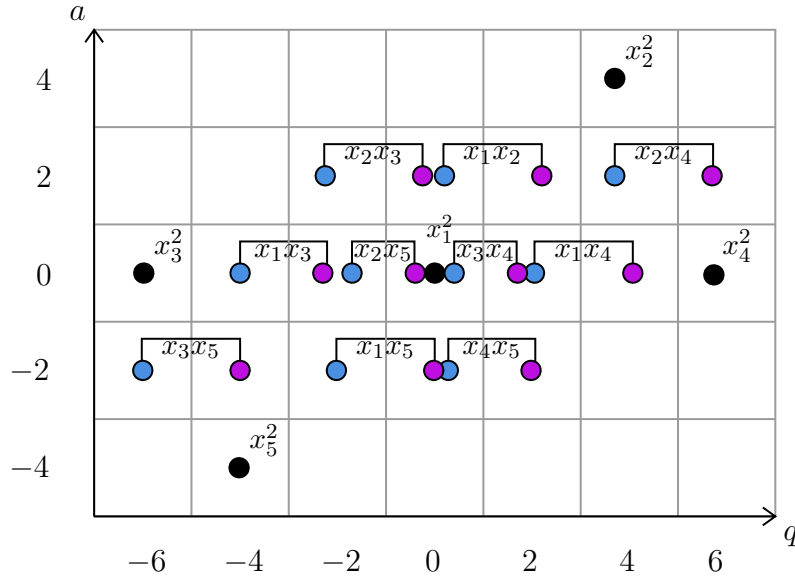


Figure 3.2: The set of generators of the S^2 -colored HOMFLY-PT homology for 4_1 knot (the labels $x_i x_j$ are consistent with the labels in figure 3.1).

For example, the S^2 -colored homology for 4_1 knot is shown in figure 3.2. There are 3 kinds of generators: 5 black nodes are in one-to-one correspondence with x_i^2 , $i = 1 \dots 5$. Blue and purple nodes correspond to $x_i x_j$ with $i \neq j$, and for each pair (i, j) there are exactly 2 generators, which we connect by an arc. The distinction between blue and purple nodes is justified by taking the common denominator in the quadratic term of the quiver series. Each term $x_i x_j$ is multiplied by $(1 + q^2)$, therefore contributing twice to the colored superpolynomial. The blue node has the q -degree $q_i + q_j + C_{ii} + 2C_{ij} + C_{jj}$, while the purple one is shifted by two: $q_i + q_j + C_{ii} + 2C_{ij} + C_{jj} + 2$. Having in mind the pairing condition inducing cancellations of all terms except those corresponding to arrows between different nodes ($2C_{ij}$), we can visualize any constraint of the form $C_{is} + C_{js} = C_{ks} + C_{ls}$ as

a parallelogram connecting nodes with the same color. For example, the constraint $C_{12} + C_{15} = C_{13} + C_{14}$ is visualized in figure 3.3.

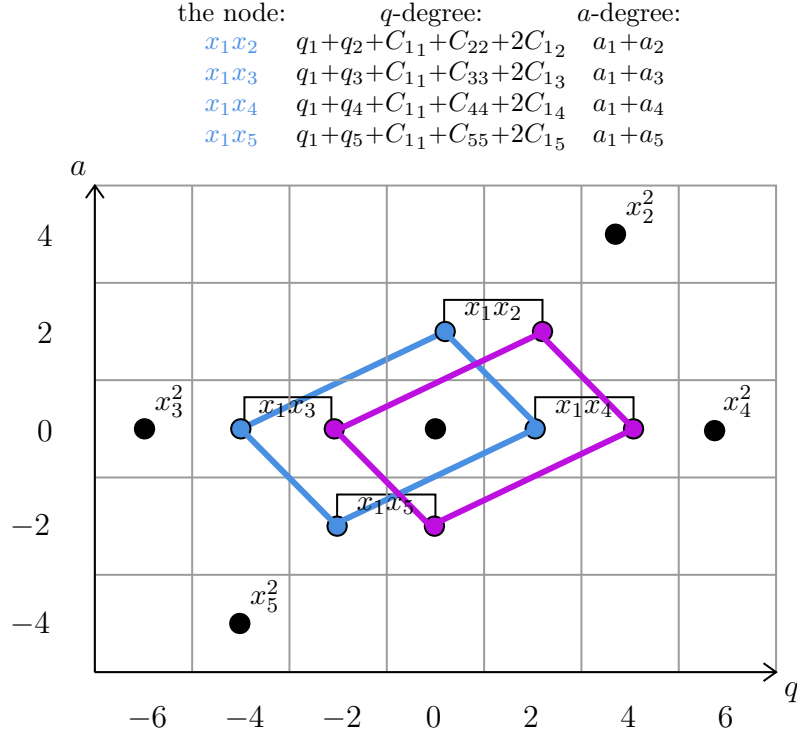


Figure 3.3: The constraint $C_{12} + C_{15} = C_{13} + C_{14}$ as a parallelogram rule. There are cancellations when equating the sums of the q - and a -degrees of x_1x_2, x_1x_5 and x_1x_3, x_1x_4 , since $\lambda_2\lambda_5 = \lambda_3\lambda_4$ implies $q_2 + q_5 = q_3 + q_4$ and $a_2 + a_5 = a_3 + a_4$.

3.2.3 Proof of the local equivalence theorem

We proceed to prove the local equivalence theorem 2. We may have multiple possible transpositions for a given quiver matrix C . Thanks to the fact that each transposition is an independent symmetry, we can consider a general form of one such transposition and show that it preserves the generating function. This automatically implies that if C and C' are connected by a sequence of such transformations, then they correspond to the same knot.

Say that C corresponds to K , $\lambda'_i = \lambda_i$ for $1 \leq i \leq m$, and we have $C'_{ij} = C_{ij}$ except for the transposition $C_{ab} \leftrightarrow C_{cd}$ with pairwise different $1 \leq a, b, c, d \leq m$. We further demand that

$$\lambda_a\lambda_b = \lambda_c\lambda_d, \quad C_{cd} = C_{ab} - 1, \quad C_{ci} + C_{di} = C_{ai} + C_{bi} - \delta_{ai} - \delta_{bi}, \quad 1 \leq i \leq m \quad (3.2.3)$$

and analogous constraints for C' ²

To prove that C' is also associated with K . Next, we unlink nodes a, b in C and

²The case $C_{ab} = C_{cd} - 1$ is obtain by relabelling $ab \leftrightarrow cd$.

nodes c, d in C' ³

$$\begin{aligned}
\tilde{C}'_{ij} &= C_{ij} \quad i, j \neq a, b & \tilde{C}'_{ij} &= C'_{ij} \quad i, j \neq c, d \\
\tilde{C}'_{ab} &= C_{ab} - 1 & \tilde{C}'_{cd} &= C'_{cd} - 1 \\
\tilde{C}'_{in} &= C_{ai} + C_{bi} - \delta_{ai} - \delta_{bi}, & \tilde{C}'_{in} &= C'_{ci} + C'_{di} - \delta_{ci} - \delta_{di}, \\
\tilde{C}'_{nn} &= C_{aa} + 2C_{ab} + C_{bb} - 1, & \tilde{C}'_{nn} &= C'_{cc} + 2C'_{cd} + C'_{dd} - 1.
\end{aligned} \tag{3.2.4}$$

These equations imply

$$\begin{aligned}
\tilde{C}'_{ab} &= C'_{ab} = C_{cd} = C_{ab} - 1 = \tilde{C}_{ab}, \\
\tilde{C}'_{cd} &= C'_{cd} - 1 = C_{ab} - 1 = C_{cd} = \tilde{C}_{cd}, \\
\tilde{C}'_{an} &= C'_{ac} + C'_{ad} = C_{ac} + C_{ad} = C_{aa} + C_{ab} - 1 = \tilde{C}_{an}, \\
\tilde{C}'_{bn} &= C'_{bc} + C'_{bd} = C_{bc} + C_{bd} = C_{ab} + C_{bb} - 1 = \tilde{C}_{bn}, \\
\tilde{C}'_{cn} &= C'_{cc} + C'_{cd} - 1 = C'_{ac} + C'_{bc} = C_{ac} + C_{bc} = \tilde{C}_{cn}, \\
\tilde{C}'_{dn} &= C'_{cd} + C'_{dd} - 1 = C'_{ad} + C'_{bd} = C_{ad} + C_{bd} = \tilde{C}_{dn}, \\
\tilde{C}'_{in} &= C'_{ci} + C'_{di} = C_{ci} + C_{di} = C_{ai} + C_{bi} = \tilde{C}_{in}, \quad \forall i \neq a, b, c, d, \\
\tilde{C}'_{nn} &= C'_{cc} + 2C'_{cd} + C'_{dd} - 1 = C_{cc} + 2C_{ab} + C_{dd} - 1 = \tilde{C}_{nn}, \\
\tilde{C}'_{ij} &= C'_{ij} = C_{ij} = \tilde{C}_{ij} \quad \text{for all other cases,}
\end{aligned} \tag{3.2.5}$$

in a few words $\tilde{C}' = \tilde{C}$.

When unlinking C' and C we can choose the knots-quivers change of variables for the new nodes. We may take

$$\tilde{\lambda}'_n = q^{-1} \lambda_c \lambda_d = q^{-1} \lambda_a \lambda_b = \tilde{\lambda}_n, \tag{3.2.6}$$

together with (3.1.3) we obtain

$$P_{Q'}(\mathbf{x}, q)|_{x_i=x\lambda'_i} = P_{\tilde{Q}'}(\mathbf{x}, q)|_{x_i=x\lambda'_i, x_n=x\tilde{\lambda}'_n} = P_{\tilde{Q}}(\mathbf{x}, q)|_{x_i=x\lambda_i, x_n=x\tilde{\lambda}_n} = P_Q(\mathbf{x}, q)|_{x_i=x\lambda_i}.$$

Thus

$$P_{Q'}(\mathbf{x}, q)|_{\mathbf{x}=x\lambda'} = P_Q(\mathbf{x}, q)|_{\mathbf{x}=x\lambda} = P_K(x, a, q, t), \tag{3.2.7}$$

which leads us to conclude that C' also corresponds to K .

3.3 Global structure and permutohedra graphs

As a quick recap, in the previous section 3.2 we proved that there could exist equivalent quiver matrices associated to the same knot. We derived a set of constraints (3.2.4) both the quiver matrix and the knot change of variables (2.3.2) need to satisfy to admit an equivalent quiver. In this section we will construct the form of general quiver matrix that satisfies the constraints (3.2.4). This general form of the quiver matrix depends on a couple of arbitrary parameters $k, l \in \mathbb{Z}$. On top of that, the general form of the solution can be also obtained from an operation we will call

³Given that unlinking yields the same quiver series, if C is associated to \mathcal{K} so will C' .

(k, l) -splitting, acting on a symmetric matrix that we will call the *pre-quiver* and we denote as \tilde{C} .

The next step is to study what happens when there is more than one transposition that produces a symmetry of the quiver matrix. It turns out that the possible compositions of these transpositions produce a highly complex network of equivalent quivers. To keep track of the transpositions, we represent them in terms of a graph. The equivalent quiver matrices are the nodes and the edges are the symmetry transpositions relating two equivalent quiver matrices. We discovered that these graphs of equivalent quivers can be constructed out of simple subgraphs known as *permutohedra*. The permutohedra naturally arise due to the combinatorial interpretation of transpositions from theorem 2 and we will show various examples of this phenomenon in the next section.

3.3.1 General solution of constraints for one transposition

Lets begin by solving the center of mass condition (3.2.4a). Our line of thought is analogous to the separation of variables method for PDE's. Suppose $\lambda_a \neq 0$ and $\lambda_b \neq 0$, then we may rewrite the center of mass condition as

$$\frac{\lambda_d}{\lambda_a} = \frac{\lambda_b}{\lambda_c} = \kappa, \quad \implies \quad \boxed{\lambda_d = \kappa\lambda_a, \quad \lambda_b = \kappa\lambda_c} \quad (3.3.1)$$

where κ is a monomial in a, q and t . This relation essentially means that out of four λ s two are truly independent.

The above relation between lambdas leads to a simplification of the infinite sums in the quiver series (2.1.40) involving λ_c and λ_d . However, for the sake of clarity and generality, we will show how to rewrite a generic power series

$$F(x_a, x_b, x_c, x_d) = \sum_{d_a, d_b, d_c, d_d \geq 0} x_a^{d_a} x_b^{d_b} x_c^{d_c} x_d^{d_d} f_{d_a, d_b, d_c, d_d} \quad (3.3.2)$$

where f_{d_a, d_b, d_c, d_d} are arbitrary coefficients, $x_i = \lambda_i x$ and lambdas satisfy (3.3.1). We substitute then (3.3.1) into (3.3.2) and gives

$$\begin{aligned} F(x_a = \lambda_a x, x_b = \lambda_b x, x_c = \kappa\lambda_b x, x_d = \kappa\lambda_a x) &= \\ &= \sum_{d_a, d_b, d_c, d_d \geq 0} x^{d_a + d_b + d_c + d_d} \lambda_a^{d_a} (\kappa\lambda_c)^{d_b} \lambda_c^{d_c} (\kappa\lambda_a)^{d_d} f_{d_a, d_b, d_c, d_d} \\ &= \sum_{\check{d}_a, \check{d}_c \geq 0} x^{\check{d}_a + \check{d}_b} \lambda_a^{\check{d}_a} \lambda_c^{\check{d}_c} \sum_{\alpha_a + \beta_a = \check{d}_a} \sum_{\alpha_c + \beta_c = \check{d}_c} \kappa^{\beta_a + \beta_c} f_{\alpha_a, \beta_a, \alpha_c, \beta_c} \end{aligned} \quad (3.3.3)$$

where to go from from the middle row to the last row, we changed the summation indices $d_a = \alpha_a$, $d_d = \beta_a$, $d_c = \alpha_c$, $d_b = \beta_c$, together with $\check{d}_a = \alpha_a + \beta_a$ plus $\check{d}_c = \alpha_c + \beta_c$.

If we think of x_i as the entries of a four-vector, it will be profitable to preform the relabelling of x_i in order to have x_d next to x_a . This is equivalent to the permutation $b \leftrightarrow d$

$$\begin{bmatrix} x_a \\ x_b \\ x_c \\ x_d \end{bmatrix} = P_{b \leftrightarrow d} \cdot \begin{bmatrix} x_a \\ x_d \\ x_c \\ x_b \end{bmatrix}, \quad P_{b \leftrightarrow d} = \begin{bmatrix} 1 & 0 & 0 & 0 \\ 0 & 0 & 0 & 1 \\ 0 & 0 & 1 & 0 \\ 0 & 1 & 0 & 0 \end{bmatrix} \quad (3.3.4)$$

In the relabeled form we have the following factorization in terms of the tensor product \otimes

$$\begin{bmatrix} x_a \\ x_d \\ x_c \\ x_b \end{bmatrix} = x \begin{bmatrix} \lambda_a \\ \kappa\lambda_a \\ \lambda_c \\ \kappa\lambda_c \end{bmatrix} = x \begin{bmatrix} \lambda_a \begin{bmatrix} 1 \\ \kappa \end{bmatrix} \\ \lambda_c \begin{bmatrix} 1 \\ \kappa \end{bmatrix} \end{bmatrix} = x \begin{bmatrix} \lambda_a \\ \lambda_c \end{bmatrix} \otimes \begin{bmatrix} 1 \\ \kappa \end{bmatrix}. \quad (3.3.5)$$

This tensor product factorization can also be seen for the summation indices

$$\begin{bmatrix} d_a \\ d_d \\ d_c \\ d_b \end{bmatrix} = \begin{bmatrix} \alpha_a \\ \beta_a \\ \alpha_c \\ \beta_c \end{bmatrix} = \begin{bmatrix} 1 \\ 0 \end{bmatrix} \otimes \begin{bmatrix} \alpha_a \\ \beta_a \end{bmatrix} + \begin{bmatrix} 0 \\ 1 \end{bmatrix} \otimes \begin{bmatrix} \alpha_c \\ \beta_c \end{bmatrix} \quad (3.3.6)$$

Our next step is to solve the constraints on the quiver matrix (3.2.4b) we notice that we can always find parameters $k, l \in \mathbb{Z}$ such that $C_{ad} = C_{aa} + k$ and $C_{dd} = C_{aa} + l$. Inserting this into the constraints (3.2.4b) with $i = a$ we obtain $C_{ab} = C_{ac} + C_{ad} - C_{aa} = C_{ac} + k$. Analogously, (3.2.4b) with $i = b$ it reduces to $C_{ad} + C_{bd} = C_{dd} + C_{cd} - 1$. We can combine the first equation in (3.2.4b) and the previous relations to produce $C_{bd} = C_{ac} + l$. In a similar fashion, (3.2.4b) with $i = c$ and $i = d$ implies respectively $C_{cb} = C_{cc} + k$ and $C_{bb} = C_{cc} + l$.

After all this manipulations, we may express the 4×4 submatrix of C with elements $\Gamma_{ij} = C_{ij}$ for $i, j = a, b, c, d$ as

$$\left[\begin{array}{cc|cc} C_{aa} & C_{ad} & C_{ac} & C_{ab} \\ C_{ad} & C_{dd} & C_{cd} & C_{bd} \\ \hline C_{ac} & C_{cd} & C_{cc} & C_{bc} \\ C_{ab} & C_{bd} & C_{bc} & C_{bb} \end{array} \right] = \left[\begin{array}{cc|cc} C_{aa} & C_{aa} + k & C_{ac} & C_{ac} + k \\ C_{aa} + k & C_{aa} + l & C_{ac} + k + 1 & C_{ac} + l \\ \hline C_{ac} & C_{ac} + k + 1 & C_{cc} & C_{cc} + k \\ C_{ac} + k & C_{ac} + l & C_{cc} + k & C_{cc} + l \end{array} \right], \quad (3.3.7)$$

where we have used the same relabelling of the nodes $b \leftrightarrow d$ to give the afore submatrix a block structure⁴. This block structure takes a simpler form when rewriting, again, using the tensor product

$$\Gamma = \begin{bmatrix} C_{aa} & C_{ac} \\ C_{ac} & C_{cc} \end{bmatrix} \otimes \begin{bmatrix} 1 & 1 \\ 1 & 1 \end{bmatrix} + \begin{bmatrix} 1 & 1 \\ 1 & 1 \end{bmatrix} \otimes \begin{bmatrix} 0 & k \\ k & l \end{bmatrix} + \begin{bmatrix} 0 & 1 \\ 0 & 0 \end{bmatrix} \otimes \begin{bmatrix} 0 & 0 \\ 1 & 0 \end{bmatrix} + \begin{bmatrix} 0 & 0 \\ 1 & 0 \end{bmatrix} \otimes \begin{bmatrix} 0 & 1 \\ 0 & 0 \end{bmatrix}. \quad (3.3.8)$$

The afore expression can be written more conveniently in the short hand notation as

$$\Gamma = \check{C} \otimes 1_{2 \times 2} + 1_{2 \times 2} \otimes \Lambda + L_{2 \times 2}^T \otimes L_{2 \times 2} + L_{2 \times 2} \otimes L_{2 \times 2}^T \quad (3.3.9)$$

where each term and factor corresponds exactly to those in (3.3.8). The first term $\check{C} = \begin{bmatrix} C_{aa} & C_{ac} \\ C_{ac} & C_{cc} \end{bmatrix}$ and we will refer to it as the *prequiver*⁵. Then, $1_{r \times s}$ with $r, s \in \mathbb{N}$ is the $r \times s$ matrix with all entries equal to one. In the second term $\Lambda = \begin{bmatrix} 0 & k \\ k & l \end{bmatrix}$ contains

⁴The relabelling of quiver nodes acts on the quiver matrix as $P_{b \leftrightarrow d} C P_{b \leftrightarrow d}^T$. We may perform relabellings at will since the quiver series (2.1.40) is invariant under this transformation.

⁵The origin of the name prequiver will be clear ones we substitute our general solution back into the quiver series.

all dependence on the k and l parameters. In the third term, $L_{r \times s}$ is an $r \times s$ matrix with ones below the main diagonal, zeros on the main diagonal, and zeros below the main diagonal.

In the tensor product form (3.3.8), the symmetry transpositions $C_{ab} \leftrightarrow C_{cd}$ from theorem 2 have a very familiar representation. Suppose we apply the aforementioned transposition on the l.h.s. of (2.3.17). On the r.h.s. the transposition amounts to swapping the $+1$ term from the C_{ab} entry to the C_{cd} one. When the same operation is preformed on the tensor product form (3.3.8) the last term changes as

$$\begin{aligned} & \begin{bmatrix} 0 & 1 \\ 0 & 0 \end{bmatrix} \otimes \begin{bmatrix} 0 & 1 \\ 0 & 0 \end{bmatrix} + \begin{bmatrix} 0 & 0 \\ 1 & 0 \end{bmatrix} \otimes \begin{bmatrix} 0 & 0 \\ 1 & 0 \end{bmatrix} = \\ & \left(\begin{bmatrix} 0 & 1 \\ 1 & 0 \end{bmatrix} \otimes I_{2 \times 2} \right) \cdot (L_{2 \times 2}^T \otimes L_{2 \times 2} + L_{2 \times 2} \otimes L_{2 \times 2}^T) \left(\begin{bmatrix} 0 & 1 \\ 1 & 0 \end{bmatrix} \otimes I_{2 \times 2} \right)^T \end{aligned} \quad (3.3.10)$$

where $\begin{bmatrix} 0 & 1 \\ 1 & 0 \end{bmatrix}$ is the matrix representation of the permutation of two elements and $I_{n \times n}$ is the identity matrix of size n .

To finish our general solution, we now turn our attention to the remaining $m - 2$ quiver nodes, which are unaffected by the transposition $C_{ab} \leftrightarrow C_{cd}$. These nodes are $i \neq a, b, c, d$ and we will call them *spectator nodes*. Similarly, we call *spectator constraints* the part of (3.2.4b), which involves the spectator nodes. We solve these constraints in the same way as we did in (3.3.7), by rewriting them as $C_{bi} - C_{ci} = C_{di} - C_{ai} = h_i$, which in turn implies

$$C_{bi} = C_{ci} + h_i, \quad C_{di} = C_{ai} + h_i, \quad (3.3.11)$$

for some $h_i \in \mathbb{Z}$.

It is convenient to write explicitly the final form of the quiver matrix satisfying all constraints (3.2.4b). Since we can always relabel the nodes of the quiver and the quiver series is invariant, then we can always bring the quiver matrix C to a block form. In that block form, the submatrix Γ is the first diagonal block and the remaining blocks correspond to the spectator nodes. For concreteness, say the number of nodes $m = 6$, plus we assume nodes e and f are spectators. Then, we have the following quiver matrix

$$\begin{aligned} & \left[\begin{array}{cc|cc|cc} C_{aa} & C_{ad} & C_{ac} & C_{ab} & C_{ae} & C_{af} \\ C_{ad} & C_{dd} & C_{cd} & C_{bd} & C_{de} & C_{df} \\ \hline C_{ac} & C_{cd} & C_{cc} & C_{bc} & C_{ce} & C_{cf} \\ C_{ab} & C_{bd} & C_{bc} & C_{bb} & C_{be} & C_{bf} \\ \hline C_{ae} & C_{de} & C_{ce} & C_{be} & C_{ee} & C_{ef} \\ C_{af} & C_{df} & C_{cf} & C_{bf} & C_{ef} & C_{ff} \end{array} \right] = \left[\begin{array}{c|c} \Gamma & \Phi \\ \hline \Phi^T & \Sigma \end{array} \right] = \\ & \left[\begin{array}{cc|cc|cc} C_{aa} & C_{aa} + k & C_{ac} & C_{ac} + k & C_{ae} & C_{af} \\ C_{aa} + k & C_{aa} + l & C_{ac} + k + 1 & C_{ac} + l & C_{ae} + h_e & C_{af} + h_f \\ \hline C_{ac} & C_{ac} + k + 1 & C_{cc} & C_{cc} + k & C_{ce} & C_{cf} \\ C_{ac} + k & C_{ac} + l & C_{cc} + k & C_{cc} + l & C_{ce} + h_e & C_{cf} + h_f \\ \hline C_{ae} & C_{ae} + h_e & C_{ce} & C_{ce} + h_e & C_{ee} & C_{ef} \\ C_{af} & C_{af} + h_f & C_{cf} & C_{cf} + h_f & C_{ef} & C_{ff} \end{array} \right], \end{aligned} \quad (3.3.12)$$

where we have taken advantage of the block structure and introduced matrices representing each block. We can think of the above as a definition for the matrices

Γ , Φ and Σ ; each of which is of size 4×4 , 4×2 and 2×2 respectively. The submatrix Γ is for the subquiver where the transposition acts, Σ is the submatrix for the spectator nodes, and Φ represents the arrows between the nodes the subquivers Γ and Φ .

We may further simplify Φ , given by the third equality in (3.3.12), using the tensor product

$$\begin{aligned} \Phi &= \begin{bmatrix} C_{ae} & C_{af} \\ C_{ae} & C_{cf} \end{bmatrix} \otimes \begin{bmatrix} 1 \\ 1 \end{bmatrix} + \begin{bmatrix} 1 \\ 1 \end{bmatrix} \otimes [h_e, h_f] \otimes \begin{bmatrix} 0 \\ 1 \end{bmatrix}, \\ &= \check{\Phi} \otimes 1_{2 \times 1} + 1_{2 \times 1} \otimes H \otimes L_{1,2} \end{aligned} \quad (3.3.13)$$

where, similarly to (3.3.8), $\check{\Phi} = \begin{bmatrix} C_{ae} & C_{af} \\ C_{ae} & C_{cf} \end{bmatrix}$ is the part associated to the prequiver \check{C} , and $H = [h_e, h_f]$ carries all the parameter dependence.

From (3.3.12) we deduce that the prequiver \check{C} is

$$\check{C} = \left[\begin{array}{cc|cc} C_{aa} & C_{ac} & C_{ae} & C_{af} \\ C_{ac} & C_{cc} & C_{ce} & C_{cf} \\ \hline C_{ae} & C_{ce} & C_{ee} & C_{ef} \\ C_{af} & C_{cf} & C_{ef} & C_{ff} \end{array} \right] = \left[\begin{array}{c|c} \check{\Gamma} & \check{\Phi} \\ \hline \check{\Phi}^T & \Sigma \end{array} \right] \quad (3.3.14)$$

where we can see the same block structure from (3.3.12).

In general, for a $m \times m$ quiver matrix C with a nontrivial transposition symmetry as in theorem 2, its prequiver its prequiver \check{C} is of size $(m - 2) \times (m - 2)$. The two removed nodes are two of the four nodes involved in the transposition. In our case, we have chosen to remove b and d . An equally possible choice could be one of the pair (a, b) , together with another node from the pair (c, d) .

The next important step is to compute the quadratic form $\vec{d}^T C \vec{d}$, which appears in the quiver generating series (2.1.40). From (3.3.12) we notice that the quadratic form may also be divided into three parts: the prequiver, the (k, l) and h_i parameters and the matrix of zeros and ones.

First, the prequiver part \check{C} from (3.3.14) produces the standard term $\vec{d}^T \check{C} \vec{d}$, where $\check{d}_a = d_a + d_d$ and $\check{d}_c = d_c + d_b$, as in (3.3.3), plus $\check{d}_e = d_e$ and $\check{d}_f = d_e$.

Secondly, the (k, l) -parameters give the quadratic term

$$\begin{bmatrix} d_a \\ d_d \\ d_c \\ d_b \end{bmatrix}^T \left[\begin{array}{cc|cc} 0 & k & 0 & k \\ k & l & k & l \\ \hline 0 & k & 0 & k \\ k & l & k & l \end{array} \right] \begin{bmatrix} d_a \\ d_d \\ d_c \\ d_b \end{bmatrix} = [2k(\alpha_a + \alpha_c) + l(\beta_a + \beta_c)] (\beta_a + \beta_c), \quad (3.3.15)$$

where in agreement with (3.3.3), $d_a = \alpha_a$, $d_d = \beta_a$, $d_c = \alpha_c$, $d_b = \beta_c$. Meanwhile, for the contribution arising from the spectator nodes, we have the term $2(\beta_a + \beta_c)(h_e \check{d}_e + h_f \check{d}_f)$.

Lastly, the term with zeros and ones from (3.3.12) produces $2\beta_a \alpha_c$. This term is the responsible one for the transposition symmetry of theorem 2, which acts as the transformation $\beta_a \alpha_c \leftrightarrow \beta_c \alpha_a$.

Having reviewed the three contributions, we are able to substitute the above formulas for $\vec{d}^T C \vec{d}$, along with (3.3.3) and its respective summation indices into the

quiver series (2.1.40), leading to

$$P_C(x_a = \lambda_a x, x_b = \kappa \lambda_c x, x_c = \lambda_c x, x_d = \kappa \lambda_a x, x_e = \lambda_e x, x_f = \lambda_f x) = \sum_{\check{d}_a, \check{d}_c, \check{d}_e, \check{d}_f \geq 0} \frac{(x \lambda_a)^{\check{d}_a} (x \lambda_c)^{\check{d}_c} (x \lambda_e)^{\check{d}_e} (x \lambda_f)^{\check{d}_f}}{(q^2)_{\check{d}_a} (q^2)_{\check{d}_c} (q^2)_{\check{d}_e} (q^2)_{\check{d}_f}} (-q)^{\sum_{i,j} \check{C}_{\check{d}_i \check{d}_j}} \Pi_{\check{d}_a, \check{d}_c, \check{d}_e, \check{d}_f}, \quad (3.3.16)$$

where

$$\frac{\Pi_{\check{d}_a, \check{d}_c, \check{d}_e, \check{d}_f}}{(q^2)_{\check{d}_a} (q^2)_{\check{d}_c}} = \sum_{\alpha_a + \beta_a = \check{d}_a} \sum_{\alpha_c + \beta_c = \check{d}_c} \frac{\kappa^{\beta_a + \beta_c} (-q)^{\pi(\alpha_a, \alpha_c; \beta_a, \beta_c)}}{(q^2)_{\alpha_a} (q^2)_{\beta_a} (q^2)_{\alpha_c} (q^2)_{\beta_c}}, \quad (3.3.17)$$

and

$$\pi(\alpha_a, \alpha_c; \beta_a, \beta_c) = 2\beta_a \alpha_c + \left[2k(\alpha_a + \alpha_c) + l(\beta_a + \beta_c) + 2(h_e \check{d}_e + h_f \check{d}_f) \right] (\beta_a + \beta_c). \quad (3.3.18)$$

The transposition symmetry (3.2.3) now reduces to the simple invariance of the Π factor under $\check{d}_a \leftrightarrow \check{d}_c$, or more formally stated

$$\boxed{\Pi_{\check{d}_c, \check{d}_a, \check{d}_e, \check{d}_f} = \Pi_{\check{d}_a, \check{d}_c, \check{d}_e, \check{d}_f}}. \quad (3.3.19)$$

At first sight, (3.3.16) might seem like a more complicated series than the original quiver series (2.1.40) we started from. Nevertheless, we actually reduced the number of infinite series and independent variables x_i , from $m = 6$ to $m - 2 = 4$ thanks to the symmetry. The situation is analogous to the use of symmetries in other areas of physics where a symmetry reduces the number of degrees of freedom of a system. The method is very similar too, a symmetry leads to constraints, which after a change of variables yield equations or partition functions that are manifestly invariant under such symmetry.

In fact, the Π factor takes a remarkably simple form when $l = 2k + 1$. For that value, we can use the q -binomial theorem [31, Lemma 4.5] to write the two partial sums as a single q -Pochhammer symbol

$$\frac{(\xi)_{\check{d}_a + \check{d}_c}}{(q)_{\check{d}_a} (q^2)_{\check{d}_c}} = \sum_{\alpha_a + \beta_a = \check{d}_a} \sum_{\alpha_c + \beta_c = \check{d}_c} \frac{(\xi q^{-1})^{\beta_a + \beta_c} (-q)^{\beta_a^2 + \beta_c^2 + 2\beta_c \check{d}_a}}{(q^2)_{\alpha_a} (q^2)_{\beta_a} (q^2)_{\alpha_c} (q^2)_{\beta_c}} = \frac{\Pi_{\check{d}_a, \check{d}_c, \check{d}_e, \check{d}_f}}{(q^2)_{\check{d}_a} (q^2)_{\check{d}_c}}, \quad (3.3.20)$$

with

$$\xi = \kappa q^{2(h_e \check{d}_e + h_f \check{d}_f) + 2k(\check{d}_a + \check{d}_c) + 1}. \quad (3.3.21)$$

In this form, the symmetry (3.3.19) under the exchange of indices $\check{d}_a \leftrightarrow \check{d}_c$ is quite explicit.

In what follows we will analyse what happens when there are two or more transposition symmetries. Due to the nature of the constraints (3.2.4b), which are dependent on all nodes, the interplay of two or more transposition symmetries is quite intricate. In certain cases, it would lead to the action of a larger permutation group, whereas in others to unfamiliar compositions of small permutation groups.

3.3.2 General solution of constraints for two or more transposition

Two overlapping symmetries

Let us continue from our last example, that is, from the quiver matrix with one symmetry and already in the block shape (3.3.12). Suppose we have a second symmetry between the nodes $C_{af} \leftrightarrow C_{be}$. Then, we may evaluate (3.3.12) into the constraints (3.2.4) yielding the following relations between its entries

$$\begin{aligned} h_e = k + 1, & & h_f = l - k & & C_{cf} = C_{ce} + k + 1 & & (3.3.22) \\ C_{af} = C_{ae} + k, & & C_{ef} = C_{ee} + k & & C_{bf} = C_{ae} + l, & & C_{ff} = C_{ee} + l. \end{aligned}$$

Plugging the above relations (3.3.26) back into the matrix (3.3.12) we obtain

$$\left[\begin{array}{cc|cc|cc} C_{aa} & C_{aa} + k & C_{ac} & C_{ac} + k & C_{ae} & C_{ae} + k \\ C_{aa} + k & C_{aa} + l & C_{ac} + k + 1 & C_{ac} + l & C_{ae} + k + 1 & C_{ae} + l \\ \hline C_{ac} & C_{ac} + k + 1 & C_{cc} & C_{cc} + k & C_{ce} & C_{ce} + k + 1 \\ C_{ac} + k & C_{ac} + l & C_{cc} + k & C_{cc} + l & C_{ce} + k + 1 & C_{ce} + l + 1 \\ \hline C_{ae} & C_{ae} + k + 1 & C_{ce} & C_{ce} + k + 1 & C_{ee} & C_{ee} + k \\ C_{ae} + k & C_{ae} + l & C_{ce} + k + 1 & C_{ce} + l + 1 & C_{ee} + k & C_{ee} + l \end{array} \right]. \quad (3.3.23)$$

This is a very interesting case, as it shows the nonintuitive relation between this symmetries. For instance, if we apply $C_{ab} \leftrightarrow C_{cd}$ it leads to an equivalent quiver, which does not have $C_{af} \leftrightarrow C_{be}$ as a symmetry. This is because, as we have argued before in subsection 3.2.1 this is due to the overlap between constraints. This results in a set of three equivalent quivers: the initial one, one with $C_{ab} \leftrightarrow C_{cd}$ and one with $C_{af} \leftrightarrow C_{be}$. We will encounter this particular scenario when studying the symmetries of the knot 5_1 .

Although we may find a prequiver for each individual transposition, it is not clear if a prequiver exist in this case for both symmetries. the block structure of the quiver matrix suggest there might be one, we still should consider the solution to the center of mass constraint (3.2.4a) that it also induces a particular change of summation indices. In this case we have the relations

$$\begin{aligned} \lambda_b = \kappa_A \lambda_c, & \quad \lambda_d = \kappa_A \lambda_c, & \quad \lambda_e = \kappa_B \lambda_a, & \quad \lambda_f = \kappa_B \kappa_A \lambda_c \\ \check{d}_a = d_a + d_d + d_e, & & \check{d}_c = d_c + d_b + d_f. & & (3.3.24) \end{aligned}$$

Two symmetries leading to three

We repeat the same analysis as in the afore example (3.3.23) with the difference that now we assume the second symmetry to be $C_{be} \leftrightarrow C_{cf}$. The reason for this is because nodes e and f were spectators for the first symmetry $C_{ab} \leftrightarrow C_{cd}$ and the second symmetry could be thought of as acting on an independent block of the quiver matrix

$$\left[\begin{array}{cc|cc|cc} C_{aa} & C_{ad} & C_{ac} & C_{ab} & C_{ae} & C_{af} \\ C_{ad} & C_{dd} & C_{cd} & C_{bd} & C_{de} & C_{df} \\ \hline C_{ac} & C_{cd} & C_{cc} & C_{bc} & C_{ce} & C_{cf} \\ C_{ab} & C_{bd} & C_{bc} & C_{bb} & C_{be} & C_{bf} \\ \hline C_{ae} & C_{de} & C_{ce} & C_{be} & C_{ee} & C_{ef} \\ C_{af} & C_{df} & C_{cf} & C_{bf} & C_{ef} & C_{ff} \end{array} \right]. \quad (3.3.25)$$

Evaluating the constraints (3.2.4) on (3.3.12) we obtain the following relations

$$\begin{aligned} h_e &= k + 1 & C_{af} &= C_{ae} + k & C_{ff} &= C_{ee} + l \\ h_f &= l - k & C_{ef} &= C_{ee} + k & C_{cf} &= C_{ce} + k \end{aligned} \quad (3.3.26)$$

which produces the quiver matrix

$$\left[\begin{array}{cc|cc|cc} C_{aa} & C_{aa} + k & C_{ac} & C_{ac} + k & C_{ae} & C_{ae} + k \\ C_{aa} + k & C_{aa} + l & C_{ac} + k + 1 & C_{ac} + l & C_{ae} + k + 1 & C_{ae} + l \\ \hline C_{ac} & C_{ac} + k + 1 & C_{cc} & C_{cc} + k & C_{ce} & C_{ce} + k \\ C_{ac} + k & C_{ac} + l & C_{cc} + k & C_{cc} + l & C_{ce} + k + 1 & C_{ce} + l \\ \hline C_{ae} & C_{ae} + k + 1 & C_{ce} & C_{ce} + k + 1 & C_{ee} & C_{ee} + k \\ C_{ae} + k & C_{ae} + l & C_{ce} + k & C_{ce} + l & C_{ee} + k & C_{ee} + l \end{array} \right] \quad (3.3.27)$$

It is important to notice that we only demand that our 6×6 quiver matrix has two independent symmetries. The way we chose them it automatically yields a third new symmetry! The third extra symmetry is $C_{af} \leftrightarrow C_{de}$ in the remaining off-diagonal block

$$\left[\begin{array}{cc|cc|cc} C_{aa} & C_{ad} & C_{ac} & C_{ab} & C_{ae} & C_{af} \\ C_{ad} & C_{dd} & C_{cd} & C_{bd} & C_{de} & C_{df} \\ \hline C_{ac} & C_{cd} & C_{cc} & C_{bc} & C_{ce} & C_{cf} \\ C_{ab} & C_{bd} & C_{bc} & C_{bb} & C_{be} & C_{bf} \\ \hline C_{ae} & C_{de} & C_{ce} & C_{be} & C_{ee} & C_{ef} \\ C_{af} & C_{df} & C_{cf} & C_{bf} & C_{ef} & C_{ff} \end{array} \right]. \quad (3.3.28)$$

We should not forget that this last symmetry is not a symmetry $C_{af} \leftrightarrow C_{de}$ for the current matrix. Due to the fact that it does not satisfy its respective constraints. In order for $C_{af} \leftrightarrow C_{de}$ to lead to a valid equivalent quiver matrix, we must first apply $C_{ab} \leftrightarrow C_{cd}$ or $C_{cf} \leftrightarrow C_{be}$, only then the constraints are satisfied.

As for the 4×4 example (3.3.8) we can decompose our quiver thanks to the tensor product as follows

$$\begin{aligned} \Gamma &= \begin{bmatrix} C_{aa} & C_{ac} & C_{ae} \\ C_{ac} & C_{cc} & C_{ce} \\ C_{ae} & C_{ce} & C_{ee} \end{bmatrix} \otimes \begin{bmatrix} 1 & 1 \\ 1 & 1 \end{bmatrix} + \begin{bmatrix} 1 & 1 & 1 \\ 1 & 1 & 1 \\ 1 & 1 & 1 \end{bmatrix} \otimes \begin{bmatrix} 0 & k \\ k & l \end{bmatrix} \\ &+ \begin{bmatrix} 0 & 0 & 0 \\ 1 & 0 & 0 \\ 1 & 1 & 0 \end{bmatrix} \otimes \begin{bmatrix} 0 & 0 \\ 1 & 0 \end{bmatrix}^T + \begin{bmatrix} 0 & 0 & 0 \\ 1 & 0 & 0 \\ 1 & 1 & 0 \end{bmatrix}^T \otimes \begin{bmatrix} 0 & 0 \\ 1 & 0 \end{bmatrix}. \end{aligned} \quad (3.3.29)$$

We can again use the short hand notation introduced in (3.3.9) and write (3.3.29) as

$$\boxed{\Gamma = \check{C} \otimes 1_{2 \times 2} + 1_{3 \times 3} \otimes \Lambda + L_{3 \times 3} \otimes L_{2 \times 2}^T + L_{3 \times 3}^T \otimes L_{2 \times 2}.} \quad (3.3.30)$$

Now the transposition $C_{ab} \leftrightarrow C_{cd}$ in the above expression acts as

$$\check{C} \otimes 1_{2 \times 2} + 1_{3 \times 3} \otimes \Lambda + \begin{bmatrix} 0 & 1 & 0 \\ 0 & 0 & 0 \\ 1 & 1 & 0 \end{bmatrix} \otimes L_{2 \times 2}^T + \begin{bmatrix} 0 & 1 & 0 \\ 0 & 0 & 0 \\ 1 & 1 & 0 \end{bmatrix}^T \otimes L_{2 \times 2}, \quad (3.3.31)$$

which we rewrite in terms of $L_{3 \times 3}$

$$\begin{bmatrix} 0 & 1 & 0 \\ 0 & 0 & 0 \\ 1 & 1 & 0 \end{bmatrix} = \begin{bmatrix} 0 & 1 & 0 \\ 1 & 0 & 0 \\ 0 & 0 & 1 \end{bmatrix} \begin{bmatrix} 0 & 0 & 0 \\ 1 & 0 & 0 \\ 1 & 1 & 0 \end{bmatrix} \begin{bmatrix} 0 & 1 & 0 \\ 1 & 0 & 0 \\ 0 & 0 & 1 \end{bmatrix}^T = G_{(12)} \cdot L_{3 \times 3} \cdot G_{(12)}^T. \quad (3.3.32)$$

We recognise that $G_{(12)}$ is one of the generators of S_3 representing the permutation $(1, 2, 3) \rightarrow (2, 1, 3)$. Ultimately, the symmetry $C_{ab} \leftrightarrow C_{cd}$ can be nicely written as

$$\check{C} \otimes 1_{2 \times 2} + 1_{3 \times 3} \otimes \Lambda + [G_{(12)} \cdot L_{3 \times 3} \cdot G_{(12)}^T] \otimes L_{2 \times 2}^T + [G_{(12)} \cdot L_{3 \times 3} \cdot G_{(12)}^T]^T \otimes L_{2 \times 2} \quad (3.3.33)$$

Likewise, if we apply $C_{cf} \leftrightarrow C_{be}$ we get

$$\check{C} \otimes 1_{2 \times 2} + 1_{3 \times 3} \otimes \Lambda + \begin{bmatrix} 0 & 0 & 0 \\ 1 & 0 & 1 \\ 1 & 0 & 0 \end{bmatrix} \otimes L_{2 \times 2}^T + \begin{bmatrix} 0 & 0 & 0 \\ 1 & 0 & 1 \\ 1 & 0 & 0 \end{bmatrix}^T \otimes L_{2 \times 2}. \quad (3.3.34)$$

Again, we can represent this as a permutation

$$\begin{bmatrix} 0 & 0 & 0 \\ 1 & 0 & 1 \\ 1 & 0 & 0 \end{bmatrix} = \begin{bmatrix} 1 & 0 & 0 \\ 0 & 0 & 1 \\ 0 & 1 & 0 \end{bmatrix} \begin{bmatrix} 0 & 0 & 0 \\ 1 & 0 & 0 \\ 1 & 1 & 0 \end{bmatrix} \begin{bmatrix} 1 & 0 & 0 \\ 0 & 0 & 1 \\ 0 & 1 & 0 \end{bmatrix}^T = G_{(23)} \cdot L_{3 \times 3} \cdot G_{(23)}^T. \quad (3.3.35)$$

It is now crystal clear that $G_{(2,3)}$ is the second generator of S_3 , the one responsible for the permutation $(1, 2, 3) \rightarrow (1, 3, 2)$. This also produces the simple representation of $C_{cf} \leftrightarrow C_{be}$ in tensor product form

$$\check{C} \otimes 1_{2 \times 2} + 1_{3 \times 3} \otimes \Lambda + (G_{(23)} \cdot L_{3 \times 3} \cdot G_{(23)}^T) \otimes L_{2 \times 2}^T + (G_{(23)} \cdot L_{3 \times 3} \cdot G_{(23)}^T)^T \otimes L_{2 \times 2}. \quad (3.3.36)$$

So far, we have shown that there is a one-to-one correspondence between transpositions on the quiver matrix and the transpositions that generate the permutation group S_3 . Thus, it is logical to expect that the symmetry group for acting on the quiver matrix is S_3 , or that we have $3! = 6$ equivalent quivers. Surprisingly, this intuition is only partially correct! To determine where our intuition fails, let's look at the remaining equivalent quivers and how they are represented in terms of permutation matrices.

Suppose we apply either $C_{ab} \leftrightarrow C_{cd}$, or $C_{cf} \leftrightarrow C_{be}$, then we are able to perform the third transposition $C_{cf} \leftrightarrow C_{be}$. This leads to the remaining three equivalent quiver matrices

$$\begin{aligned} \begin{bmatrix} 0 & 1 & 1 \\ 0 & 0 & 0 \\ 0 & 1 & 0 \end{bmatrix} &= \begin{bmatrix} 0 & 0 & 1 \\ 1 & 0 & 0 \\ 0 & 1 & 0 \end{bmatrix} \begin{bmatrix} 0 & 0 & 0 \\ 1 & 0 & 0 \\ 1 & 1 & 0 \end{bmatrix} \begin{bmatrix} 0 & 0 & 1 \\ 1 & 0 & 0 \\ 0 & 1 & 0 \end{bmatrix}^T = \tau_{(132)} L_{3 \times 3} \tau_{(132)}^T, \\ \begin{bmatrix} 0 & 0 & 1 \\ 1 & 0 & 1 \\ 0 & 0 & 0 \end{bmatrix} &= \begin{bmatrix} 0 & 1 & 0 \\ 0 & 0 & 1 \\ 1 & 0 & 0 \end{bmatrix} \begin{bmatrix} 0 & 0 & 0 \\ 1 & 0 & 0 \\ 1 & 1 & 0 \end{bmatrix} \begin{bmatrix} 0 & 1 & 0 \\ 0 & 0 & 1 \\ 1 & 0 & 0 \end{bmatrix}^T = \tau_{(123)} L_{3 \times 3} \tau_{(123)}^T, \\ \begin{bmatrix} 0 & 1 & 1 \\ 0 & 0 & 1 \\ 0 & 0 & 0 \end{bmatrix} &= \begin{bmatrix} 0 & 0 & 1 \\ 0 & 1 & 0 \\ 1 & 0 & 0 \end{bmatrix} \begin{bmatrix} 0 & 0 & 0 \\ 1 & 0 & 0 \\ 1 & 1 & 0 \end{bmatrix} \begin{bmatrix} 0 & 0 & 1 \\ 0 & 1 & 0 \\ 1 & 0 & 0 \end{bmatrix}^T = \tau_{(13)} L_{3 \times 3} \tau_{(13)}^T, \end{aligned} \quad (3.3.37)$$

were $\tau_{(123)}$ is the corresponding cyclic permutation in cyclic notation, and so for the other two τ 's. Since $C_{af} \leftrightarrow C_{de}$ does not correspond to $\tau_{(13)}$, this reveals that transpositions on the quiver matrix are not in one-to-one correspondence with the three transpositions of S_3 .

In other words, the equivalent quivers, in this case, do correspond to the set permutations of the set of three elements, but the transpositions of the quiver matrix do not correspond to the group S_3 . This is easy to appreciate from the fact that one of the group axioms is that we can always compose any two elements of the group and obtain a third element also in the group. Here, we know we can not apply $C_{ab} \leftrightarrow C_{cd}$ after $C_{cf} \leftrightarrow C_{be}$, or vice versa, because that would lead to a quiver, which is not equivalent.

The correct notion is that the transpositions on the quiver matrix correspond to *inversions* of a permutation. The notion of an inversion is quite intuitive, is a way to quantify how much a permutation disorders a set. The more precise definition says: Suppose that we have the set $\{1, \dots, n\}$, this set has the natural ascending order. We say that a permutation $\tau \in S_n$ has an inversion for each pair of elements that are out of their natural order, e.g. $i < j$, while $\tau(i) > \tau(j)$. We will denote an inversion by (i, j) and a permutation is uniquely specified by all its inversions. Lastly, the number of possible inversions for a permutation of n elements is the triangular number $n(n-1)/2$.

For instance, in the case of S_3 we have the permutation $G_{(12)}$. On the other hand we know $1 < 2$, but $G_{(12)}(1) = 2 > G_{(12)}(2) = 1$. So the permutation set for $G_{(12)}$ is $\{(G_{(12)}(1) = 2, G_{(12)}(2) = 1)\}$. Here is the permutation set associated to each permutation in S_3 (without the identity permutation)

$$\begin{aligned} G_{(12)} &\equiv \{(2, 1)\}, & G_{(23)} &\equiv \{(3, 2)\}, & \tau_{(132)} &\equiv \{(3, 1), (3, 2)\}, \\ \tau_{(123)} &\equiv \{(2, 1), (3, 1)\}, & \tau_{(13)} &\equiv \{(3, 1), (3, 2), (2, 1)\}. \end{aligned} \quad (3.3.38)$$

In this presentation, the relation to transposition on the quiver matrix is much clearer. Lets take (3.3.27) as the starting (unpermuted) matrix. When we decompose it in using the tensor product as in (3.3.29), all information about transpositions is now in $L_{3 \times 3}$. When we apply the transposition $C_{ab} \leftrightarrow C_{cd}$, or $G_{(12)}$, the action it has on $L_{3 \times 3}$ we can see on the l.h.s. of (3.3.32) is to swap the elements of the entries $(1, 2) \leftrightarrow (2, 1)$. In general, we can think of the off-diagonal entries of $L_{3 \times 3}$ as inversions, and if a permutation has an inversions (i, j) , or $(\tau(i), \tau(j))$, we take them as indicating entries on $L_{3 \times 3}$ and swap $L_{i,j} = 0 \leftrightarrow L_{\tau(i), \tau(j)} = 1$.

As now expected, the identification between transpositions and inversions in our case is

$$\boxed{C_{ab} \leftrightarrow C_{cd} \equiv (2, 1), \quad C_{cf} \leftrightarrow C_{be} \equiv (3, 2), \quad C_{cf} \leftrightarrow C_{be} \equiv (3, 1).} \quad (3.3.39)$$

This also explains why we are not able to apply $C_{cf} \leftrightarrow C_{be}$ directly on (3.3.27). Namely, permutations containing that transposition also invert other elements, or contain the other transpositions too.

Regarding the center of mass conditions (3.2.4a) we have the following relations

$$\begin{aligned} \lambda_d &= \kappa \lambda_a, & \lambda_b &= \kappa \lambda_c, & \lambda_f &= \kappa \lambda_e, & (3.3.40) \\ \check{d}_a &= d_a + d_d, & \check{d}_c &= d_c + d_b, & \check{d}_e &= d_e + d_f, \end{aligned}$$

with $\alpha_a = d_a$, $\beta_a = d_d$, $\alpha_c = d_c$, $\beta_c = d_b$, $\alpha_e = d_e$ and $\beta_e = d_f$.

We can substitute (3.3.29) into the quiver series along with the afore relations (3.3.40) to obtain

$$\sum_{\check{d}_a, \check{d}_c, \check{d}_e, \geq 0} \frac{(x\lambda_a)^{\check{d}_a} (x\lambda_c)^{\check{d}_c} (x\lambda_e)^{\check{d}_e}}{(q^2)_{\check{d}_a} (q^2)_{\check{d}_b} (q^2)_{\check{d}_e}} (-q)^{\sum_{i,j} \check{C}_{\check{d}_i \check{d}_j}} \Pi_{\check{d}_a, \check{d}_c, \check{d}_e}, \quad (3.3.41)$$

with

$$\frac{\Pi_{\check{d}_a, \check{d}_c, \check{d}_e}}{(q^2)_{\check{d}_a} (q^2)_{\check{d}_c} (q^2)_{\check{d}_e}} = \sum_{\alpha_a + \beta_a = \check{d}_a} \sum_{\alpha_c + \beta_c = \check{d}_c} \sum_{\alpha_e + \beta_e = \check{d}_e} \frac{\kappa^{\beta_a + \beta_c + \beta_e} (-q)^{\pi(\alpha_a, \alpha_c, \alpha_e; \beta_a, \beta_c, \alpha_e)}}{(q^2)_{\alpha_a} (q^2)_{\beta_a} (q^2)_{\alpha_c} (q^2)_{\beta_c}}, \quad (3.3.42)$$

and

$$\begin{aligned} \pi(\alpha_a, \alpha_c, \alpha_e; \beta_a, \beta_c, \beta_e) = \\ 2(\beta_a \alpha_c + \beta_c \alpha_e) + [2k(\alpha_a + \alpha_c + \alpha_e) + l(\beta_a + \beta_c + \beta_e)](\beta_a + \beta_c + \beta_e). \end{aligned} \quad (3.3.43)$$

This is a generalized version of (3.3.16) for a quiver with three symmetries (3.3.25). Similarly as for the one symmetry (3.3.19) case $\Pi_{\check{d}_a, \check{d}_c, \check{d}_e}$ factor in (3.3.42) is invariant under any permutation of its three indices. This crucial observation allows us to finally make contact with S_3 . All equivalent quivers that arise from transpositions on (3.3.28) can be identified with a permutation of the indices of $\Pi_{\check{d}_a, \check{d}_c, \check{d}_e}$. Moreover, we now can correctly define the action of S_3 on $\Pi_{\check{d}_a, \check{d}_c, \check{d}_e}$ as the symmetry group behind the equivalent quivers.

Moreover, the starting two transpositions $C_{ab} \leftrightarrow C_{cd}$ and $C_{cf} \leftrightarrow C_{be}$ correspond to the two transpositions $\Pi_{\check{d}_c, \check{d}_a, \check{d}_e}$ and $\Pi_{\check{d}_a, \check{d}_e, \check{d}_c}$, respectively. This is why any quiver matrix having the afore symmetries leads automatically to a third one.

Again (3.3.42) has the nice simplification when $l = 2k + 1$

$$\frac{(\xi)_{\check{d}_a + \check{d}_c + \check{d}_e}}{(q)_{\check{d}_a} (q^2)_{\check{d}_c} (q^2)_{\check{d}_e}} = \sum_{\alpha_a + \beta_a = \check{d}_a} \sum_{\alpha_c + \beta_c = \check{d}_c} \sum_{\alpha_e + \beta_e = \check{d}_e} \frac{(\xi q^{-1})^{\beta_a + \beta_c + \beta_e} (-q)^{\beta_a^2 + \beta_c^2 + \beta_e^2 + 2(\beta_c \check{d}_a + \beta_e \check{d}_c)}}{(q^2)_{\alpha_a} (q^2)_{\beta_a} (q^2)_{\alpha_c} (q^2)_{\beta_c} (q^2)_{\alpha_e} (q^2)_{\beta_e}}, \quad (3.3.44)$$

with

$$\xi = \kappa q^{2k(\check{d}_a + \check{d}_c + \check{d}_e) + 1}. \quad (3.3.45)$$

n symmetries leading to S_{n+1}

All generating functions for the superpolynomials we will encounter are written in terms of the q -Pochhammer symbol. This will be the origin of several, but not all the symmetries we will study in our quiver. Without further ado, here we present the general formula for decomposing a q -Pochhammer with \check{d}_s , for $s = 1, \dots, n$ indices into n partial sums

$$\begin{aligned} \frac{(\xi)_{\check{d}_1 + \dots + \check{d}_n}}{(q^2)_{\check{d}_1} \dots (q^2)_{\check{d}_n}} = \sum_{\alpha_1 + \beta_1 = \check{d}_1} \dots \sum_{\alpha_n + \beta_n = \check{d}_n} (-q)^{\beta_1^2 + \dots + \beta_n^2 + 2 \sum_{i=1}^{n-1} \beta_{i+1} (\check{d}_1 + \dots + \check{d}_i)} \times \\ \times \frac{(\xi q^{-1})^{\beta_1 + \dots + \beta_n}}{(q^2)_{\alpha_1} (q^2)_{\beta_1} \dots (q^2)_{\alpha_n} (q^2)_{\beta_n}}. \end{aligned} \quad (3.3.46)$$

The relevant observation is that the l.h.s. of (3.3.46) is manifestly invariant under any permutation of its indices \check{d}_s . This implies that the r.h.s. must also be invariant under such permutations. In the exponent of $(-q)$ we have $\sum_{i=1}^{n-1} \beta_{i+1}(\check{d}_1 + \dots + \check{d}_i) = \sum_{i>j} \beta_i \alpha_j + \sum_{i>j} \beta_i \beta_j$, so the first term $\sum_{i>j} \beta_i \alpha_j$ is responsible for the equivalent quivers, while $\sum_{i>j} \beta_i \beta_j$ is the second elementary symmetric polynomial, which is symmetric in all β_i .

To make contact with the symmetries arising from quiver matrices like (3.3.21) and (3.3.45) we define ξ to be

$$\xi = \kappa q^{2(h_{n+1}\check{d}_{n+1} + \dots + h_{m-n}\check{d}_{m-n}) + 2k(\check{d}_1 + \dots + \check{d}_n) + 1}, \quad (3.3.47)$$

where we are assuming that we have a quiver with m nodes and we have $m - n$ spectator nodes with respective $h_s \in \mathbb{Z}$ as in (3.3.11). Also, κ and k are the parameters arising from the solutions to the constraints (3.2.4b)

As we have argued before, the q -Pochhammer (3.3.46) is a very convenient and compact way to encode the symmetries arising from the quiver matrix. Nevertheless, there is a way to introduce an extra l parameter which gives us the generality we need for any symmetry in the quiver matrix arising from theorem 2. Namely, we refer to the $\Pi_{\check{d}_1, \dots, \check{d}_n}$ factor of the form

$$\begin{aligned} \frac{\Pi_{\check{d}_1, \dots, \check{d}_n}}{(q^2)_{\check{d}_1} \cdots (q^2)_{\check{d}_n}} &= \sum_{\alpha_1 + \beta_1 = \check{d}_1} \cdots \sum_{\alpha_n + \beta_n = \check{d}_n} \frac{\kappa^{\beta_1 + \dots + \beta_n}}{(q^2)_{\alpha_1} (q^2)_{\beta_1} \cdots (q^2)_{\alpha_n} (q^2)_{\beta_n}} \\ &\times (-q)^{2\sum_{i<j} \beta_i \alpha_j + (2\sum_{s=n+1}^{m-n} h_s \check{d}_s + 2k(\alpha_1 + \dots + \alpha_n) + l(\beta_1 + \dots + \beta_n))(\beta_1 + \dots + \beta_n)}, \end{aligned} \quad (3.3.48)$$

where we have the special case when $l = 2k + 1$ the formula reduces to (3.3.46). We do not know, if there is a compact product formula for $\Pi_{\check{d}_1, \dots, \check{d}_n}$ for generic l , however it is not an obstacle for us, since all we need its invariance under permutation of its indices \check{d}_s .

The above formula will be so important for us that we will define it as an operation relating a quiver and a prequiver.

Definition 3. Let \check{C} be an $(m - n) \times (m - n)$ prequiver matrix with $m \geq 2n \geq 4$ written as

$$\check{C} = \left[\begin{array}{ccc|ccc} \check{C}_{1,1} & \cdots & \check{C}_{1,n} & \check{C}_{1,n+1} & \cdots & \check{C}_{1,m-n} \\ \vdots & \ddots & \vdots & \vdots & \ddots & \vdots \\ \check{C}_{1,n} & \cdots & \check{C}_{n,n} & \check{C}_{n,n+1} & \cdots & \check{C}_{n,m-n} \\ \hline \check{C}_{1,n+1} & \cdots & \check{C}_{n,n+1} & \check{C}_{n+1,n+1} & \cdots & \check{C}_{n+1,m-n} \\ \vdots & \ddots & \vdots & \vdots & \ddots & \vdots \\ \check{C}_{1,m-n} & \cdots & \check{C}_{n,m-n} & \check{C}_{n+1,m-n} & \cdots & \check{C}_{m-n,m-n} \end{array} \right] = \left[\begin{array}{c|c} \check{\Gamma} & \check{\Phi} \\ \check{\Phi}^T & \Sigma \end{array} \right], \quad (3.3.49)$$

with the respective λ s from the knot change of variables (2.3.2)

$$\check{\lambda} = \left[\check{\lambda}_1, \dots, \check{\lambda}_n \mid \check{\lambda}_{n+1}, \dots, \check{\lambda}_{m-n} \right]^T = \left[\check{\lambda}_\gamma \mid \check{\lambda}_\sigma \right]^T, \quad (3.3.50)$$

where $\gamma = 1, \dots, n$ and $\sigma = n + 1, \dots, m - n$.

Then, a (k, l) -splitting of n nodes of the prequiver in the presence of $m - 2n$ spectator nodes (with corresponding integer shifts h_σ) yields the following quiver matrix C of size $m \times m$

$$\check{C} \longrightarrow C = \left[\begin{array}{c|c} \Gamma & \Phi \\ \hline \Phi^T & \Sigma \end{array} \right], \quad (3.3.51)$$

where Γ and Φ are given by

$$\Gamma = \check{\Gamma} \otimes 1_{2 \times 2} + 1_{n \times n} \otimes \Lambda + L_{n \times n} \otimes L_{2 \times 2}^T + L_{n \times n}^T \otimes L_{2 \times 2}, \quad (3.3.52)$$

with Λ , $1_{r \times s}$ and $L_{r \times s}$ are defined in (3.3.9); whereas

$$\Phi = \check{\Phi} \otimes 1_{2 \times 1} + 1_{n \times 1} \otimes H \otimes L_{1,2}^T, \quad H = [h_{n+1}, h_{n+2}, \dots, h_{m-n}]. \quad (3.3.53)$$

When the splitting is in unpermuted, or in its natural order, we obtain $L_{n \times n}$ in the tensor decomposition (3.3.52). It will be convenient sometimes to give the permuted version of the quiver matrix $\tau L_{n \times n} \tau^T$, where $\tau \in S_n$ in the matrix representation. In that case we specify τ in terms of its inversion set. In our convention for two splitted nodes in the prequiver matrix are inverted if i and j , $i < j$, but $\tau(i) > \tau(j)$, then $L_{i,j} \leftrightarrow L_{\tau(i),\tau(j)}$. If $i < j$, and $\tau(i) < \tau(j)$, then $L_{i,j}$ and $L_{\tau(i),\tau(j)}$ are unchanged.

Lastly, (k, l) -splitting also transforms $\check{\lambda}$ as follows

$$\check{\lambda} \longrightarrow \lambda = \left[\check{\lambda}_1, \kappa \check{\lambda}_1, \check{\lambda}_2, \kappa \check{\lambda}_2, \dots, \check{\lambda}_n, \kappa \check{\lambda}_n \mid \check{\lambda}_{n+1}, \dots, \check{\lambda}_{m-n} \right]^T = \left[\check{\lambda}_\gamma \otimes [1, \kappa] \mid \check{\lambda}_\sigma \right]^T \quad (3.3.54)$$

It is worth mentioning that, in practice we will not always provide the prequiver in a block structure as in (3.3.49). In those situations, we will explicitly state which nodes of the prequiver we will be (k, l) -splitting and which are the spectators. In addition, we will specify the values of all parameters k , l and h_σ .

To better grasp the reason why we introduced the notion of (k, l) -splitting it is worth looking at the simplest examples. For instance, take the prequiver \check{C} in (3.3.14), which has $m = 6$ and $n = 2$. If we perform (k, l) -splitting on that prequiver, we obtain (3.3.12), which was the general form of a quiver matrix that admits the transposition $C_{ab} \leftrightarrow C_{cd}$. Additionally, that transposition could be thought as the generator $G_{(12)}$ of the group S_2 .

Similarly, if we start from the prequiver (3.3.29), with $m = 6$ and $n = 3$. We may also apply (k, l) -splitting to that prequiver to obtain (3.3.25), which we obtain as the most general solution to the constraints for the two symmetries $C_{ab} \leftrightarrow C_{cd}$ and $C_{be} \leftrightarrow C_{cf}$. There we also noticed that those two symmetries can be identified with the two generators $G_{(12)}$ and $G_{(2,3)}$ of S_3 .

On the other hand, it is not possible to write (3.3.23) as a (k, l) -splitting. Although the form of that quiver matrix is almost identical to that of a (3.3.25), their λ_i and \check{d}_i are considerably different. What it is possible in this case is to find a prequiver and a (k, l) -splitting for of each transpositions $C_{ab} \leftrightarrow C_{cd}$ and $C_{af} \leftrightarrow C_{be}$ separately. In this sense, we may say that (k, l) -splitting is the operation relating all equivalent quivers.

To summarize, we could say that starting from the quiver matrix, finding its symmetries, and solving the constraints leads us to a prequiver. Whereas (k, l) -splitting is the inverse, we start from a prequiver and we obtain a quiver matrix which satisfies the constraints and has the desired symmetries.

The other advantage of using (k, l) -splitting, on n nodes of the prequiver, is that it automatically gives the whole $n!$ equivalent quivers. Working the other way around is much harder. Starting from a quiver matrix and determining if a set of symmetries reduces to a (k, l) -splitting in principle would require to identify all $n(n-1)/2$ symmetries, one by one.

In practice, as we have seen, we do not need to derive all $n(n-1)/2$ symmetries to bring it to a (k, l) -splitting form (3.3.51). As we noticed in (3.3.28), we started from two symmetries that gave the quiver matrix (3.3.25) a block structure. Those two symmetries were enough to determine the (k, l) -splitting structure, this because they are identified with the generators of S_3 .

This means that in general, we only need to find $n-1$ symmetries. Next, take the submatrix Γ of the quiver matrix C where those symmetries act on, and verify it Γ has a block structure. Each block should be a 2×2 matrix, and the blocks containing the transposable elements should lie on the supradiagonal of Γ ⁶. If all the afore conditions are satisfied, the $n-1$ blocks on the supradiagonal will correspond to the generators of S_n . Having identified the generators of S_n , the remaining $(n-1)(n-2)/2$ symmetries and the (k, l) -splitting form (3.3.51) directly follow.

Lastly, $N_C(s) \geq 1$ is the number of equivalent quiver matrices to C , as a function of the number of symmetries $s \geq 0$, with $N_C(s=0) = 1$. We will provide some simple lower and upper bounds for $N_C(s)$.

The lower bound is obtained when we can not compose any two symmetries. This because applying one would spoil the constraints of the other. In this situation, we can apply each transposition at most once, then undo it, in order to apply the next one. This gives one more equivalent quiver matrix for each symmetry, namely, $N_C(s) \geq s+1$.

The upper bound on is the opposite scenario. Suppose that we are free to apply any transposition after another. Consequently, this leads to $N_C(s) \leq 2^s$.

Therefore, if $N_C(s)$ is bounded by

$$1 \leq s+1 \leq N_C(s) \leq 2^s. \quad (3.3.55)$$

We see that this is also satisfied in the case of (k, l) -splitting when those s symmetries are identified with the $n-1$ generators of S_n as $n-1 = s$,

$$1 \leq s+1 \leq N_C(s) = (s+1)! \leq 2^{\frac{s(s+1)}{2}}. \quad (3.3.56)$$

3.3.3 Permutohedra – what they are and why they arise

We begin by recalling that a *permutohedron* of order n , denoted Π_n , is an $(n-1)$ -dimensional polytope whose vertices represent permutations of n objects $\{1, \dots, n\}$ and edges correspond to flips (transpositions) of adjacent neighbors [43, 84]. In figure 3.4 we can see examples of the first few permutohedra. To represent some of this higher-dimensional objects, we take the skeleton of the polytope (the graph consisting of vertices and edges) and embed it in a plane.

Some useful facts about the permutohedron Π_n are that it has $n!$ vertices and each vertex has $n-1$ immediate neighbors. Π_n has also $(n-1)n!/2$ edges; each

⁶The supradiagonal is the diagonal above the main diagonal of a square matrix.

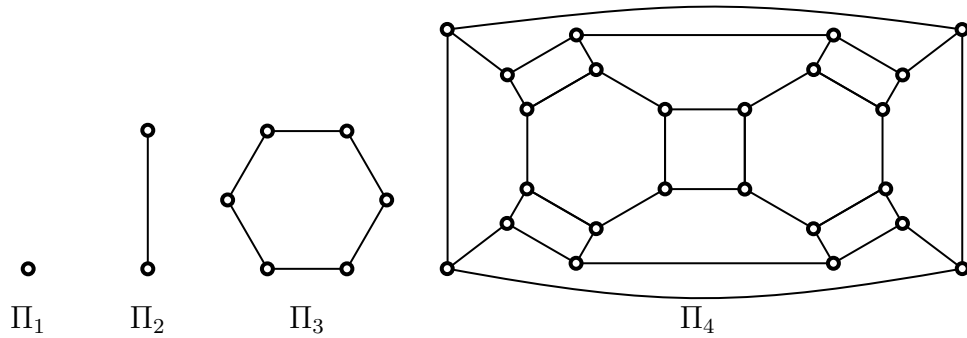


Figure 3.4: Planar realizations of permutohedra Π_n of orders 1, 2, 3, 4. One quadrangular face of Π_4 is represented by an external region. Three-dimensional representation of permutohedron Π_4 is shown in figure 3.6.

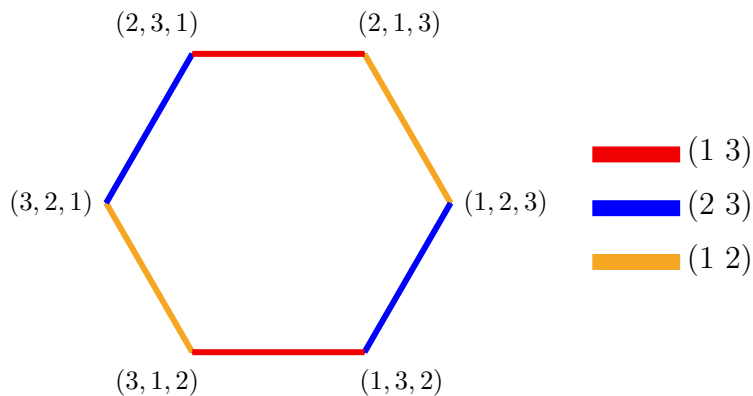


Figure 3.5: Permutohedron Π_3 . Each vertex represents a particular permutation of 3 elements. Two vertices are connected by an edge if corresponding permutations differ by a flip of immediate neighbors. There are 3 types of flips, $(1\ 2)$, $(2\ 3)$ and $(1\ 3)$, which are represented by different colors in the figure.

edge corresponds to one of $n(n - 1)/2$ types of flips (or transposition) $(i\ j)$ (for $1 \leq i < j \leq n$)⁷. To keep track of the flips, it is convenient to assign colors to each of them; in that way we construct a colored version of the permutohedra, see for example figures 3.6 and 3.5.

In figure 3.5 we can see that Π_3 is a hexagon. On the other hand, Π_4 is a (3-dimensional) truncated octahedron consisting of $4! = 24$ vertices. It has 36 edges of 6 different types, such that 3 edges meet at each vertex, and its faces form 6 quadrangles and 8 hexagons, see figure 3.6.

In a few words, a permutohedra is a very convenient visual representation of the permutation of n elements, which encodes transpositions as edges. The map relating the permutohedra to the (k, l) -splitting is that:

- Vertices correspond to equivalent quiver matrices.
- Edges correspond to symmetries, or inversions.
- $n - 1$ edges at each vertex match the generators of S_n .

⁷We refer to them as flips to distinguish them from transpositions of elements of quiver matrices. Although, transpositions in quiver matrices are equivalent to flips.

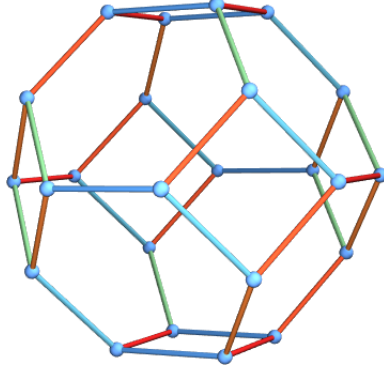


Figure 3.6: Permutohedron Π_4 . Its vertices are labeled by permutations of elements $\{1, 2, 3, 4\}$, and different colors of edges correspond to different types of transpositions $(i j)$ (for $1 \leq i < j \leq 4$). Vertices connected by an edge differ by one transposition of neighboring elements.

- Colors represent which elements in the quiver matrix are transposed.

This visual representation will prove itself extremely useful when we start in the next section when we investigate the quivers associated to knots.

3.4 Equivalent quivers for knots

In this section, we analyze in detail the equivalent quivers and the structure of their symmetry graphs, which we will refer to as permutohedra graphs, for knots 3_1 , 4_1 , 5_1 , 5_2 , 6_1 and 7_1 . After that, we present the knots 6_2 , 6_3 and 7_3 , which are neither torus knots, nor twist knots, and we take them as stand-alone examples. At the end of this section, we summarise our results in table 3.1.

Remark 4. *To have more compact expressions, let us introduce the bold font notation used in [42]*

$$\mathbf{x} = [x_1, x_2, \dots, x_m]^T, \quad \boldsymbol{\lambda} = [\lambda_1, \lambda_2, \dots, \lambda_m]^T, \quad \mathbf{d} = [d_1, d_2, \dots, d_m]^T, \\ \mathbf{x}^{\mathbf{d}} = x_1^{d_1} x_2^{d_2} \dots x_m^{d_m}, \quad (q^2)^{\mathbf{d}} = (q^2)_{d_1} (q^2)_{d_2} \dots (q^2)_{d_m}, \quad (3.4.1)$$

and analogously for $\check{\mathbf{x}}$, $\check{\boldsymbol{\lambda}}$ and $\check{\mathbf{d}}$.

In terms of the new variables, the quiver generating series (2.1.40) takes the more compact form

$$P_Q(\mathbf{x}, q) = \sum_{\mathbf{d}} (-q)^{\mathbf{d} \cdot \mathbf{C} \cdot \mathbf{d}} \frac{\mathbf{x}^{\mathbf{d}}}{(q^2; q^2)_{\mathbf{d}}} \equiv \sum_{d_1, \dots, d_m \geq 0} (-q)^{\sum_{i,j=1}^m C_{ij} d_i d_j} \frac{x_1^{d_1} \dots x_m^{d_m}}{(q^2; q^2)_{d_1} \dots (q^2; q^2)_{d_m}}. \quad (3.4.2)$$

3.4.1 Trefoil knot, 3_1

The generating function of superpolynomials of the knot 3_1 is given by [27]

$$P_{3_1}(x, a, q, t) = \sum_{r=0}^{\infty} \frac{x^r a^{2r} q^{-2r}}{(q^2)_r} \sum_{k=0}^r \begin{bmatrix} r \\ k \end{bmatrix} q^{2k(r+1)} t^{2k} (-a^2 q^{-2} t)_k, \quad (3.4.3)$$

where we use the q -binomial

$$\begin{bmatrix} r \\ k \end{bmatrix} = \frac{(q^2)_r}{(q^2)_{r-k}(q^2)_k}. \quad (3.4.4)$$

The coefficient of the first-order term ($r = 1$) of (3.4.3) is the uncolored superpolynomial $P_1(a, q, t) = a^2q^{-2} + a^2q^2t^2 + a^4t^3$. Its homological diagram consists of one zig-zag composed of 3 nodes, see figure 3.7.

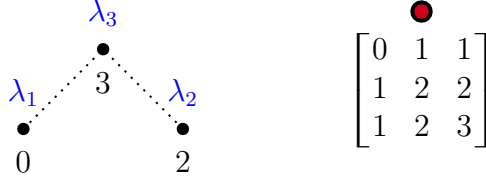


Figure 3.7: Homology diagram and a quiver matrix for 3_1 knot. The labels 0, 2 and 3 are t -degrees of generators, while λ_i arise in specialization of quiver generating parameters. For 3_1 knot the quiver is unique, so the permutohedra graph consists of one vertex (shown in red).

Let us derive the trefoil quiver taking advantage of the formula for a q -Pochhammer with several indices (3.3.46). First, if we keep the q -Pochhammer $(-a^2q^{-2}t)_k$ aside, the rest of $P_{3_1}(x, a, q, t)$ can be expressed in a quiver form. To do that, we use (3.4.4) to rewrite the q -binomial and cancel $(q^2)_r$:

$$\sum_{r=0}^{\infty} \frac{x^r a^{2r} q^{-2r}}{(q^2)_r} \sum_{k=0}^r \begin{bmatrix} r \\ k \end{bmatrix} q^{2k(r+1)} t^{2k} = \sum_{r=0}^{\infty} x^r a^{2r} q^{-2r} \sum_{k=0}^r \frac{1}{(q^2)_{r-k}(q^2)_k} q^{2k(r+1)} t^{2k}. \quad (3.4.5)$$

Then, we introduce new summation indices: $\check{d}_1 = r - k$ and $\check{d}_2 = k$, which brings (3.4.5) closer to a motivic generating function for the prequiver:

$$\sum_{\check{d}_1, \check{d}_2 \geq 0} (-q)^{2\check{d}_1\check{d}_2 + 2\check{d}_2^2} \frac{(xa^2q^{-2})^{\check{d}_1} (xa^2(-t)^2)^{\check{d}_2}}{(q^2)_{\check{d}_1}(q^2)_{\check{d}_2}} = \sum_{\check{d}} (-q)^{\check{d} \cdot \check{C} \cdot \check{d}} \frac{\check{x}^{\check{d}}}{(q^2)_{\check{d}}} \Bigg|_{\check{x} = x\check{\lambda}}, \quad (3.4.6)$$

$$\check{C} = \begin{bmatrix} 0 & 1 \\ 1 & 2 \end{bmatrix}, \quad \check{\lambda} = \begin{bmatrix} a^2q^{-2} \\ a^2(-t)^2 \end{bmatrix}.$$

Lets reintroduce $(-a^2q^{-2}t)_k$ with $k = \check{d}_2$ and use (3.3.46) for splitting one node (because only one \check{d}_i enters k):

$$\frac{(\xi)_{\check{d}_i}}{(q^2)_{\check{d}_i}} = \sum_{\alpha_i + \beta_i = \check{d}_i} (-q)^{\beta_i^2} \frac{(\xi q^{-1})^{\beta_i}}{(q^2)_{\alpha_i}(q^2)_{\beta_i}}, \quad (3.4.7)$$

with $\xi = -a^2q^{-2}t$ and $i = 2$. We then have

$$P_{3_1}(x, a, q, t) = \sum_{d_1, \alpha_2, \beta_2 \geq 0} \frac{(xa^2q^{-2})^{d_1} (xa^2(-t)^2)^{\alpha_2} (xa^4q^{-3}(-t)^2)^{\beta_2}}{(q^2)_{d_1}(q^2)_{\alpha_2}(q^2)_{\beta_2}} \times (-q)^{2d_1\alpha_2 + 2d_1\beta_2 + 2\alpha_2^2 + 2\alpha_2\beta_2 + 3\beta_2^2}, \quad (3.4.8)$$

which equals $P_Q(\mathbf{x}, q)|_{\mathbf{x}=x\boldsymbol{\lambda}}$ for

$$C = \left[\begin{array}{c|cc} 0 & 1 & 1 \\ \hline 1 & 2 & 2 \\ 1 & 2 & 3 \end{array} \right], \quad \boldsymbol{\lambda} = \begin{bmatrix} a^2q^{-2} \\ a^2(-t)^2 \\ a^4q^{-3}(-t)^3 \end{bmatrix}. \quad (3.4.9)$$

This is the quiver already obtained in [30, 31]; in terms of splitting 3 this quiver arises from (3.4.6) by (0, 1)-splitting of the second node, with trivial permutation $\sigma(2) = 2$, $h_1 = 0$, and $\kappa = -a^2q^{-3}t$:

$$\begin{aligned} \check{C} = \left[\begin{array}{c|c} 0 & 1 \\ \hline 1 & 2 \end{array} \right] &\longrightarrow C = \left[\begin{array}{c|cc} 0 & 1 & 1+0 \\ \hline 1 & 2 & 2+0 \\ 1+0 & 2+0 & 2+1 \end{array} \right], \\ \check{\boldsymbol{\lambda}} = \begin{bmatrix} a^2q^{-2} \\ a^2(-t)^2 \end{bmatrix} &\longrightarrow \boldsymbol{\lambda} = \begin{bmatrix} a^2q^{-2} \\ a^2(-t)^2 \\ a^2(-t)^2 \times a^2q^{-3}(-t) \end{bmatrix}. \end{aligned} \quad (3.4.10)$$

We expect that the above quiver (3.4.10) is unique. The reason being that there are no possible permutations when splitting a single node. A sufficient independent argument is that, since the trefoil knot is thin, and quiver equivalences come from permutations of off-diagonal matrix entries. However, to make a pairing we need at least a 4×4 matrix, and our matrix is 3×3 . Hence, there are no other permutation possible. This is the first nontrivial confirmation of our conjecture 1.

3.4.2 Figure-eight knot, 4_1

The two equivalent quivers for the figure-eight knot were found in [31, 39]. In that reference the authors proved the equivalence of the two quivers using unlinking (3.1.3). That is why it is instructive to arrive to the same conclusion, but through the prequiver and splitting. The generating function of superpolynomials of the figure-eight knot is [27]:

$$P_{4_1}(x, a, q, t) = \sum_{r=0}^{\infty} \sum_{k=0}^r \frac{x^r (-1)^k a^{-2k} t^{-2k} q^{-k^2+3k} (q^{-2r})_k (-a^2 q^{-2} t)_k (-a^2 q^{2r} t^3)_k}{(q^2)_r (q^2)_k}.$$

The uncolored superpolynomial is $P_1(a, q, t) = 1 + a^{-2}t^{-2} + q^{-2}t^{-1} + q^2t + a^2t^2$. Its homological diagram is made of a degenerate zig-zag that reduces to a single node, and a diamond, as in figure 3.8.

First, we need $(q^{-2r})_k = (-1)^k q^{-2rk+k(k-1)} \frac{(q^2)_r}{(q^2)_{r-k}}$, together with as (3.4.7) for $(-a^2 q^{2r} t^3)_k / (q^2)_k$, this gives us the prequiver

$$\sum_{0 \leq k \leq r} \frac{x^r (-1)^k a^{-2k} t^{-2k} q^{-k^2+3k} (q^{-2r})_k (-a^2 q^{2r} t^3)_k}{(q^2)_r (q^2)_k} = \sum_{\check{\mathbf{d}}} \frac{(-q)^{\check{C} \cdot \check{\mathbf{d}}} \check{\mathbf{x}}^{\check{\mathbf{d}}}}{(q^2)_{\check{\mathbf{d}}}} \Big|_{\check{\mathbf{x}}=x\check{\boldsymbol{\lambda}}},$$

$$\check{C} = \left[\begin{array}{c|cc} 0 & -1 & 0 \\ \hline -1 & -2 & -1 \\ 0 & -1 & 1 \end{array} \right], \quad \check{\boldsymbol{\lambda}} = \begin{bmatrix} 1 \\ a^{-2}q^2(-t)^{-2} \\ q(-t) \end{bmatrix}, \quad (3.4.11)$$

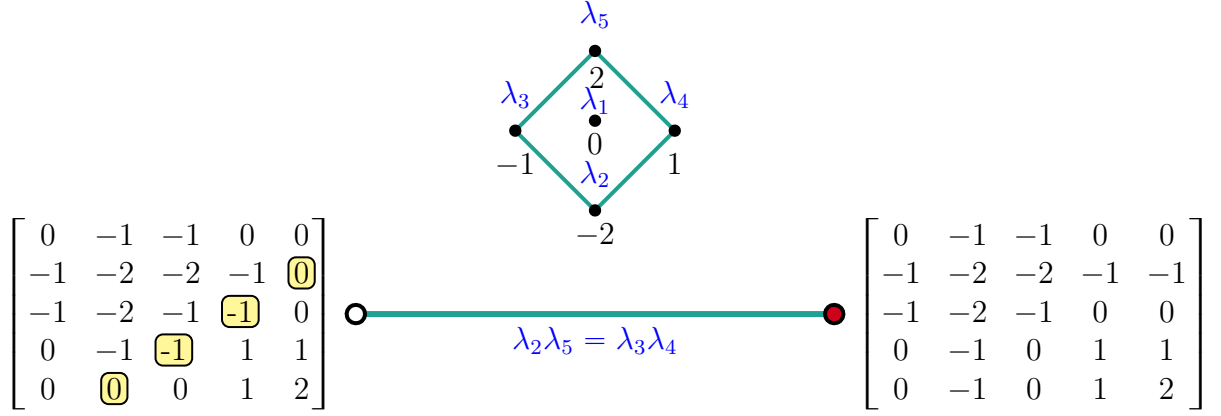


Figure 3.8: Homological diagram for 4_1 knot, with labels λ_i assigned to various nodes (top). In the bottom the two equivalent quivers are shown, which differ by a transposition of elements $C_{2,5}$ and $C_{3,4}$ of the quiver matrix (shown in yellow, together with their symmetric companions). The positions of these elements are encoded in combinations $\lambda_2\lambda_5$ and $\lambda_3\lambda_4$, which are equal to each other (satisfy the center of mass condition).

where we substitute $r-k = \check{d}_1$ and $k = \check{d}_2 + \check{d}_3$. In addition, we rewrite the remaining term $(-a^2q^{-2}t)_k \equiv (-a^2q^{-2}t)_{\check{d}_2+\check{d}_3}$, using (3.3.46) for $n = 2$:

$$\frac{(\xi)_{\check{d}_i+\check{d}_j}}{(q^2)_{\check{d}_i}(q^2)_{\check{d}_j}} = \sum_{\alpha_i+\beta_i=\check{d}_i} \sum_{\alpha_j+\beta_j=\check{d}_j} (-q)^{\beta_i^2+\beta_j^2+2\beta_i(\alpha_j+\beta_j)} \frac{(\xi q^{-1})^{\beta_i}}{(q^2)_{\alpha_i}(q^2)_{\beta_i}} \frac{(\xi q^{-1})^{\beta_j}}{(q^2)_{\alpha_j}(q^2)_{\beta_j}}. \quad (3.4.12)$$

The appearance of the two equivalent quivers is due to the two possibilities (i, j) in the term $\beta_i\alpha_j$, or (j, i) $\beta_j\alpha_i$. Taking $(i, j) = (2, 3)$, the quadratic terms in the exponent of $(-q)$ we derive the quiver matrix:

$$C = \left[\begin{array}{c|ccc|cc} 0 & -1 & -1 & 0 & 0 \\ -1 & -2 & -2 & -1 & -1 \\ -1 & -2 & -1 & 0 & 0 \\ \hline 0 & -1 & 0 & 1 & 1 \\ 0 & -1 & 0 & 1 & 2 \end{array} \right], \quad \lambda = \begin{bmatrix} 1 \\ a^{-2}q^2(-t)^{-2} \\ q^{-1}(-t)^{-1} \\ q(-t) \\ a^2q^{-2}(-t)^2 \end{bmatrix} \quad (3.4.13)$$

which is the one obtained in [31] (up to a permutation of rows and columns). We assign it to the red dot in figure 3.8.

Meanwhile, having $(i, j) = (3, 2)$ produces

$$C = \left[\begin{array}{c|ccc|cc} 0 & -1 & -1 & 0 & 0 \\ -1 & -2 & -2 & -1 & 0 \\ -1 & -2 & -1 & -1 & 0 \\ \hline 0 & -1 & -1 & 1 & 1 \\ 0 & 0 & 0 & 1 & 2 \end{array} \right], \quad \lambda = \begin{bmatrix} 1 \\ a^{-2}q^2(-t)^{-2} \\ q^{-1}(-t)^{-1} \\ q(-t) \\ a^2q^{-2}(-t)^2 \end{bmatrix} \quad (3.4.14)$$

which yields the second quiver found in [39]. We can see the same two quivers in figure 3.8, both are related by a transposition of elements highlighted in yellow. This transposition corresponds to the unique inversion possible for $\beta_i\alpha_j$ in (3.4.12).

We say that the two quivers (3.4.13) and (3.4.14) appear thanks to a (0, 1)-splitting of nodes number 2 and 3 of the prequiver (3.4.11). Since we split two nodes, there are 2 possible permutations. For the identity permutation ($\sigma(2) = 2$, $\sigma(3) = 3$) we obtain (3.4.13)

$$\check{C} = \left[\begin{array}{c|c|c} 0 & -1 & 0 \\ \hline -1 & -2 & -1 \\ \hline 0 & -1 & 1 \end{array} \right] \xrightarrow{\sigma(2) < \sigma(3)} \quad (3.4.15)$$

$$C = \left[\begin{array}{c|cc|cc} 0 & -1 & -1+0 & 0 & 0+0 \\ \hline -1 & -2 & -2+0 & -1 & -1+0 \\ -1+0 & -2+0 & -2+1 & -1+0+1 & -1+1 \\ \hline 0 & -1 & -1+0+1 & 1 & 1+0 \\ 0+0 & -1+0 & -1+1 & 1+0 & 1+1 \end{array} \right].$$

On the other hand, for a transposition $\sigma = (2\ 3)$ (i.e. $\sigma(2) = 3$, $\sigma(3) = 2$) we get

$$\check{C} = \left[\begin{array}{c|c|c} 0 & -1 & 0 \\ \hline -1 & -2 & -1 \\ \hline 0 & -1 & 1 \end{array} \right] \xrightarrow{\sigma(2) > \sigma(3)} \quad (3.4.16)$$

$$C = \left[\begin{array}{c|cc|cc} 0 & -1 & -1+0 & 0 & 0+0 \\ \hline -1 & -2 & -2+0 & -1 & -1+0+1 \\ -1+0 & -2+0 & -2+1 & -1+0 & -1+1 \\ \hline 0 & -1 & -1+0 & 1 & 1+0 \\ 0+0 & -1+0+1 & -1+1 & 1+0 & 1+1 \end{array} \right].$$

In both cases we have $h_1 = 0$ and $\kappa = -a^2q^{-3}t$.

The center of mass condition (3.2.4a) as $\lambda_2\lambda_5 = \lambda_3\lambda_4$ is also satisfied, thus concluding that it is a symmetry. The permutohedra graph is Π_2 as seen in figure 3.8. Thanks to the thinnes of 4_1 any equivalent quiver arises from permutations of off-diagonal entries of C . Nevertheless, there are no more pairings aside of $\lambda_2\lambda_5 = \lambda_3\lambda_4$, this means these are all equivalent quivers and confirms our conjecture 1.

3.4.3 Cinquefoil knot, 5_1

Moving on to the 5_1 knot. Its generating function of its colored superpolynomials is given by [27]

$$P_{5_1}(x, a, q, t) = \sum_{r=0}^{\infty} \frac{x^r a^{4r} q^{-4r}}{(q^2)_r} \sum_{0 \leq k_2 \leq k_1 \leq r} \begin{bmatrix} r \\ k_1 \end{bmatrix} \begin{bmatrix} k_1 \\ k_2 \end{bmatrix} (-a^2 q^{-2} t)_{k_1} \times q^{2[(2r+1)(k_1+k_2) - rk_1 - k_1 k_2]} t^{2(k_1+k_2)}, \quad (3.4.17)$$

again $r = 1$ gives the superpolynomial $P_1(a, q, t) = a^4 q^{-4} + a^4 t^2 + a^6 q^{-2} t^3 + a^4 q^4 t^4 + a^6 q^2 t^5$. Its homological diagram is a zig-zag consisting of 5 nodes, depicted in figure 3.9.

We can split the q -Pochhammer $(-a^2 q^{-2} t)_{k_1}$ in terms of the indices $k_1 = (k_1 -$

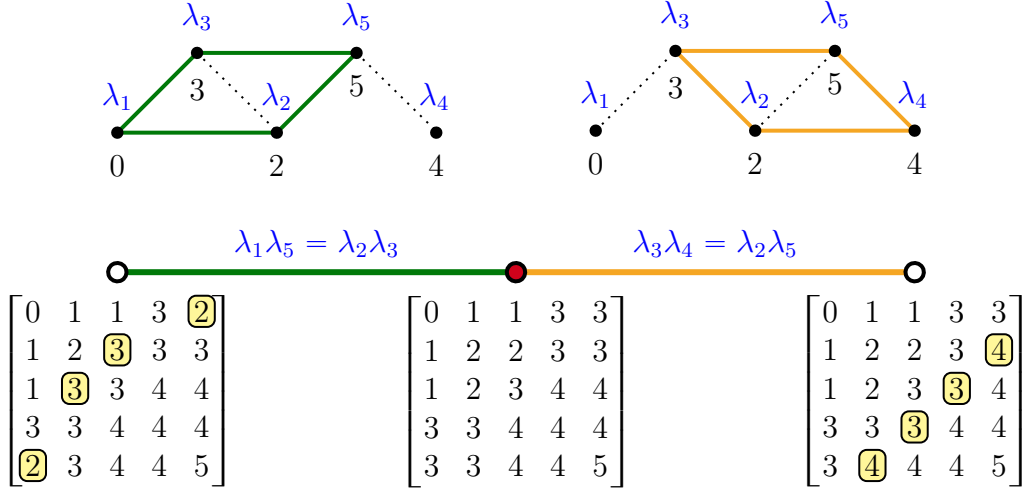


Figure 3.9: Two copies of the homological diagram for 5_1 knot are shown on top. On each copy we denoted a parallelogram that encodes a symmetry, i.e. a transposition of two matrix elements that yields an equivalent quiver. In total there are 3 equivalent quivers, shown in bottom, which correspond to 3 vertices of the permutohedra graph. The permutohedra graph is made of two Π_2 that share a common vertex (in red).

$k_2) + k_2 = \check{d}_2 + \check{d}_3$ (3.4.17), while the rest gives the prequiver

$$P_{5_1}(x, a, q, t) = \sum_{\check{d}} (-q)^{\check{d} \cdot \check{C} \cdot \check{d}} \frac{\mathbf{x}^{\check{d}}}{(q^2)^{\check{d}}} (-a^2 q^{-2} t)^{\check{d}_2 + \check{d}_3} \Big|_{\check{x} = x \check{\lambda}} \quad (3.4.18)$$

$$\check{C} = \left[\begin{array}{c|cc|cc} 0 & 1 & 3 & 3 & 3 \\ \hline 1 & 2 & 3 & 3 & 3 \\ \hline 3 & 3 & 4 & 4 & 4 \\ \hline 3 & 3 & 4 & 4 & 4 \\ \hline 2 & 3 & 4 & 4 & 5 \end{array} \right], \quad \check{\lambda} = \begin{bmatrix} a^4 q^{-4} \\ a^4 q^{-2} (-t)^2 \\ a^4 (-t)^4 \end{bmatrix}.$$

Substituting (3.3.46) results in a $(0, 1)$ -splitting of nodes 2 and 3 (the node 1 is a spectator with $h_1 = 0$; $\kappa = -a^2 q^{-3} t$). The identity permutation ($\sigma(2) = 2, \sigma(3) = 3$) leads to

$$C = \left[\begin{array}{c|cc|cc} 0 & 1 & 1 & 3 & 3 \\ \hline 1 & 2 & 2 & 3 & 3 \\ \hline 1 & 2 & 3 & 4 & 4 \\ \hline 3 & 3 & 4 & 4 & 4 \\ \hline 3 & 3 & 4 & 4 & 5 \end{array} \right], \quad \lambda = \begin{bmatrix} a^4 q^{-4} \\ a^4 q^{-2} (-t)^2 \\ a^6 q^{-5} (-t)^3 \\ a^4 (-t)^4 \\ a^6 q^{-3} (-t)^5 \end{bmatrix} \quad (3.4.19)$$

On the other hand, $\sigma = (2 \ 3)$ yields

$$C = \left[\begin{array}{c|cc|cc} 0 & 1 & 1 & 3 & 3 \\ \hline 1 & 2 & 2 & 3 & 4 \\ \hline 1 & 2 & 3 & 3 & 4 \\ \hline 3 & 3 & 3 & 4 & 4 \\ \hline 3 & 4 & 4 & 4 & 5 \end{array} \right], \quad \lambda = \begin{bmatrix} a^4 q^{-4} \\ a^4 q^{-2} (-t)^2 \\ a^6 q^{-5} (-t)^3 \\ a^4 (-t)^4 \\ a^6 q^{-3} (-t)^5 \end{bmatrix} \quad (3.4.20)$$

We can see that the center of mass condition (3.2.4a) is satisfied in terms of the parallelogram $\lambda_3 \lambda_4 = \lambda_2 \lambda_5$ (shown in orange in figure 3.9). Nevertheless, 5_1 has a

second pairing $\lambda_1\lambda_5 = \lambda_2\lambda_3$ (shown in green in figure 3.9). The second pairing also produces a symmetry. Interestingly, we can obtain the same quiver in (3.4.19) from a (1, 3)-splitting on a distinct prequiver.⁸ In concrete, P_{5_1} can be rewritten as

$$P_{5_1}(x, a, q, t) = \sum_{\check{d}} (-q)^{\check{d}\check{c}\check{d}} \frac{\check{x}^{\check{d}}}{(q^2)_{\check{d}}} (-a^2 q^{2r} t^3)_{\check{d}_2 + \check{d}_3} \Big|_{\check{x}=x\check{\lambda}} \quad (3.4.21)$$

$$\check{C} = \begin{bmatrix} 4 & 3 & 3 \\ 3 & 0 & 1 \\ 3 & 1 & 2 \end{bmatrix}, \quad \check{\lambda} = \begin{bmatrix} a^4(-t)^4 \\ a^4 q^{-4} \\ a^4 q^{-2}(-t)^2 \end{bmatrix},$$

producing (3.4.19) by (1, 3)-splitting of nodes 2 and 3 (the node 1 is a spectator with $h_1 = 1$) with permutation $\sigma = (2\ 3)$ and $\kappa = -a^2 q^{-1} t^3$. But we now we can preform the same splitting with the identity permutation, which leads to the other equivalent quiver

$$C = \begin{bmatrix} 4 & 3 & 4 & 3 & 4 \\ 3 & 0 & 1 & 1 & \textcircled{2} \\ 4 & 1 & 3 & \textcircled{3} & 4 \\ 3 & 1 & \textcircled{3} & 2 & 3 \\ 4 & \textcircled{2} & 4 & 3 & 5 \end{bmatrix}, \quad \lambda = \begin{bmatrix} a^4(-t)^4 \\ a^4 q^{-4} \\ a^6 q^{-5}(-t)^3 \\ a^4 q^{-2}(-t)^2 \\ a^6 q^{-3}(-t)^5 \end{bmatrix}, \quad (3.4.22)$$

which, up to relabelling of the quiver nodes, is the matrix on the l.h.s of figure 3.9.

As we have seen in subsection 3.3.2, if the two transpositions overlap as in (3.3.23) the symmetries can be composed. This means that, 5_1 has only three equivalent quivers, and its permutohedra graph is made out of gluing of two Π_2 along a common middle vertex. Lastly, 5_1 is thin, it has no more pairings. Therefore, we found all equivalent quivers, confirming again our conjecture 1.

3.4.4 5_2 knot

The knot 5_2 is a much more exciting and intricate example. This because it has 6 symmetries and 12 equivalent quivers. The structure of the permutohedra graph is an interesting gluing of three Π_3 . For compactness we will present only the three prequivers and their respective splittings leading to all equivalent quivers. To see the 12 equivalent matrices we encourage to reader to consult [42, Appendix A]).

As for previous knots, the generating function of superpolynomials [31] for 5_2 is

$$P_{5_2}(x, a, q, t) = \sum_{r=0}^{\infty} \frac{x^r}{(q^2)_r} \sum_{0 \leq k_2 \leq k_1 \leq r} \begin{bmatrix} r \\ k_1 \end{bmatrix} \begin{bmatrix} k_1 \\ k_2 \end{bmatrix} (-1)^{r+k_1} (-a^2 q^{-2} t)_{k_1} (-a^2 q^{2r} t^3)_{k_1} a^{2k_2} q^{k_1^2 + k_1 + 2(k_2^2 - k_2 - r k_1)} t^{2k_2 - r}. \quad (3.4.23)$$

With the superpolynomial $P_1(a, q, t) = a^2 q^2 t^2 + a^2 q^{-2} + a^4 t^3 + a^2 t + a^4 q^2 t^4 + a^4 q^{-2} t^2 + a^6 t^5$. The homological diagram consists of a diamond and a zig-zag of length three, see figure 3.10.

⁸In fact it admits also the inverse of (1, 2)-splitting with $h_1 = 0$ and $h_1 = 2$, but they capture the same symmetries.

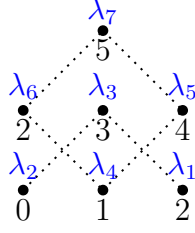


Figure 3.10: Homology diagram for 5_2 knot; labels λ_i are consistent with (3.4.30).

We can derive the first prequiver in the same fashion as in for the previous knots. Starting from (3.4.23)) we get

$$P_{5_2}(x, a, q, t) = \sum_{\check{d}} (-q)^{\check{d} \cdot \check{C} \cdot \check{d}} \frac{\mathbf{x}^{\check{d}}}{(q^2)_{\check{d}}} (-a^2 q^{-2} t)_{\check{d}_2 + \check{d}_3 + \check{d}_4} \Big|_{\mathbf{x} = x \check{\lambda}}, \quad (3.4.24)$$

$$\check{C} = \begin{bmatrix} 0 & 0 & 1 & 1 \\ 0 & 1 & 1 & 2 \\ 1 & 1 & 2 & 2 \\ 1 & 2 & 2 & 4 \end{bmatrix}, \quad \check{\lambda} = \begin{bmatrix} a^2 q^{-2} \\ a^2 q^{-1} (-t) \\ a^2 (-t)^2 \\ a^4 q^{-2} (-t)^4 \end{bmatrix}.$$

Applying (0,1)-splitting to the nodes 2, 3 and 4 with trivial permutation, $h_1 = 0$, and $\kappa = -a^2 q^{-3} t$ leads to

$$C = \begin{bmatrix} 0 & 0 & 0 & 1 & 1 & 1 & 1 \\ 0 & 1 & 1 & 1 & 1 & 2 & 2 \\ 0 & 1 & 2 & 2 & 2 & 3 & 3 \\ 1 & 1 & 2 & 2 & 2 & 2 & 2 \\ 1 & 1 & 2 & 2 & 3 & 3 & 3 \\ 1 & 2 & 3 & 2 & 3 & 4 & 4 \\ 1 & 2 & 3 & 2 & 3 & 4 & 5 \end{bmatrix}, \quad \lambda = \begin{bmatrix} a^2 q^{-2} \\ a^2 q^{-1} (-t) \\ a^4 q^{-4} (-t)^2 \\ a^2 (-t)^2 \\ a^4 q^{-3} (-t)^3 \\ a^4 q^{-2} (-t)^4 \\ a^6 q^{-5} (-t)^5 \end{bmatrix}. \quad (3.4.25)$$

Due to the fact that we splitted three nodes, as we explained in subsection 3.3.2 the resulting symmetry group is S_3 and the permutohedra graph is the hexagon Π_3 .

Additionally, (3.4.23) has the alternative form

$$P_{5_2}(x, a, q, t) = \sum_{\check{d}} (-q)^{\check{d} \cdot \check{C} \cdot \check{d}} \frac{\mathbf{x}^{\check{d}}}{(q^2)_{\check{d}}} \Pi_{\check{d}_2, \check{d}_3, \check{d}_4} \Big|_{\mathbf{x} = x \check{\lambda}}$$

$$\check{C} = \begin{bmatrix} 1 & 0 & 1 & 1 \\ 0 & 0 & 1 & 1 \\ 1 & 1 & 2 & 2 \\ 1 & 1 & 2 & 3 \end{bmatrix}, \quad \check{\lambda} = \begin{bmatrix} a^2 q^{-1} (-t) \\ a^2 q^{-2} \\ a^2 (-t)^2 \\ a^4 q^{-3} (-t)^3 \end{bmatrix}, \quad (3.4.26)$$

$$\Pi_{\check{d}_2, \check{d}_3, \check{d}_4} = \sum_{\alpha_2 + \beta_2 = \check{d}_2} \sum_{\alpha_3 + \beta_3 = \check{d}_3} \sum_{\alpha_4 + \beta_4 = \check{d}_4} (-q)^{2\check{d}_1(\beta_2 + \beta_3 + \beta_4) + 2(\beta_2 + \beta_3 + \beta_4)^2 + 2(\beta_2 \alpha_3 + \beta_2 \alpha_4 + \beta_3 \alpha_4)}$$

$$\times \frac{(a^2 q^{-2} t^2)^{(\beta_2 + \beta_3 + \beta_4)} (q^2)_{\check{d}_2} (q^2)_{\check{d}_3} (q^2)_{\check{d}_4}}{(q^2)_{\alpha_2} (q^2)_{\beta_2} (q^2)_{\alpha_3} (q^2)_{\beta_3} (q^2)_{\alpha_4} (q^2)_{\beta_4}}.$$

Here Π_{d_2, d_3, d_4} stands for a $(0, 2)$ -splitting of the last three nodes with trivial permutation, $h_1 = 1$, and $\kappa = a^2 q^{-2} t^2$, which leads to a relabelled version of (3.4.25):

$$C = \left[\begin{array}{c|ccc|ccc} 1 & 0 & 1 & 1 & 2 & 1 & 2 \\ 0 & 0 & 0 & 1 & \textcircled{1} & 1 & 1 \\ 1 & 0 & 2 & \textcircled{2} & 3 & 2 & 3 \\ \hline 1 & 1 & \textcircled{2} & 2 & 2 & 2 & 2 \\ 2 & \textcircled{1} & 3 & 2 & 4 & 3 & 4 \\ \hline 1 & 1 & 2 & 2 & 3 & 3 & 3 \\ 2 & 1 & 3 & 2 & 4 & 3 & 5 \end{array} \right], \quad \lambda = \begin{bmatrix} a^2 q^{-1} (-t) \\ a^2 q^{-2} \\ a^2 (-t)^2 \\ a^4 q^{-4} (-t)^2 \\ a^4 q^{-2} (-t)^4 \\ a^4 q^{-3} (-t)^3 \\ a^6 q^{-5} (-t)^5 \end{bmatrix}. \quad (3.4.27)$$

Again, we have a Π_3 , and one of its vertices, is shared with previous Π_3 . That common vertex is the one representing the above matrix. In fact, there is yet another quiver shared by both Π_3 , the one corresponding to the transposition $C_{1,7} \leftrightarrow C_{3,5}$. For the record, a $(0, 2)$ -splitting of prequiver (3.4.26) with permutation $\sigma = (2\ 3)$ reproduces the quiver for 5_2 previously derived in [31]:

$$C = \left[\begin{array}{c|ccc|ccc} 1 & 0 & 1 & 1 & 2 & 1 & 2 \\ 0 & 0 & 0 & 1 & \textcircled{2} & 1 & 1 \\ 1 & 0 & 2 & \textcircled{1} & 3 & 2 & 3 \\ \hline 1 & 1 & \textcircled{1} & 2 & 2 & 2 & 2 \\ 2 & \textcircled{2} & 3 & 2 & 4 & 3 & 4 \\ \hline 1 & 1 & 2 & 2 & 3 & 3 & 3 \\ 2 & 1 & 3 & 2 & 4 & 3 & 5 \end{array} \right], \quad \lambda = \begin{bmatrix} a^2 q^{-1} (-t) \\ a^2 q^{-2} \\ a^2 (-t)^2 \\ a^4 q^{-4} (-t)^2 \\ a^4 q^{-2} (-t)^4 \\ a^4 q^{-3} (-t)^3 \\ a^6 q^{-5} (-t)^5 \end{bmatrix}. \quad (3.4.28)$$

The transposition needed to go from (3.4.27) to (3.4.28) is highlighted in yellow.

Moreover, we can obtain (3.4.28) from a different splitting. This leads to an equivalent version of (3.4.23):

$$P_{5_2}(x, a, q, t) = \sum_{\check{a}} (-q)^{\check{a} \cdot \check{C} \cdot \check{a}} \frac{\mathbf{x}^{\check{a}}}{(q^2)_{\check{a}}} (-a^2 q^{2r} t^3)_{\check{a}_2 + \check{a}_3 + \check{a}_4} \Big|_{\mathbf{x} = x \check{\lambda}} \quad (3.4.29)$$

$$\check{C} = \left[\begin{array}{c|ccc|ccc} 2 & 1 & 1 & 1 & 1 & 1 & 1 \\ 1 & 0 & 0 & 0 & 0 & 0 & 0 \\ 1 & 0 & 1 & 1 & 1 & 1 & 1 \\ \hline 1 & 0 & 1 & 1 & 2 & 2 & 2 \end{array} \right] \quad \check{\lambda} = \begin{bmatrix} a^2 (-t)^2 \\ a^2 q^{-2} \\ a^2 q^{-1} (-t) \\ a^4 q^{-4} (-t)^2 \end{bmatrix}.$$

Having a $(1, 3)$ -splitting of the last three nodes with permutation $\sigma = (2\ 3)$, $h_1 = 1$, and $\kappa = -a^2 q^{-1} t^3$ yielding

$$C = \left[\begin{array}{c|ccc|ccc} 2 & 1 & 2 & 1 & 2 & 1 & 2 \\ 1 & 0 & 1 & 0 & 2 & 0 & 1 \\ 2 & 1 & 3 & 1 & 3 & 2 & 3 \\ \hline 1 & 0 & 1 & 1 & 2 & 1 & 2 \\ 2 & 2 & 3 & 2 & 4 & 3 & 4 \\ \hline 1 & 0 & 2 & 1 & 3 & 2 & 3 \\ 2 & 1 & 3 & 2 & 4 & 3 & 5 \end{array} \right], \quad \lambda = \begin{bmatrix} a^2 (-t)^2 \\ a^2 q^{-2} \\ a^4 q^{-3} (-t)^3 \\ a^2 q^{-1} (-t) \\ a^4 q^{-2} (-t)^4 \\ a^4 q^{-4} (-t)^2 \\ a^6 q^{-5} (-t)^5 \end{bmatrix}, \quad (3.4.30)$$

up to relabelling, it leads back to (3.4.28), which is the shared vertex with the previous Π_3 . Thus (3.4.29) is responsible for the remaining Π_3 .

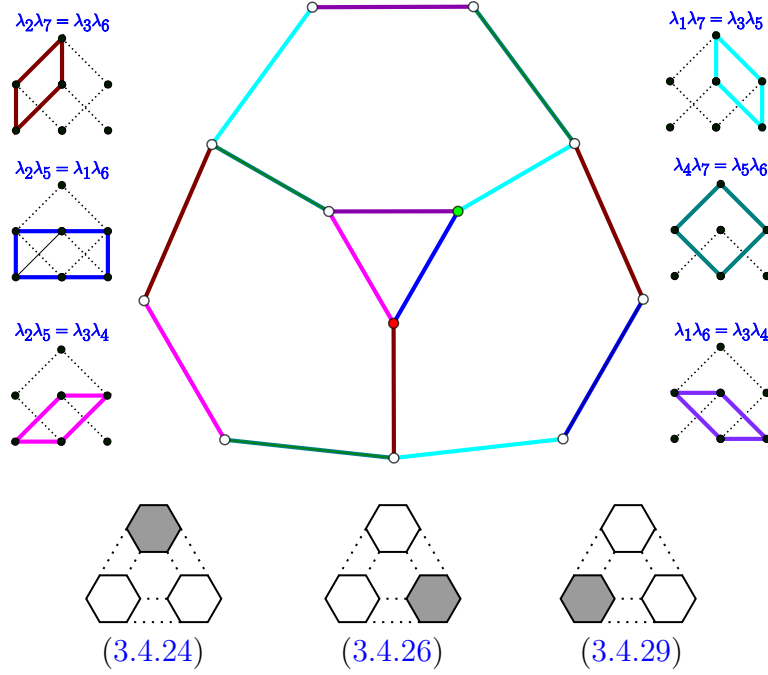


Figure 3.11: The permutohedra graph for 5_2 knot consists of three Π_3 (shown schematically in bottom together with the formulas they correspond to) glued along common edges. The edges in this graph correspond to 6 types of transpositions arising from various quadruples of homology generators, which are also shown in various colors on the homological diagrams.

All-in-all, the structure of the equivalence class of quivers for 5_2 is nicely depicted in 3.11. The hexagon representing the 6 permutations of the $(0, 1)$ -splitting of the prequiver (3.4.24) is on the top of the graph. The bottom-right Π_3 comes from all possible $(0, 2)$ -splittings of the prequiver (3.4.26). The last permutohedra, coming from $(1, 3)$ -splittings of (3.4.29) lead on the bottom-left. The green dot stands for the quiver (3.4.25), whereas the red one represents the quiver (3.4.28). The transposition joining the two quivers is the blue edge. In short, the whole permutohedra graph is the result of 3 Π_3 glued along their edges, as shown in figure 3.11.

An important remark is in order, we mentioned that in general it is not possible to compose transpositions into a three-cycles; yet there is clearly a triangle in the center of the diagram. This is not actually a contradiction, to see this, remember that Π_3 is a representation of S_3 permuting the set $\{1, 2, 3\}$, what if instead it acted on $\{1, 2, 1\}$? This is what is known as a *generalized permutohedra* [43, pag 24]. Then, certain distinct permutations lead to the same point on the graph. Thus, the triangle can be thought as a degenerate hexagon, when thought of as a generalized permutohedra. This is further justified by noticing that the elements in the permuted entries are actually $\{1, 2, 1\}$.

A nice way to visualize the symmetries, edges of the permutohedron graph, is by looking at the pairings on the homology diagram. This is the first example where we are not able to guarantee that we found the whole set of equivalent quivers, still based on the evidence, we conjecture that this is indeed the case 1.

3.4.5 7_1 knot

The reason why we jump from knots with seven crossings to 7_1 with seven is because in terms of complexity of the permutohedra graph and number of equivalent quivers this is the adequate next step. We obtain a total of 13 equivalent quivers, whose explicit quiver matrices can be found in [42, Appendix A]. The structure of the graph reveals two Π_3 glued at one vertex, plus two additional Π_2 glued to each Π_3 .

As usual, we start from the generating function of colored superpolynomials taken from [85, 86]

$$P_{7_1}(x, a, q, t) = \sum_{r=0}^{\infty} \frac{x^r a^{6r} q^{-6r}}{(q^2)^r} \sum_{0 \leq k_3 \leq k_2 \leq k_1 \leq r} \begin{bmatrix} r \\ k_1 \end{bmatrix} \begin{bmatrix} k_1 \\ k_2 \end{bmatrix} \begin{bmatrix} k_2 \\ k_3 \end{bmatrix} (-a^2 q^{-2} t)_{k_1} \times q^{2[(2r+1)(k_1+k_2+k_3) - rk_1 - k_1 k_2 - k_2 k_3]} t^{2(k_1+k_2+k_3)}. \quad (3.4.31)$$

Setting $r = 1$ yields the uncolored superpolynomial $P_1(a, q, t) = a^6 q^{-6} + a^6 q^{-2} t^2 + a^8 q^{-4} t^3 + a^6 q^2 t^4 + a^8 t^5 + a^6 q^6 t^6 + a^8 q^4 t^7$. Its homological diagram consists of one zig-zag made of 7 nodes, see figure 3.12.

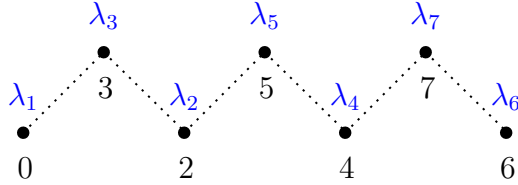


Figure 3.12: Homology diagram for 7_1 knot; labels λ_i are consistent with (3.4.33).

Next, we obtain its prequiver (3.4.31):

$$P_{7_1}(x, a, q, t) = \sum_{\check{a}} (-q)^{\check{a} \cdot \check{C} \cdot \check{a}} \frac{\check{x}^{\check{a}}}{(q^2)^{\check{a}}} (-a^2 q^{-2} t)_{\check{a}_2 + \check{a}_3 + \check{a}_4} \Big|_{\check{x} = x \check{\lambda}} \quad (3.4.32)$$

$$\check{C} = \begin{bmatrix} 0 & 1 & 3 & 5 \\ 1 & 2 & 3 & 5 \\ 3 & 3 & 4 & 5 \\ 5 & 5 & 5 & 6 \end{bmatrix}, \quad \check{\lambda} = \begin{bmatrix} a^6 q^{-6} \\ a^6 q^{-4} (-t)^2 \\ a^6 q^{-2} (-t)^4 \\ a^6 (-t)^6 \end{bmatrix}.$$

We further perform a (0,1)-splitting of the last three nodes with the identity permutation, $h_1 = 0$, and $\kappa = -a^2 q^{-3} t$ obtaining

$$C = \begin{bmatrix} 0 & 1 & 1 & 3 & 3 & 5 & 5 \\ 1 & 2 & 2 & 3 & 3 & 5 & 5 \\ 1 & 2 & 3 & 4 & 4 & 6 & 6 \\ 3 & 3 & 4 & 4 & 4 & 5 & 5 \\ 3 & 3 & 4 & 4 & 5 & 6 & 6 \\ 5 & 5 & 6 & 5 & 6 & 6 & 6 \\ 5 & 5 & 6 & 5 & 6 & 6 & 7 \end{bmatrix}, \quad \lambda = \begin{bmatrix} a^6 q^{-6} \\ a^6 q^{-4} (-t)^2 \\ a^8 q^{-7} (-t)^3 \\ a^6 q^{-2} (-t)^4 \\ a^8 q^{-5} (-t)^5 \\ a^6 (-t)^6 \\ a^8 q^{-3} (-t)^7 \end{bmatrix}, \quad (3.4.33)$$

which is the quiver also derived in [31]. Here we have the added advantage that we know how to obtain the remaining five equivalent quivers corresponding to the nontrivial permutations of S_3 .

Moreover, we may re-express (3.4.31) as

$$P_{7_1}(x, a, q, t) = \sum_{\check{d}} (-q)^{\check{d} \cdot \check{C} \cdot \check{d}} \frac{\check{x}^{\check{d}}}{(q^2)^{\check{d}}} (-a^2 q^{2r} t^3)_{\check{d}_2 + \check{d}_3 + \check{d}_4} \Big|_{\check{x} = x \check{\lambda}} \quad (3.4.34)$$

$$\check{C} = \begin{bmatrix} 6 & 5 & 5 & 5 \\ 5 & 0 & 1 & 3 \\ 5 & 1 & 2 & 3 \\ 5 & 3 & 3 & 4 \end{bmatrix}, \quad \check{\lambda} = \begin{bmatrix} a^6(-t)^6 \\ a^6 q^{-6} \\ a^6 q^{-4}(-t)^2 \\ a^6 q^{-2}(-t)^4 \end{bmatrix}.$$

After performing a (1, 3)-splitting of the last three nodes with permutation $\sigma = (2\ 4)$, $h_1 = 1$, and $\kappa = -a^2 q^{-1} t^3$ gives a relabelling of the quiver (3.4.33):

$$C = \begin{bmatrix} 6 & 5 & 6 & 5 & 6 & 5 & 6 \\ 5 & 0 & 1 & 1 & 3 & 3 & 5 \\ 6 & 1 & 3 & 2 & 4 & 4 & 6 \\ 5 & 1 & 2 & 2 & 3 & 3 & 5 \\ 6 & 3 & 4 & 3 & 5 & 4 & 6 \\ 5 & 3 & 4 & 3 & 4 & 4 & 5 \\ 6 & 5 & 6 & 5 & 6 & 5 & 7 \end{bmatrix}, \quad \lambda = \begin{bmatrix} a^6(-t)^6 \\ a^6 q^{-6} \\ a^8 q^{-7}(-t)^3 \\ a^6 q^{-4}(-t)^2 \\ a^8 q^{-5}(-t)^5 \\ a^6 q^{-2}(-t)^4 \\ a^8 q^{-3}(-t)^7 \end{bmatrix}, \quad (3.4.35)$$

considering the equivalent quiver matrices associated with other permutations in S_3 we get the second Π_3 . Ultimately, we recognize that both Π have a common vertex, namely (3.4.33).

Coming back to the initial Π_3 associated with the prequiver (3.4.32). Surprisingly, there is one equivalent quiver which possess an extra symmetry, that is

$$C = \begin{bmatrix} 0 & 1 & 1 & 3 & 3 & 5 & 5 \\ 1 & 2 & 2 & 3 & 4 & 5 & 6 \\ 1 & 2 & 3 & 3 & 4 & 5 & 6 \\ 3 & 3 & 3 & 4 & 4 & 5 & 6 \\ 3 & 4 & 4 & 4 & 5 & 5 & 6 \\ 5 & 5 & 5 & 5 & 5 & 6 & 6 \\ 5 & 6 & 6 & 6 & 6 & 6 & 7 \end{bmatrix}, \quad \lambda = \begin{bmatrix} a^6 q^{-6} \\ a^6 q^{-4}(-t)^2 \\ a^8 q^{-7}(-t)^3 \\ a^6 q^{-2}(-t)^4 \\ a^8 q^{-5}(-t)^5 \\ a^6(-t)^6 \\ a^8 q^{-3}(-t)^7 \end{bmatrix}, \quad (3.4.36)$$

which comes after a (0,1)-splitting of (3.4.32) with permutation $\sigma = (2\ 4)$. Indeed, (0,1)-splitting of the last two nodes of the prequiver

$$\check{C} = \begin{bmatrix} 0 & 1 & 5 & 1 & 3 \\ 1 & 2 & 6 & 2 & 4 \\ 5 & 6 & 7 & 6 & 6 \\ 1 & 2 & 6 & 3 & 4 \\ 3 & 4 & 6 & 4 & 5 \end{bmatrix}, \quad \check{\lambda} = \begin{bmatrix} a^6 q^{-6} \\ a^6 q^{-4}(-t)^2 \\ a^8 q^{-3}(-t)^7 \\ a^8 q^{-7}(-t)^3 \\ a^8 q^{-5}(-t)^5 \end{bmatrix}, \quad (3.4.37)$$

with permutation $\sigma = (4\ 5)$, $h_1 = 2$, $h_2 = 1$, $h_3 = 0$, and $\kappa = -a^{-2} q^5 t$ leads to

$$C = \begin{bmatrix} 0 & 1 & 5 & 1 & 3 & 3 & 5 \\ 1 & 2 & 6 & 2 & 3 & 4 & 5 \\ 5 & 6 & 7 & 6 & 6 & 6 & 6 \\ 1 & 2 & 6 & 3 & 3 & 4 & 5 \\ 3 & 3 & 6 & 3 & 4 & 4 & 5 \\ 3 & 4 & 6 & 4 & 4 & 5 & 5 \\ 5 & 5 & 6 & 5 & 5 & 5 & 6 \end{bmatrix}, \quad \lambda = \begin{bmatrix} a^6 q^{-6} \\ a^6 q^{-4}(-t)^2 \\ a^8 q^{-3}(-t)^7 \\ a^8 q^{-7}(-t)^3 \\ a^6 q^{-2}(-t)^4 \\ a^8 q^{-5}(-t)^5 \\ a^6 q^{-6} \end{bmatrix}, \quad (3.4.38)$$

which can be obtained from (3.4.36) via a relabelling. This leads to another equivalent quiver, which has a connection to (3.4.36). Thus, we represent this as a Π_2 , which is glued to a Π_3 at the vertex that represents (3.4.36).

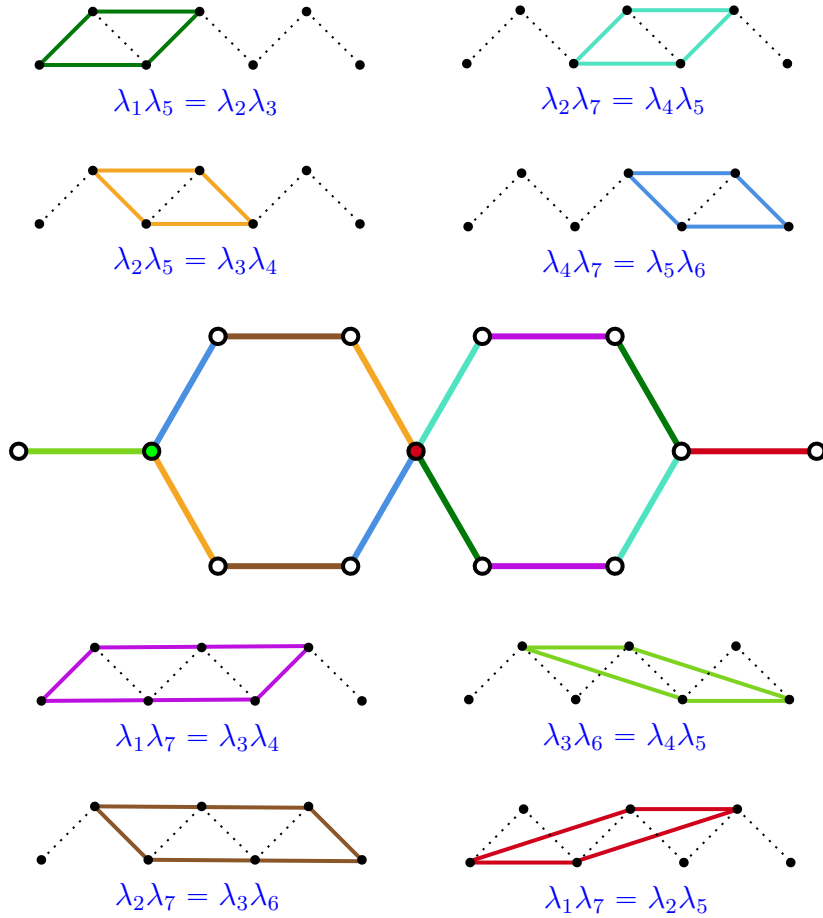


Figure 3.13: The permutohedra graph for 7_1 knot consists of two Π_3 and two Π_2 appropriately glued. Altogether it has 13 vertices representing equivalent quivers, and 8 symmetries corresponding to various quadruples of homology generators (and represented by different colors of the edges in the graph).

The same situation occurs for the second Π_3 , it also has a Π_2 attached to it. The whole graph can be appreciated in figure 3.13. The initial quiver (3.4.33), was the first derived in [31], is the center of the entire graph, and the graph is symmetric with respect to it; we denote it by a red dot. The Π_3 on the left originates from (3.4.32), whereas the right one corresponds to the prequiver (3.4.34). The green dot, which adheres Π_2 to Π_3 , represents the quiver (3.4.36).

Lastly, we tested whether there were any further equivalent quivers, but were unable to discover more. Therefore, following conjecture 1, we expect this is the complete list of equivalent quivers for 7_1 .

3.4.6 6_1 knot

We are now focused on the 6_1 knot. This seemingly simple knot already has 141 equivalent quivers and 16 symmetries, together build an impressive and sophisticated structure for the permutohedra graph, depicted in figure 3.14.

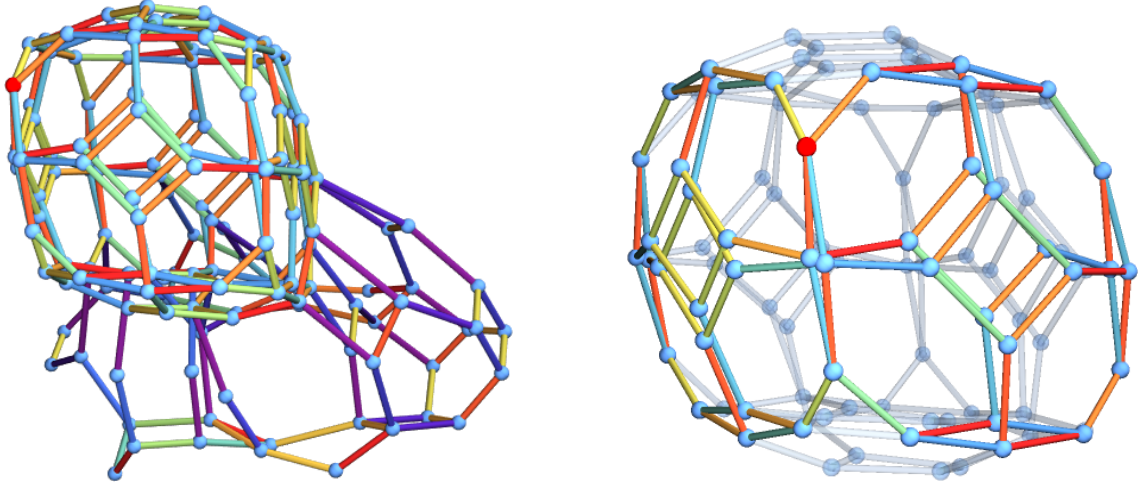


Figure 3.14: The permutohedra graph for 6_1 knot has 141 vertices that represent equivalent quivers (left). Excluding symmetries that involve λ_1 reduces the whole graph to a cube-like shape (right). Each face of this cube is one Π_4 (a bit squashed), and neighboring Π_4 's are glued along a square, which is a common face to both Π_4 's. The red vertex represents the quiver (3.4.41) (or its reordered form (3.4.43)).

The generating function of colored superpolynomials for the knot 6_1 has the form [85]:

$$P_{6_1}(x, a, q, t) = \sum_{r=0}^{\infty} \frac{x^r}{(q^2)^r} \sum_{0 \leq k_2 \leq k_1 \leq r} \begin{bmatrix} r \\ k_1 \end{bmatrix} \begin{bmatrix} k_1 \\ k_2 \end{bmatrix} (-a^{-2}q^2t^{-1}; q^{-2})_{k_1} (-a^{-2}q^{-2r}t^{-3}; q^{-2})_{k_1} \times a^{2(k_1+k_2)}t^{2(k_1+k_2)}q^{2(k_1^2+k_2^2-k_1-k_2)}. \quad (3.4.39)$$

The linear-order gives the uncolored superpolynomial $P_1(a, q, t) = 1 + a^{-2}t^{-2} + q^2t + q^{-2}t^{-1} + a^2t^2 + 1 + a^2q^2t^3 + a^2q^{-2}t + a^4t^4$. Its homological diagram, shown in figure 3.15, is made of 2 diamonds and a degenerate zig-zag of one point that coincides with one point of the upper diamond, so that $\lambda_1 = \lambda_6$.

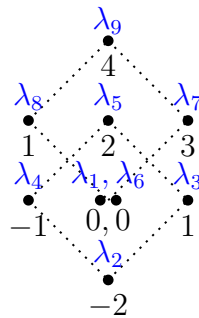


Figure 3.15: Homology diagram for 6_1 knot; labels λ_i are consistent with (3.4.41).

Let us find the prequiver from (3.4.39)

$$P_{6_1}(x, a, q, t) = \sum_{\check{d}} (-q)^{\check{d} \cdot \check{C} \cdot \check{d}} \frac{\check{x}^{\check{d}}}{(q^2)^{\check{d}}} (-a^2 q^{-2} t)_{\check{d}_2 + \check{d}_3 + \check{d}_4 + \check{d}_5} \Big|_{\check{x} = x \check{\lambda}}$$

$$\check{C} = \begin{bmatrix} 0 & -1 & -1 & -1 & -1 \\ -1 & -2 & -2 & -2 & -1 \\ -1 & -2 & -1 & -2 & -1 \\ -1 & -2 & -2 & 0 & 0 \\ -1 & -1 & -1 & 0 & 1 \end{bmatrix}, \quad \check{\lambda} = \begin{bmatrix} 1 \\ a^{-2} q^2 (-t)^{-2} \\ q^{-1} (-t)^{-1} \\ 1 \\ a^2 q^{-3} (-t) \end{bmatrix}. \quad (3.4.40)$$

With a (1, 3)-splitting of the last four nodes, associated with the permutation $\sigma = (2 \ 4 \ 5 \ 3)$, $h_1 = 1$, and $\kappa = -a^2 q^{-1} t^3$ produces the same quiver first obtained in [31]:

$$C = \begin{bmatrix} 0 & -1 & 0 & -1 & 0 & -1 & 0 & -1 & 0 \\ -1 & -2 & -1 & -2 & -1 & -2 & 0 & -1 & 0 \\ 0 & -1 & 1 & 0 & 1 & -1 & 1 & 1 & 2 \\ -1 & -2 & 0 & -1 & 0 & -2 & 0 & -1 & 1 \\ 0 & -1 & 1 & 0 & 2 & -1 & 1 & 0 & 2 \\ -1 & -2 & -1 & -2 & -1 & 0 & 1 & 0 & 1 \\ 0 & 0 & 1 & 0 & 1 & 1 & 3 & 2 & 3 \\ -1 & -1 & 1 & -1 & 0 & 0 & 2 & 1 & 2 \\ 0 & 0 & 2 & 1 & 2 & 1 & 3 & 2 & 4 \end{bmatrix}, \quad \lambda = \begin{bmatrix} 1 \\ a^{-2} q^2 (-t)^{-2} \\ q(-t) \\ q^{-1} (-t)^{-1} \\ a^2 q^{-2} (-t)^2 \\ 1 \\ a^2 q^{-1} (-t)^3 \\ a^2 q^{-3} (-t) \\ a^4 q^{-4} (-t)^4 \end{bmatrix}. \quad (3.4.41)$$

Meanwhile, 3.4.39 can be rewritten as

$$P_{6_1}(x, a, q, t) = \sum_{\check{d}} (-q)^{\check{d} \cdot \check{C} \cdot \check{d}} \frac{\check{x}^{\check{d}}}{(q^2)^{\check{d}}} \Pi_{\check{d}_2, \check{d}_3, \check{d}_4, \check{d}_5} \Big|_{\check{x} = x \check{\lambda}}$$

$$\Pi_{\check{d}_2, \check{d}_3, \check{d}_4, \check{d}_5} = \sum_{\alpha_2 + \beta_2 = \check{d}_2} \sum_{\alpha_3 + \beta_3 = \check{d}_3} \sum_{\alpha_4 + \beta_4 = \check{d}_4} \sum_{\alpha_5 + \beta_5 = \check{d}_5} \prod_{i=2}^5 \frac{(a^2 q^{-2} t^2)^{\beta_i} (q^2)^{\check{d}_i}}{(q^2)^{\alpha_i} (q^2)^{\beta_i}}$$

$$\times (-q)^{2(\beta_2 + \beta_3 + \beta_4 + \beta_5)^2 + 2(\alpha_2 \beta_3 + \alpha_2 \beta_4 + \alpha_2 \beta_5 + \alpha_3 \beta_4 + \alpha_3 \beta_5 + \alpha_4 \beta_5)}$$

$$\check{C} = \begin{bmatrix} 0 & -1 & -1 & 0 & 0 \\ -1 & -2 & -2 & -1 & -1 \\ -1 & -2 & -1 & 0 & 0 \\ 0 & -1 & 0 & 1 & 1 \\ 0 & -1 & 0 & 1 & 2 \end{bmatrix}, \quad \check{\lambda} = \begin{bmatrix} 1 \\ a^{-2} q^2 (-t)^{-2} \\ q^{-1} (-t)^{-1} \\ q(-t) \\ a^2 q^{-2} (-t)^2 \end{bmatrix}, \quad (3.4.42)$$

After a (0, 2)-splitting of the last four nodes with permutation $\sigma = (2 \ 5)(3 \ 4)$, $h_1 = 0$

and $\kappa = a^2q^{-2}t^2$ we get

$$C = \left[\begin{array}{c|cc|cc|cc|cc} 0 & -1 & -1 & -1 & -1 & 0 & 0 & 0 & 0 \\ -1 & -2 & -2 & -2 & -1 & -1 & 0 & -1 & 0 \\ -1 & -2 & 0 & -2 & 0 & -1 & 1 & -1 & 1 \\ \hline -1 & -2 & -2 & -1 & -1 & 0 & 1 & 0 & 1 \\ -1 & -1 & 0 & -1 & 1 & 0 & 2 & 0 & 2 \\ \hline 0 & -1 & -1 & 0 & 0 & 1 & 1 & 1 & 2 \\ 0 & 0 & 1 & 1 & 2 & 1 & 3 & 1 & 3 \\ \hline 0 & -1 & -1 & 0 & 0 & 1 & 1 & 2 & 2 \\ 0 & 0 & 1 & 1 & 2 & 2 & 3 & 2 & 4 \end{array} \right], \quad \boldsymbol{\lambda} = \left[\begin{array}{c} 1 \\ a^{-2}q^2(-t)^{-2} \\ 1 \\ q^{-1}(-t)^{-1} \\ a^2q^{-3}(-t) \\ q(-t) \\ a^2q^{-1}(-t)^3 \\ a^2q^{-2}(-t)^2 \\ a^4q^{-4}(-t)^4 \end{array} \right]. \quad (3.4.43)$$

which is a rearrangement of (3.4.41). This implies that the afore quiver is a shared vertex of two permutohedra Π_4 , and is represented with a the red dot in figure 3.14. We offer a planar embedding perspective of the two Π_4 , together with the eight symmetries that generate them in 3.16. The Π_4 to the right of the red dot in figure 3.14, arises thanks to the prequiver (3.4.40); whereas the second Π_4 to the left of the red dot originates from the prequiver (3.4.42). In spirit of conjecture 1 we assume that we have found all equivalent quivers.

3.4.7 $6_2, 6_3, 7_3$ knots

As one would expect, $6_2, 6_3$ and 7_3 , are left until the end of our discussion because their number of equivalent quivers and symmetries is several orders of magnitude higher, see table 3.1. That is why we limit ourselves to present an equivalent quiver matrix C , their $\boldsymbol{\lambda}$, their homological diagrams, and a few of their symmetries. The quiver matrices are taken from [31] and [80].

6_2 knot We hit it off with the 6_2 knot. Its quiver and $\boldsymbol{\lambda}$ found in [31] are

$$C = \left[\begin{array}{cccccccccccc} -2 & -2 & -1 & -1 & -1 & -1 & 0 & -1 & 1 & 1 & 1 \\ -2 & -1 & -1 & 0 & 0 & 0 & 1 & 0 & 1 & 2 & 2 \\ -1 & -1 & 0 & 1 & 0 & 0 & 1 & 0 & 1 & 2 & 2 \\ -1 & 0 & 1 & 0 & 0 & 0 & 1 & 0 & 2 & 1 & 1 \\ -1 & 0 & 0 & 0 & 1 & 1 & 1 & 1 & 2 & 2 & 2 \\ -1 & 0 & 0 & 0 & 1 & 1 & 1 & 1 & 2 & 2 & 2 \\ 0 & 1 & 1 & 1 & 1 & 1 & 2 & 1 & 2 & 2 & 2 \\ -1 & 0 & 0 & 0 & 1 & 1 & 1 & 2 & 2 & 3 & 3 \\ 1 & 1 & 1 & 2 & 2 & 2 & 2 & 2 & 3 & 3 & 3 \\ 1 & 2 & 2 & 1 & 2 & 2 & 2 & 3 & 3 & 3 & 3 \\ 1 & 2 & 2 & 1 & 2 & 2 & 2 & 3 & 3 & 3 & 4 \end{array} \right], \quad \boldsymbol{\lambda} = \left[\begin{array}{c} q^{-2}(-t)^{-2} \\ a^2q^{-4}(-t)^{-1} \\ a^2q^{-2} \\ q^2 \\ a^2(-t) \\ a^2(-t) \\ a^2q^2(-t)^2 \\ a^4q^{-2}(-t)^2 \\ a^4(-t)^3 \\ a^2q^4(-t)^3 \\ a^4q^2(-t)^4 \end{array} \right]. \quad (3.4.44)$$

The matrix of the quiver above (3.4.44) has eight local symmetries⁹ associated

⁹Those that can be applied to the quiver matrix as it stands. In the permutohedra graph, these local symmetries would be the edges incident to the vertex that represents (3.4.44).

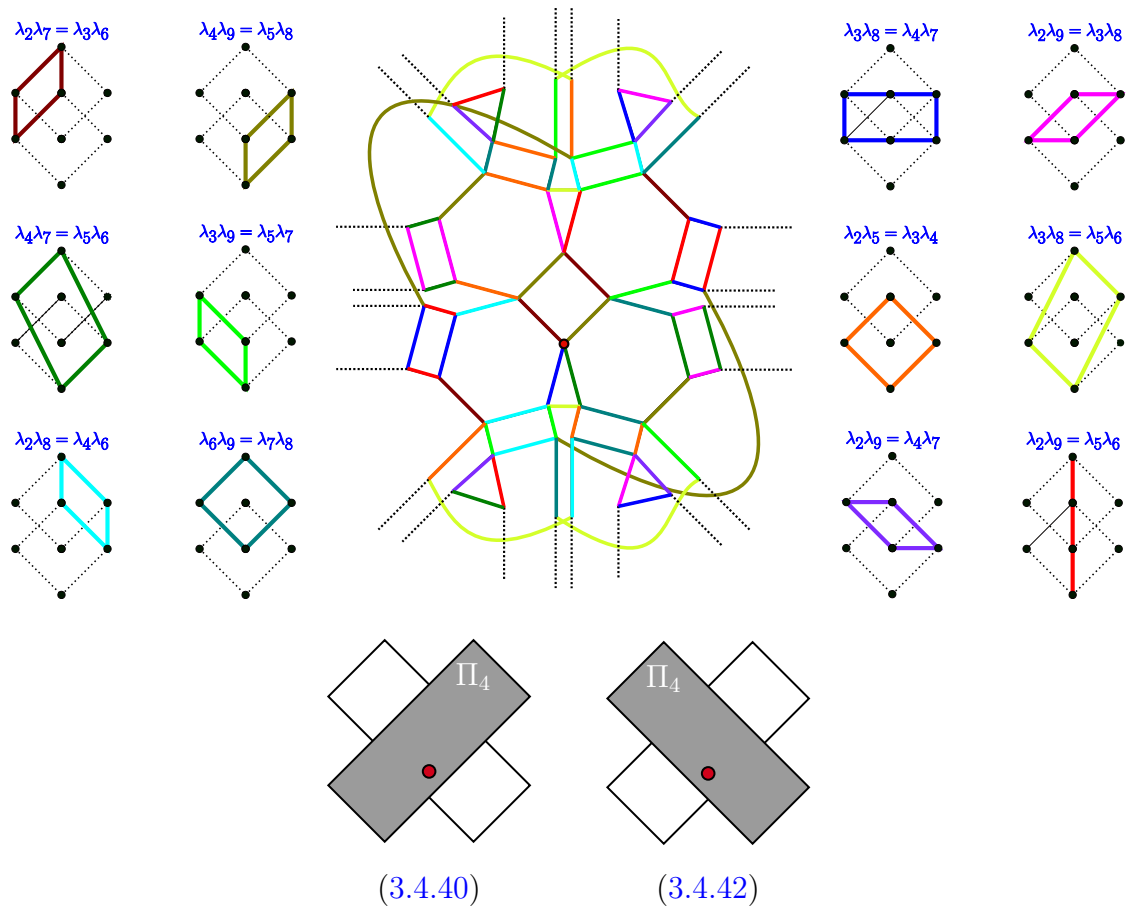


Figure 3.16: Planar projection of a part of the permutohedra graph for 6_1 knot. In homological diagrams (on left and right) it is indicated how some of its symmetries, corresponding to edges of the graph, arise from quadruples of homology generators. The positions of two permutohedra Π_4 mentioned in the text are indicated schematically in the bottom.

with :

$$\begin{array}{llll}
 \lambda_1\lambda_7 = \lambda_3\lambda_4, & \lambda_1\lambda_{11} = \lambda_4\lambda_8, & \lambda_5\lambda_{11} = \lambda_8\lambda_{10}, & \lambda_6\lambda_{11} = \lambda_8\lambda_{10}, \\
 \lambda_1\lambda_9 = \lambda_3\lambda_5, & \lambda_1\lambda_9 = \lambda_3\lambda_6, & \lambda_2\lambda_7 = \lambda_3\lambda_5, & \lambda_2\lambda_7 = \lambda_3\lambda_6.
 \end{array}$$

In figure 3.17, we draw those eight symmetries in the form of parallelograms on top of the homological diagram.

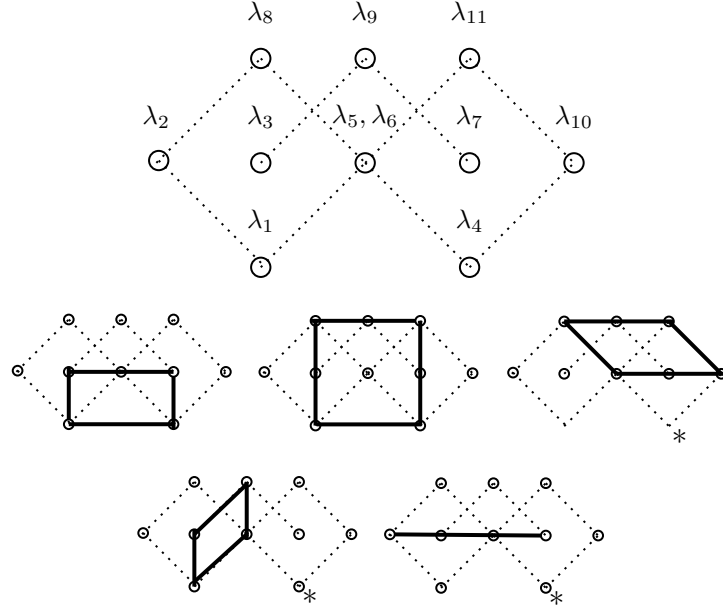


Figure 3.17: Homology diagram and local symmetries for 6_2 knot, each picture marked with * corresponds to two symmetries, due to double-valued nodes λ_5 and λ_6 .

6_3 **knot** We repeat the same procedure for the knot 6_3 . We present its quiver matrix C and λ below [31]

$$\begin{bmatrix}
 0 & 0 & 0 & -1 & -1 & 0 & 0 & -1 & -1 & 0 & 0 & -1 & -1 \\
 0 & 1 & 0 & -1 & -2 & 1 & 0 & -1 & -2 & 1 & 1 & 0 & -1 \\
 0 & 0 & 0 & -1 & -2 & 1 & 0 & 0 & -2 & 1 & 1 & 0 & 0 \\
 -1 & -1 & -1 & -2 & -3 & 0 & -1 & -2 & -3 & -1 & 0 & -2 & -2 \\
 -1 & -2 & -2 & -3 & -3 & -1 & -1 & -2 & -3 & -1 & -1 & -2 & -2 \\
 0 & 1 & 1 & 0 & -1 & 2 & 1 & 0 & -1 & 2 & 1 & 1 & -1 \\
 0 & 0 & 0 & -1 & -1 & 1 & 1 & 0 & -1 & 2 & 1 & 1 & 0 \\
 -1 & -1 & 0 & -2 & -2 & 0 & 0 & -1 & -2 & 0 & 0 & -1 & -2 \\
 -1 & -2 & -2 & -3 & -3 & -1 & -1 & -2 & -2 & 0 & -1 & -1 & -2 \\
 0 & 1 & 1 & -1 & -1 & 2 & 2 & 0 & 0 & 3 & 2 & 1 & 0 \\
 0 & 1 & 1 & 0 & -1 & 1 & 1 & 0 & -1 & 2 & 2 & 1 & 0 \\
 -1 & 0 & 0 & -2 & -2 & 1 & 1 & -1 & -1 & 1 & 1 & 0 & -1 \\
 -1 & -1 & 0 & -2 & -2 & -1 & 0 & -2 & -2 & 0 & 0 & -1 & -1
 \end{bmatrix},
 \begin{bmatrix}
 1 \\
 a^2q^{-2}(-t) \\
 1 \\
 q^{-4}(-t)^{-2} \\
 a^{-2}q^{-2}(-t)^{-3} \\
 a^2(-t)^2 \\
 q^2(-t) \\
 q^{-2}(-t)^{-1} \\
 a^{-2}(-t)^{-2} \\
 a^2q^2(-t)^3 \\
 q^4(-t)^2 \\
 1 \\
 a^{-2}q^2(-t)^{-1}
 \end{bmatrix}.
 \tag{3.4.45}$$

The previous quiver (3.4.45) has six local symmetries:

$$\begin{aligned}
 \lambda_2\lambda_8 &= \lambda_4\lambda_6, & \lambda_2\lambda_{12} &= \lambda_4\lambda_{10}, & \lambda_3\lambda_8 &= \lambda_4\lambda_7, \\
 \lambda_3\lambda_9 &= \lambda_5\lambda_7, & \lambda_3\lambda_{13} &= \lambda_5\lambda_{11}, & \lambda_6\lambda_{13} &= \lambda_8\lambda_{11},
 \end{aligned}$$

which, again, we encode as parallelograms in the homology diagram in figure 3.18.

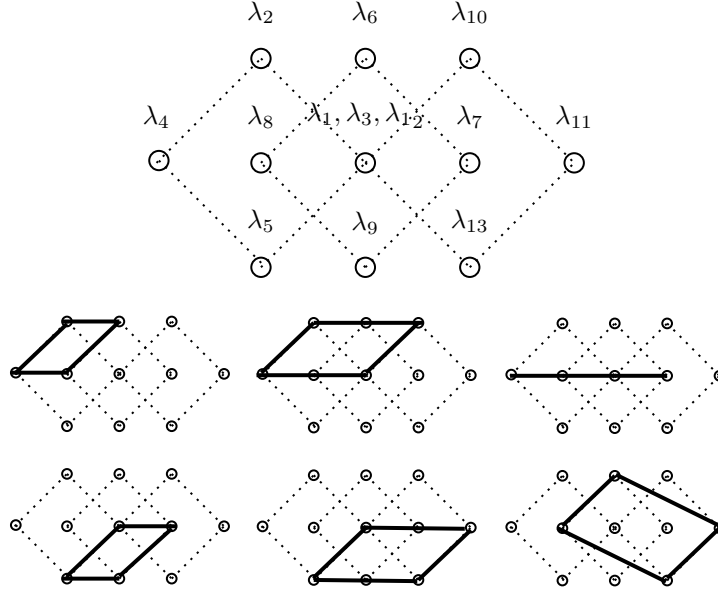


Figure 3.18: Homology diagram and local symmetries for 6_3 knot.

7₃ knot We present the quiver matrix C and λ for the 7₃ knot, following [80]

$$C = \begin{bmatrix} 2 & 0 & 3 & 2 & 1 & 5 & 4 & 3 & 3 & 2 & 5 & 4 & 3 \\ 0 & 0 & 1 & 1 & 0 & 3 & 3 & 2 & 1 & 1 & 3 & 3 & 2 \\ 3 & 1 & 4 & 2 & 2 & 5 & 4 & 4 & 4 & 2 & 5 & 4 & 4 \\ 2 & 1 & 2 & 2 & 1 & 3 & 3 & 3 & 3 & 2 & 3 & 3 & 3 \\ 1 & 0 & 2 & 1 & 1 & 3 & 2 & 2 & 2 & 1 & 3 & 2 & 2 \\ 5 & 3 & 5 & 3 & 3 & 6 & 4 & 4 & 6 & 4 & 6 & 4 & 4 \\ 4 & 3 & 4 & 3 & 2 & 4 & 4 & 3 & 5 & 4 & 5 & 4 & 3 \\ 3 & 2 & 4 & 3 & 2 & 4 & 3 & 3 & 4 & 3 & 5 & 4 & 3 \\ 3 & 1 & 4 & 3 & 2 & 6 & 5 & 4 & 5 & 3 & 6 & 5 & 4 \\ 2 & 1 & 2 & 2 & 1 & 4 & 4 & 3 & 3 & 3 & 4 & 4 & 3 \\ 5 & 3 & 5 & 3 & 3 & 6 & 5 & 5 & 6 & 4 & 7 & 5 & 5 \\ 4 & 3 & 4 & 3 & 2 & 4 & 4 & 4 & 5 & 4 & 5 & 5 & 4 \\ 3 & 2 & 4 & 3 & 2 & 4 & 3 & 3 & 4 & 3 & 5 & 4 & 4 \end{bmatrix}, \quad \lambda = \begin{bmatrix} a^6 q^{-4} (-t)^2 \\ a^4 q^{-4} \\ a^6 (-t)^4 \\ a^4 (-t)^2 \\ a^4 q^{-2} (-t) \\ a^6 q^4 (-t)^6 \\ a^4 q^4 (-t)^4 \\ a^4 q^2 (-t)^3 \\ a^8 q^{-2} (-t)^5 \\ a^6 q^{-2} (-t)^3 \\ a^8 q^2 (-t)^7 \\ a^6 q^2 (-t)^5 \\ a^6 (-t)^4 \end{bmatrix}. \quad (3.4.46)$$

This quiver (3.4.46) enjoys the following seven local symmetries:

$$\begin{aligned} \lambda_1 \lambda_{10} &= \lambda_2 \lambda_9, & \lambda_2 \lambda_{11} &= \lambda_3 \lambda_{10}, & \lambda_3 \lambda_{10} &= \lambda_4 \lambda_9, & \lambda_3 \lambda_{12} &= \lambda_4 \lambda_{11}, \\ \lambda_4 \lambda_{13} &= \lambda_5 \lambda_{12}, & \lambda_6 \lambda_{12} &= \lambda_7 \lambda_{11}, & \lambda_7 \lambda_{13} &= \lambda_8 \lambda_{12}. \end{aligned}$$

For the last time, in figure 3.19, we depict those seven symmetries as parallelograms on the homology diagram.

For our grand finale, we condense all the information regarding the equivalent quivers, pairings, and symmetries for various knots in the following table 3.1. For the examples at hand, point out that for torus knots and twist knots, the growth in the number of equivalent quivers is clearly factorial. Nevertheless, as seen by the standalone examples, seemingly simple knots may have a baffling number of equivalent quivers. This means that to study knots with a larger number of crossings, new methods are needed, to make counting tractable.

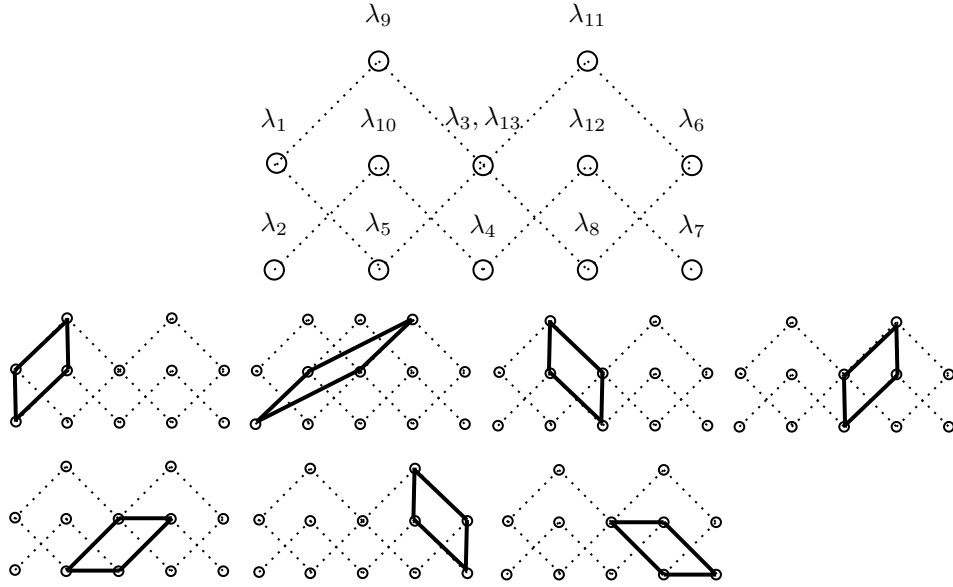


Figure 3.19: Homology diagram and local symmetries for 7_3 knot.

Knot		Pairings	Symmetries	Equivalent quivers
Unknot	0_1	0	0	1
	3_1	0	0	1
Torus knots $T_{2,2p+1}$	5_1	2	2	3
	7_1	9	8	13
	9_1	24	20	68
	11_1	50	40	405
	13_1	90	70	2684
	15_1	147	112	19557
	\vdots	\vdots	\vdots	\vdots
	$(2p+1)_1$	$p^2(p-1)/2$	$p(p^2-1)/3$	$\sim 2p!$
Twists knots $TK_{2 p +2}$	4_1	1	1	2
	6_1	24	16	141
	8_1	105	61	36555
Twists knots TK_{2p+1}	5_2	8	6	12
	7_2	52	34	1983
Stand-alone examples	6_2	46	36	3534
	6_3	101	72	142368
	7_3	86	67	109636

Table 3.1: The number of pairings, symmetries, and equivalent quivers that we have found for $(2, 2p+1)$ torus knots, twist knots, and $6_2, 6_3, 7_3$ knots.

Chapter 4

Quiver A-polynomials

The purpose of this chapter is to introduce a new object that we call quiver A-polynomial. We begin by proving the existence of the quantum A-polynomial for any quiver and the classical one immediately follows. After that we focus on the classification of the classical A-polynomials in terms of their genus. We named them quiver A-polynomials, since when the quiver is associated with a knot, the quiver A-polynomial reduces to the A-polynomial for this knot.

To construct the quantum A-polynomial we start from the equations that the quiver partition function satisfies. These are encoded in a set of linear operators, which when they act on the quiver series (2.1.40) from the left-hand side, then the right-hand side is equal to zero. These arise from the recursion relations satisfied by the series of quivers as a q -difference equation. These operators will be the building blocks used to construct the quantum quiver A-polynomial. We will present a few examples of 2×2 quiver matrices, for which this procedure can be carried out in detail. The reason for concentrating on these rather small quiver matrices is that they provide the simplest tractable examples. In that case, we achieve a complete classification.

We also study the classical version of these operator equations. The leading term in the asymptotic is encoded in the classical quiver A-polynomial. Thus, the zero set of this polynomial is an algebraic curve which encodes the BPS spectrum of the 3d SUSY gauge theory. The results are also presented in [44].

It is worth reminding ourselves that the quivers we consider now are not necessarily associated to knots, meaning that we concentrate on any 2-node quiver. Additionally, that this is the first time, that we know of, that the concept of a quiver A-polynomial is introduced, both in its classical and quantum version.

Remark 5. In [44] the authors used the notation $q \rightarrow q^{1/2}$. We follow their notation for this chapter. The reason is that, although at first sight it introduces an unnecessary square root, it actually simplifies the formulas for the resulting A-polynomials. This also facilitates cross-checks with their results.

4.1 Quantum derivation and definition

As it is customary in combinatorics, whenever we have a sequence, we look for its generating function. Then, the recursion relations of the sequence turn into equations for the generating function. Let us apply this strategy to the coefficients

of the quiver series (2.1.40)

$$P_{d_1, \dots, d_m} = \frac{(-q^{1/2})^{\sum_{i,j=1}^m C_{ij} d_i d_j}}{(q^2)_{d_1} \dots (q^2)_{d_m}}, \quad (4.1.1)$$

they satisfy the simple first order linear recurrence relation

$$P_{d_1, \dots, d_{k+1}, \dots, d_m} = \frac{(-q^{1/2})^{\sum_{i,j=1}^m C_{ij} (d_i + \delta_{ik})(d_j + \delta_{jk})}}{(q)_{d_1} \dots (q)_{d_{k+1}} \dots (q)_{d_m}} = \frac{(-q^{1/2})^{C_{kk} + 2 \sum_{i=1}^m C_{ik} d_i}}{1 - q^{d_k + 1}} P_{d_1, \dots, d_m}. \quad (4.1.2)$$

Then, we introduce the operators \hat{z}_i , for $i = 1, \dots, m$ with the commutation relation $\hat{z}_i \hat{x}_k = q^{\delta_{ki}} \hat{x}_k \hat{z}_i$. In terms of operators acting on the quiver series (2.1.40) the above recursion relation takes the form

$$\sum_{(d_1, \dots, d_m) \geq 0} P_{d_1, \dots, d_{k+1}, \dots, d_m} \prod_i^m x_i^{d_i + \delta_{ki}} = \left[(1 - \hat{z}_k)^{-1} (-q^{1/2})^{C_{kk}} \hat{x}_k \prod_j^m \hat{z}_j^{C_{kj}} \right] \cdot P(x_1, \dots, x_m). \quad (4.1.3)$$

Multiplying by $1 - \hat{z}_k$ on both sides leads to

$$\boxed{\hat{H}_k \cdot P(x_1, \dots, x_m) = 0, \quad \hat{H}_k = (-q^{1/2})^{C_{kk}} \hat{x}_k \prod_j^m \hat{z}_j^{C_{kj}} + \hat{z}_k - 1} \quad (4.1.4)$$

for reasons we will explain in a moment we refer to the above (4.1.4) as the *quantum Nahm equations*.

To obtain the classical equations, we notice that the q -Pochhammers in the denominator lead to poles when $q \rightarrow 1$. We can make the change of variables $q = e^{\hbar}$ to construct a WKB expansion around the singularity $\hbar \rightarrow 0$ with the ansatz

$$P(x_1, \dots, x_m) \sim e^{\sum_{k=-1}^{\infty} \hbar^k S_k(x_1, \dots, x_m)}. \quad (4.1.5)$$

The next step is substitute the ansatz into the quantum Nahm equations and take the limit $\hbar \rightarrow 0$

$$P^{-1} \hat{H}_i \cdot P = 0 \xrightarrow{\hbar \rightarrow 0} \boxed{H_i = (-1)^{C_{ii}} x_i \prod_{j=1}^m z_j^{C_{ij}} + z_i - 1 = 0, \quad z_i = e^{x_i \partial_{x_i} S_{-1}}}. \quad (4.1.6)$$

the above are the well-known Nahm equations¹ [58, 59, 63]. These equations can be also obtained by applying the saddle-point method directly to the quiver series.

In the previous chapter 3 we noticed that to make contact with knot invariants we needed to perform the knot change of variables (2.3.2) $x_i = \lambda_i x$. Furthermore, as we explained in subsection 2.2.2, the equation satisfied by the generating function of superpolynomials (2.2.14) is itself a knot invariant known as the quantum A-polynomial (2.2.39). The quantum A-polynomial is expressed in terms of a single \hat{x} and \hat{y} satisfying the commutation relation $\hat{y} \hat{x} = q \hat{x} \hat{y}$.

Obviously, $\hat{y} \neq \hat{z}_i$, since they act on different variables. Still, there is a way to relate the action of \hat{y} to that of \hat{z}_i after the change of variables

$$\hat{y} \cdot P(\lambda_1 x, \dots, \lambda_m x) = P(q \lambda_1 x, \dots, q \lambda_m x) = \prod_{i=1}^m \hat{z}_i \cdot P(x_1, \dots, x_m) \Big|_{x_i = \lambda_i x}. \quad (4.1.7)$$

¹Not to be confused with the Nahm equations for monopoles in gauge theories.

This means that any operator written in terms of x_i and $\prod_{i=1}^m \hat{z}_i$ can easily be matched to an operator in the two variables x and \hat{y} . Thus, the main questions of this chapter:

- Given a quiver series $P_C(x_1, \dots, x_m)$ and its operators $\hat{H} \cdot P_C(x_1, \dots, x_m) = 0$, how can we derive the equation for $\hat{A}(\hat{x}, \hat{y}) \cdot P_C(x_1 = \lambda_1 x, \dots, \lambda_m x) = 0$?

As it turns out, this is a well-known and solved mathematical problem known as *non-commutative elimination*. To see the connection, we start from the set of operators \hat{H}_i . Their main property is that when they act on the quiver series, they set it to zero (4.1.4), we say they *annihilate* the quiver series. But there is more structure than meets the eye at first sight, take any operator \hat{F} in terms of \hat{x}_i and \hat{z}_i , in general $\hat{F} \cdot P \neq 0$. However, if we multiply any \hat{H}_i from the left by \hat{F} the resulting operator does annihilate the quiver series $(\hat{F}\hat{H}_i) \cdot P_C(x_1, \dots, x_m) = 0$.

We can further add any two $\hat{H}_i + \hat{H}_j$ and the resulting operator will still annihilate the quiver series. We can summarize these two observations in the more general statement

$$\left(\sum_{i=1}^m \hat{F}_i \hat{H}_i \right) \cdot P_C(x_1, \dots, x_m) = 0, \quad (4.1.8)$$

where \hat{F}_i are arbitrary operators in \hat{x}_i and \hat{z}_i . The above equation (4.1.8) implies that the set of operators that annihilate the series of quivers is closed by addition and multiplication from the left. Any set closed under these operations is called an *ideal*, and in the particular case of operators annihilating a function is known as *left sided annihilation ideal*. Since any operator belonging to this ideal can be expressed in terms of $\langle \hat{H}_1, \dots, \hat{H}_m \rangle$, we say that they are *generators of the ideal*.

Now that we know that the quantum Nahm equations (4.1.4) generate an ideal, we can use the operations of the ideal to construct the *quiver quantum A-polynomial*

$$\boxed{\hat{A} \left(\hat{x}_1, \dots, \hat{x}_m, \prod_{i=1}^m \hat{z}_i \right) \cdot P_C(x_1, \dots, x_m) \Big|_{x_j = \lambda_j x} = \hat{A}(\hat{x}, \hat{y}) \cdot P_C(x) = 0.} \quad (4.1.9)$$

To that end, we can rewrite (4.1.7) as an operator annihilating the quiver series

$$\boxed{P_C^{-1} \left(\hat{y} - \prod_{i=1}^m \hat{z}_i \right) \cdot P_C = 0 \xrightarrow{h \rightarrow 0} y = e^{\sum_{i=1}^m x_i \partial_{x_i} S_{-1}}.} \quad (4.1.10)$$

We can treat this equation as an extra generator of the ideal $\langle \hat{H}_1, \dots, \hat{H}_m, \hat{y} - \prod_{i=1}^m \hat{z}_i \rangle$. In this way, our setup is analogous to the problem of solving a set of polynomial equations. Each generator produces an independent equation, $m + 1$ in total, and we can think of \hat{y} and \hat{z}_i as $m + 1$ non-commutative variables. Therefore, we can use the equations to progressively eliminate non-commutative variables \hat{z}_i . We can repeat this process until we obtain an equation in terms of \hat{y} alone. This strategy is the non-commutative elimination algorithm we mentioned before.

Next, we present a couple of important properties of the quiver series which are passed on to the quiver A-polynomial. Lastly, it is worth mentioning that we focus special attention in deriving quiver A-polynomials, which have genus zero as

complex curves. The reason is because in [44] we proposed to recover the quantum A-polynomial from the classical one, using a technique known as *topological recursion*. For more on that topic, we encourage the reader to look at [44, 73] and references therein.

4.1.1 Properties of the quiver A-polynomial

Framing As we discussed earlier in subsection (2.2.1), there is an ambiguity in various knot invariants called framing. Framing inserts an extra factor in the generating function for colored superpolynomials (2.2.14) as

$$P^{\mathcal{K}}(a, q, t, x) = \sum_{r=0}^{\infty} \frac{x^r}{(q)_r} (-q^{1/2})^{fr^2} P_r^{\mathcal{K}}(a, q, t), \quad f \in \mathbb{Z}. \quad (4.1.11)$$

Due to the quadratic exponent r^2 , when reexpressing this in a quiver series, with $r = d_1 + \dots + d_m$, framing acts on the quiver matrix as an overall shift of its entries

$$C \longrightarrow C + f1_{m \times m}, \quad (4.1.12)$$

where we recall that $1_{m \times m}$ stands for the $m \times m$ matrix with ones in all its entries.

At the level of the quantum Nahm equations (4.1.4) they lead to

$$\begin{aligned} \widehat{H}_k' &= (-q^{1/2})^{C_{kk}+f} \widehat{x}_k \prod_j^m \widehat{z}_j^{C_{kj}+f} + \widehat{z}_k - 1 = (-q^{1/2})^{C_{kk}} \widehat{x}_k' \prod_j^m \widehat{z}_j^{C_{kj}} + \widehat{z}_k - 1, \\ \widehat{x}_k' &= \widehat{x}_k (-q^{1/2} \widehat{y})^f, \end{aligned} \quad (4.1.13)$$

where we should think of \widehat{x}_i' as a new operator, not as a change of variables. It is straightforward to check that it does not change the commutation relations $\widehat{z}_i \widehat{x}_j' = q^{\delta_{ij}} \widehat{x}_j' \widehat{z}_i$ and $\widehat{x}_i' \widehat{x}_j' = \widehat{x}_j' \widehat{x}_i'$.

In other words, if we find the quiver quantum A-polynomial for a quiver matrix C , then it suffices to transform $\widehat{x}_i \rightarrow \widehat{x}_i \widehat{y}^f$

$$\boxed{\widehat{A}_{C+f1_{m \times m}}(\widehat{x}_i, \widehat{y}) = \widehat{A}_C(\widehat{x}_i (-q^{1/2} \widehat{y})^f, \widehat{y})}. \quad (4.1.14)$$

We should keep in mind that if we want to normal order it, say all \widehat{y} to the right, that will produce extra q -factors from products of x s, as $\widehat{x}_i \widehat{x}_j \rightarrow \widehat{x}_i \widehat{y}^f \widehat{x}_j \widehat{y}^f = \widehat{x}_i q^f \widehat{x}_j \widehat{y}^{2f}$.

Mirror transform The second operation we import from the realm of knot invariants is the mirror image of a knot. That is, when we invert the orientation of the knot from the skein relation (2.2.17) we can see that it takes $q \rightarrow q^{-1}$. In the quiver series, this transformation actually produces a symmetry if we further perform $C \rightarrow I - C$

$$P_{I-C}(x_1, \dots, x_m; q^{-1}) = P_C(q^{1/2} x_1, \dots, q^{1/2} x_m; q) \quad (4.1.15)$$

where the q -prefactor in front of x_i arises from the q -Pochhammers on the denominator thanks to the identity $(q^{-1})_d = (-q^{-1/2})^{d^2} q^{-d/2} (q)_d$. We call the matrix $I - C$ the *reciprocal* of C , and the reason behind this name is due to the operation it induces on the quiver A-polynomial.

To see the effect $C \rightarrow I - C$ has on the quantum A polynomial of the quiver, we shall first look at the transformation of the quantum Nahm equations (4.1.4)

$$\begin{aligned}
\widehat{H}_{i,I-C}(\widehat{x}_i, \widehat{z}_j; q) &= (-q^{1/2})^{\delta_{ii}-C_{ii}} \widehat{x}_i \prod_{j=1}^m \widehat{z}_j^{\delta_{ij}-C_{ij}} + \widehat{z}_i - 1 \\
&= (-\widehat{z}_i) \left[(-q^{-1/2})^{C_{ii}} q^{-1/2} \widehat{x}_i \prod_{j=1}^m \widehat{z}_j^{-C_{ij}} - 1 + \widehat{z}_i^{-1} \right] \\
&= (-\widehat{z}_i) \widehat{H}_{i,C}(q^{-1/2} \widehat{x}_i, \widehat{z}_i^{-1}, q^{-1}).
\end{aligned} \tag{4.1.16}$$

We can tell that it inverts $\widehat{z}_i \rightarrow \widehat{z}_i^{-1}$. Hence, to have a similar set of equations, let us modify the equation for \widehat{y} , in terms of \widehat{z}_i^{-1}

$$\widehat{y} - \prod_{i=1}^m \widehat{z}_i = -\widehat{y} \prod_{j=1}^m \widehat{z}_j \left(\widehat{y}^{-1} - \prod_{i=1}^m \widehat{z}_i^{-1} \right). \tag{4.1.17}$$

Based on the fact that the quantum Nahm equations form an ideal, we may always discard the prefactors on the l.h.s. of (4.1.16) and (4.1.17). Finally, as expected, the effect of $C \rightarrow I - C$ on the equations is $q \rightarrow q^{-1}$, $\widehat{z}_i \rightarrow \widehat{z}_i^{-1}$, $\widehat{y} \rightarrow \widehat{y}^{-1}$, while rescaling $\widehat{x}_i \rightarrow q^{-1/2} \widehat{x}_i$. Since, rescaling \widehat{x}_i does not affect the rest of the operators, in the end, this leads to the following transformation on the quiver quantum A-polynomial

$$\boxed{\widehat{A}_{I-C}(\widehat{x}_i, \widehat{y}; q) = \widehat{A}_C(q^{-1/2} \widehat{x}_i, \widehat{y}^{-1}; q^{-1})}. \tag{4.1.18}$$

This operation in the context of polynomials is known as taking the reciprocal of a polynomial in the variables \widehat{y} and q , and therefore we refer to it as the reciprocal quiver.

These two properties would be very very important for us when deriving A-polynomials for quivers. Thanks to them, if two quivers are related by the above transformations, then for us their quiver A-polynomials will be practically equivalent. We will concentrate then on quivers which are not equivalent and derive the A-polynomial for its simplest representative.

4.2 Examples of explicit quiver A-polynomials

4.2.1 One node quiver

The first quiver in our list is the one node quiver. The quiver matrix is pure framing $C = f$

$$P_C(x) = \sum_{d=0}^{\infty} (-q^{1/2})^{fd^2} \frac{x^d}{(q)_d}. \tag{4.2.1}$$

Directly upon setting $m = 1$ in the quantum Nahm equations (4.1.4) we obtain the quantum (and classical) A-polynomial

$$A(\widehat{x}, \widehat{y}) = \widehat{x}(-q^{1/2} \widehat{y})^f + \widehat{y} - 1 \xrightarrow{h \rightarrow 0} A(x, y) = x(-y)^f + y - 1 = 0. \tag{4.2.2}$$

It is easy to show that the classical A-polynomial is a genus zero complex curve. This because it is linear in x and we can easily solve the previous equation for x in terms of y and introduce the following rational parametrization

$$x(t) = \frac{1-t}{(-t)^f}, \quad y(t) = t, \quad t \in \mathbb{C}. \quad (4.2.3)$$

This particular quiver is the one associated to the colored superpolynomials of the unknot.

4.2.2 Homogeneous quiver

The straightforward generalization of the one-node quiver is the $m \times m$ homogeneous quiver $C = f1_{m \times m}$. This quiver is essentially pure framing, so we can derive the unframed version of the A-polynomial and reintroduce frame dependence at the end.

The quantum Nahm equations with $f = 0$ for this quiver are

$$\begin{aligned} \hat{z}_i \cdot P_{C=0} &= [1 - (-q^{1/2})^f \hat{x}_i] \cdot P_{C=0}, \\ \left(\prod_{j \neq i} \hat{z}_j \right) \hat{z}_i \cdot P_{C=0} &= \left(\prod_{j \neq i} \hat{z}_j \right) [1 - (-q^{1/2})^f \hat{x}_i] \cdot P_{C=0} \\ \prod_{i=1}^m \hat{z}_i \cdot P_{C=0} &= \prod_{i=1}^m [1 - (-q^{1/2})^f \hat{x}_i] \cdot P_{C=0}. \end{aligned} \quad (4.2.4)$$

This clearly leads us to the following quiver A-polynomials

$$\hat{A}(\hat{x}_i, \hat{y}) = \prod_{i=1}^m [1 - \hat{x}_i (-q^{1/2} \hat{y})^f] - \hat{y} \xrightarrow{h \rightarrow 0} A(x_i, y) = \prod_{i=1}^m (1 - x_i (-y)^f) - y = 0. \quad (4.2.5)$$

Then, upon the change of variables $x_i = \lambda_i x$ the classical A-polynomial is a genus zero curve. To see this, we take the unframed A-polynomial $f = 0$ solve for y and take $x(t) = t$ as a parameter

$$x(t) = \frac{t}{(-y)^f(t)}, \quad y(t) = - \prod_{i=1}^m (1 - \lambda_i x), \quad (4.2.6)$$

where the denominator of $x(t)$ is to reintroduce the framing dependence as mentioned in (4.1.14).

4.3 Genus zero two-node quivers

In the previous section 4.2 we have seen two examples in which the entire quiver dependence is encoded in a framing transformation. In this section, we concentrate on another set of tractable examples, the two-node quiver matrices. In general, they depend on three parameters, however, thanks to the framing transformation we will deal with diagonal quiver matrices

$$C = \begin{bmatrix} a & 0 \\ 0 & b \end{bmatrix}. \quad (4.3.1)$$

4.3.1 Diagonal $\begin{bmatrix} a & 0 \\ 0 & 1 \end{bmatrix}$

The simplest nontrivial family of quivers

$$C = \begin{bmatrix} a & 0 \\ 0 & 0 \end{bmatrix},$$

with $a \in \mathbb{Z}$. For the particular value of $a = 1$ the quiver series gives the colored superpolynomials for the unknot in the unreduced normalization [31]. Setting $a = 2$ it reproduces the extremal invariants of the trefoil knot and certain Duchon paths [52]. Lastly, for $a = 0$ it gives back the homogeneous quiver from the previous subsection 4.2.2.

The quantum Nahm equations (4.1.4) for this quiver matrix are

$$[\hat{x}_1(-q^{1/2}\hat{z}_1)^a + \hat{z}_1] \cdot P_C = P_C, \quad \hat{z}_2 \cdot P_C = [1 - \hat{x}_2] \cdot P_C. \quad (4.3.2)$$

If we multiply the first equation (with \hat{x}_1) from the left by \hat{z}_2 and use both the second equation (with \hat{x}_2) we get

$$\hat{x}_1(-q^{1/2})^a(\hat{z}_1)^{a-1}\hat{y} \cdot P_C = [1 - \hat{x}_2 - \hat{y}] \cdot P_C, \quad (4.3.3)$$

where we also isolated the term with \hat{x}_1 on the l.h.s. Finally, we can multiply the resulting equation by \hat{z}_2^{a-1} from the left. On the l.h.s. that would produce a \hat{y}^a factor, where as on the r.h.s. we may use the second quantum Nahm equation (4.3.2) leading to the quantum A-polynomial

$$\hat{A}(\hat{x}_1, \hat{x}_2, \hat{y}) = \begin{cases} \hat{x}_1(-q^{1/2}\hat{y})^a + (q\hat{x}_2; q)_{a-1}\hat{y} - (\hat{x}_2; q)_a, & a \geq 1, \\ \hat{x}_1(\hat{x}_2; q)_{1-a} + (q^{-a}\hat{x}_2 - 1 + \hat{y})(-q^{-1/2}\hat{y})^{-a}, & a \leq 0, \end{cases} \quad (4.3.4)$$

and the classical A-polynomial

$$A(x_1, x_2, y) = \begin{cases} x_1(-y)^a + (1 - x_2)^{a-1}y - (1 - x_2)^a, & a \geq 1 \\ x_1(1 - x_2)^{1-a} + (x_2 - 1 + y)(-y)^{-a}, & a \leq 0 \end{cases} \quad (4.3.5)$$

After the change of variables $x_1 = \lambda_1 x$ and $x_2 = \lambda_2 x$, the classical A-polynomial (4.3.5) is a genus zero curve, with the rational parametrization

$$x(t) = \frac{\lambda_1^{a-2}(t + (-1)^a \lambda_1)}{t^a}, \quad y(t) = \frac{t^a - \lambda_1^{a-2} \lambda_2 t + (-1)^{a+1} \lambda_1^{a-1} \lambda_2}{(-1)^{a+1} \lambda_1 t^{a-1}}. \quad (4.3.6)$$

4.3.2 Diagonal $\begin{bmatrix} a & 0 \\ 0 & 1 \end{bmatrix}$

This family of quivers also yields genus zero classical A-polynomials

$$C = \begin{bmatrix} a & 0 \\ 0 & 1 \end{bmatrix},$$

with $a \in \mathbb{Z}$. For $a = 1$ and $C \rightarrow I - C$ this quiver is equivalent to the homogeneous quiver with $f = 0$.

The quantum Nahm equations are practically the same as for the previous family (4.3.2). The difference is, the second equation (with \hat{z}_2) we transform its r.h.s.

$[1 - \hat{x}_2] \rightarrow [1 - q^{1/2}\hat{x}_2]^{-1}$. Having done that transformation, the rest of the derivation of the quantum A-polynomials is analogous, and it gives

$$\hat{A}(\hat{x}_1, \hat{x}_2, \hat{y}) = \begin{cases} \hat{x}_1(q^{1/2}\hat{x}_2; q)_a(-q^{1/2}\hat{y})^a + (1 - q^{1/2}x_2)\hat{y} - 1, & a \geq 1, \\ (q^{1/2}\hat{x}_2; q)_{a+1}\hat{y}^{a+1} + (-q^{-1/2})^a\hat{x}_1 - (q^{1/2}\hat{x}_2; q)_a\hat{y}^a, & a \leq 0. \end{cases} \quad (4.3.7)$$

The classical A-polynomial

$$A(x_1, x_2, y) = \begin{cases} x_1(1 - x_2)^a(-y)^a + (1 - x_2)y - 1, & a \geq 1, \\ (1 - x_2)^{a+1}y^{a+1} + (-1)^a x_1 - (1 - x_2)^a y^a, & a \leq 0. \end{cases} \quad (4.3.8)$$

Upon the change of variables, they are genus zero curves with the parametrization

$$x(t) = \frac{\lambda_1^{a-2}(t + (-1)^a \lambda_1)}{t^a}, \quad y = \frac{(-1)^{a+1} \lambda_1^{-1} t^{a+1}}{t^a - \lambda_1^{a-2} \lambda_2 t + (-1)^{a+1} \lambda_1^{a-1} \lambda_2} \quad (4.3.9)$$

4.3.3 Reciprocal $\begin{bmatrix} a & 0 \\ 0 & 1-a \end{bmatrix}$

This next family of quivers is invariant under the reciprocal operation (4.1.18), so that is why we refer to them as reciprocal quivers

$$C = \begin{bmatrix} a & 0 \\ 0 & 1-a \end{bmatrix},$$

where $a \in \mathbb{Z}_+$ because $a \leq 0$ is equivalent to $x_1 \leftrightarrow x_2$. For the value $a = 1$ it overlaps with the diagonal $(1, 0)$ seen in the previous subsections 4.3.2 and 4.3.1.

Its quantum A-polynomial has the form

$$\begin{aligned} \hat{A}(\hat{x}_1, \hat{x}_2, \hat{y}) &= \prod_{n=0}^{a-1} (q^a \hat{x}_1 \hat{y}^a - q^{(a-n)(a-1)+1/2} \hat{x}_2) \\ &\quad + q^{a/2} \prod_{n=0}^{a-2} (q^{n+a} \hat{x}_1 \hat{y}^{a-1} - q^{(a-n)(a-1)+1/2} \hat{x}_2) (1 - \hat{y})(-\hat{y})^{a-1} \end{aligned} \quad (4.3.10)$$

Classical A-polynomial, the blue factor, is the one that encodes the asymptotics of the quiver generating function, since is the one that satisfies $y(x=0) = 1$.

$$A(x_1, x_2, y) = (x_1 y^a - x_2)^a + (1 - y)(-y)^{a-1} (x_1 y^{a-1} - x_2)^{a-1} \quad (4.3.11a)$$

$$A(x, x, y) = (y - 1)^a x^{a-1} (x[a]_y^a - (-y)^{a-1} [a - 1]_y^{a-1}), \quad (4.3.11b)$$

where $[a]_q = (1 - y^a)/(1 - y) = \sum_{n=0}^{a-1} y^n$. In the above equation we can observe for the first time a very interesting phenomenon. When $x_1 = x_2 = x$ the classical A-polynomial factorizes into two factors, blue and red, while the quantum A-polynomial does not factorize. The reason for this degeneracy is due to the reciprocal symmetry $y^{-1}(x_1, x_2) = y(x_2, x_1)$, which in the case $y^{-1}(x) = y(x) \implies y(x) = \pm 1$. By looking directly at the quiver series (2.1.40), $P_C(x=0) = 1 \implies y(x=0) = 1$, so the blue factor in (4.3.11b) is the only component which satisfies this, thus we may discard the red factor.

In other words, we can think of the quiver series $P_{1-a}(x)$ in the classical limit, as the reciprocal of $P_a(x)$. A good example of this claim is when $a = 1$, we then have

$$P_1(q^{-1/2}x) = (x; q)_\infty = P_0^{-1}(x), \quad (4.3.12)$$

where $(x; q)_\infty$ is the infinite q -Pochhammer (2.1.31).

We found two suitable parametrizations for (4.3.11a). They are related via a simple rational transformation, still upon setting $x_1 = x_2 = x$ one parametrizes the red factor in (4.3.11b), while the second parametrizes the blue factor. The first parametrization is

$$x(t) = (t-1)(-t)^{a-1} \frac{(\lambda_1 t^{a-1} - \lambda_2)^{a-1}}{(\lambda_1 t^a - \lambda_2)^a}, \quad y(t) = t \quad (4.3.13a)$$

$$x(t) = (-t)^{a-1} \frac{[a-1]_t^{a-1}}{[a]_t^a}, \quad y(t) = t, \quad \lambda_1 = \lambda_2 = 1. \quad (4.3.13b)$$

The second parametrization, obtained from the first one after the transformation $t \rightarrow (c_2 t - 1)/(c_1 t - 1)$

$$x(t) = t \frac{[(\lambda_1 t - 1)(\lambda_2 t - 1)(-\Delta_{a-1}(t))]^{a-1}}{\Delta_a(t)^a}, \quad y(t) = \frac{\lambda_2 t - 1}{\lambda_1 t - 1} \quad (4.3.14a)$$

$$x(t) = -t \frac{[(a-2)t + 1]^{a-1}}{[(1-a)t - 1]^a}, \quad y(t) = 1, \quad \lambda_1 = \lambda_2 = 1, \quad (4.3.14b)$$

where

$$\Delta_a(t) = \frac{\lambda_1(\lambda_2 t - 1)^a - \lambda_2(\lambda_1 t - 1)^a}{(-1)^{a+1}(\lambda_2 - \lambda_1)} = 1 - \lambda_1 \lambda_2 \sum_{n=2}^a \binom{a}{n} (-t)^n \sum_{m=0}^{n-2} \lambda_1^m \lambda_2^{n-2-m} \quad (4.3.14c)$$

4.3.4 Diagonal $\begin{bmatrix} a & 0 \\ 0 & a \end{bmatrix}$

The last family of quivers yielding genus zero classical curves is the diagonal quiver

$$\begin{bmatrix} a & 0 \\ 0 & a \end{bmatrix}$$

Where $a \in \mathbb{Z}_+$, because $a < 0$ can be obtained from $a > 1$ after $C \rightarrow I - C$. The cases $a = 1$ and $a = 0$ are examples of homogeneous quiver in subsection 4.2.2 and $I - \begin{bmatrix} 0 & 0 \\ 0 & 0 \end{bmatrix}$.

We proceed to derive the quiver A-polynomial, starting from the quantum Nahm equations

$$(-q^{1/2})^a \hat{x}_1 \hat{z}_1^a \cdot P_C = (1 - \hat{z}_1) \cdot P_C, \quad (-q^{1/2})^a \hat{x}_2 \hat{z}_2^a \cdot P_C = (1 - \hat{z}_2) \cdot P_C. \quad (4.3.15)$$

We can multiply the second equation from the left by $(-q^{1/2})^a \hat{x}_1 \hat{z}_1^{a+1}$, leading to

$$q^{a+1} \hat{x}_1 \hat{x}_2 \hat{y}_2^a \cdot P_C = (\hat{z}_1 - \hat{y})(-q^{1/2})^a \hat{x}_1 \hat{z}_1^a \cdot P_C = (\hat{z}_1 - \hat{y})(1 - \hat{z}_1) \cdot P_C, \quad (4.3.16)$$

where to obtain the second equality, we have used the first quantum Nahm equation (4.3.15). The aforementioned equation can be rewritten as

$$\hat{z}_1^2 \cdot P_C = (\hat{B}_{a+1} \hat{z}_1 - \hat{y}) \cdot P_C, \quad \hat{B}_s = 1 + \hat{y} - q^s \hat{x}_1 \hat{x}_2 \hat{y}^a. \quad (4.3.17)$$

Now comes the interesting observation. We may multiply the above equation from the left \hat{z}_1 , giving

$$\hat{z}_1^3 \cdot P_C = (\hat{B}_{a+2} \hat{z}_1^2 - \hat{y} \hat{z}_1) \cdot P_C = \left[(\hat{B}_{a+2} \hat{B}_{a+1} - \hat{y}) \hat{z}_1 - \hat{B}_{a+2} \hat{y} \hat{z}_1 \right] \cdot P_C, \quad (4.3.18)$$

where we used (4.3.17) for the term \widehat{z}_1^2 in the r.h.s. This quickly leads us to the observation that any power $\widehat{z}_1^k \cdot P_C$ can be reexpressed as

$$\widehat{z}_1^k \cdot P_C = (\widehat{R}_{k,a} \widehat{z}_1 + \widehat{T}_{k,a}) \cdot P_C \quad (4.3.19)$$

where $\widehat{R}_{k,a}$ and $\widehat{T}_{k,a}$ are the resulting operators in terms of \widehat{B}_k and \widehat{y} . The second index of $\widehat{R}_{k,a}$ is associated with the index of B_s . The explicit form of these operators for the two next values of k is the following

$$\widehat{R}_{4,a} = \widehat{B}_{a+1} \widehat{B}_{a+2} \widehat{B}_{a+3} - 2\widehat{y} \widehat{B}_{a+1}, \quad T_{4,a} = -(\widehat{B}_{a+2} \widehat{B}_{a+3} - \widehat{y}) \widehat{y}, \quad (4.3.20a)$$

$$\begin{aligned} \widehat{R}_{5,a} &= \widehat{B}_{a+1} \widehat{B}_{a+2} \widehat{B}_{a+3} \widehat{B}_{a+4} \\ &\quad - 3\widehat{y} \widehat{B}_{a+1} \widehat{B}_{a+2} + \widehat{y}^2, \end{aligned} \quad T_{5,a} = -(\widehat{B}_{a+2} \widehat{B}_{a+3} \widehat{B}_{a+4} - 2\widehat{y} \widehat{B}_{a+2}) \widehat{y}. \quad (4.3.20b)$$

Actually, we can derive the recursion relation satisfied by the previous operators by multiplying \widehat{z}_1 from the left in (4.3.19),

$$\widehat{R}_{k+1,a} = \widehat{R}_{k,a+1} \widehat{B}_a + \widehat{T}_{k,a+1}, \quad \widehat{T}_{k+1,a} = -\widehat{R}_{k,a+1} \widehat{y}. \quad (4.3.21)$$

Given that this is a linear recursion relation, we can easily find the explicit solution

$$\widehat{R}_{k,a} = \sum_{n=0}^{\lfloor \frac{k+1}{2} \rfloor} \binom{k+1-n}{n} (-\widehat{y})^n \prod_{s=1}^{k+1-2n} \widehat{B}_{a+s}, \quad \widehat{T}_{k,a} = -\widehat{R}_{k-1,a+1} \widehat{y}. \quad (4.3.22)$$

So far, all this derivation has been for \widehat{z}_1 . However, we can obtain the same results for \widehat{z}_2 after $\widehat{z}_1 \rightarrow \widehat{z}_2$ and $\widehat{x}_1 \rightarrow \widehat{x}_2$, due to the symmetry of this particular quiver.

Next, the combination of the quantum Nahm equations (4.3.15) with (4.3.19) produces

$$q^a \widehat{x}_1 \widehat{x}_2 \widehat{y}^a \cdot P_C = (1 - \widehat{z}_1 - \widehat{z}_2 + \widehat{y}) \cdot P_C, \quad (4.3.23a)$$

$$(-q^{1/2})^a (\widehat{x}_1 + \widehat{x}_2) \widehat{y}^a \cdot P_C = \left[(\widehat{R}_{a,a} - \widehat{T}_{a,a+1})(\widehat{z}_1 + \widehat{z}_2) + 2(\widehat{T}_{a,a} - \widehat{R}_{a,a+1} \widehat{y}) \right] \cdot P_C. \quad (4.3.23b)$$

Lastly, we can multiply the first equation from the left by $\widehat{R}_{a,a} - \widehat{T}_{a,a+1}$, and add them together and cancel the linear terms in \widehat{z}_1 and \widehat{z}_2 . Finally, we obtain the quiver quantum A-polynomial

$$\begin{aligned} \widehat{A}(\widehat{x}_1, \widehat{x}_2, \widehat{y}) &= (\widehat{R}_{a,a} - \widehat{T}_{a,a+1})(1 + \widehat{y}) + 2(\widehat{T}_{a,a} - \widehat{R}_{a,a+1}) \widehat{y} \\ &\quad - \left[(-q^{1/2})^a (\widehat{x}_1 + \widehat{x}_2) + (\widehat{R}_{a,a} - \widehat{T}_{a,a+1}) q^a \widehat{x}_1 \widehat{x}_2 \right] \widehat{y}^a. \end{aligned} \quad (4.3.24)$$

In the classical limit, the A-polynomial simplifies to

$$A(x_1, x_2, y) = (R_a + T_a)(1 - y) - [(-1)^a (x_1 + x_2) + (R_a - T_a) x_1 x_2] y^a \quad (4.3.25)$$

with $\widehat{B}_s \xrightarrow{h \rightarrow 0} B_0$, $\widehat{R}_{k,a} \xrightarrow{h \rightarrow 0} R_{k,0} = R_k$, likewise for T_a . The fact that these variables do no longer depend on the second index produces a cancellation of terms in the first line of the quantum A-polynomial (4.3.24); resulting in the nice factorization we see in the classical case (4.3.25).

Moreover, in the classical case we can give an alternative expression for R_a and T_a . If we take the classical limit of the recursion relations (4.3.21) and write them in matrix form

$$\begin{bmatrix} R_{k+1} \\ T_{k+1} \end{bmatrix} = \begin{bmatrix} B & 1 \\ -y & 0 \end{bmatrix} \begin{bmatrix} R_k \\ T_k \end{bmatrix} = \begin{bmatrix} B & 1 \\ -y & 0 \end{bmatrix}^{k+1} \begin{bmatrix} R_0 = B_0 \\ T_0 = -y \end{bmatrix}. \quad (4.3.26)$$

Thus, to compute the k -th term, we can raise the above matrix to its k -th power. The k -th power is easily computed in terms of the eigenvalues. Then, when acting on the

$$\begin{bmatrix} B & 1 \\ -y & 0 \end{bmatrix}^k = \frac{1}{\Delta^{k/2}} \begin{bmatrix} \lambda_+^{k+1} - \lambda_-^{k+1} & \lambda_+^k - \lambda_-^k \\ \lambda_+ \lambda_- (\lambda_-^k - \lambda_+^k) & \lambda_+ \lambda_- (\lambda_-^{k-1} - \lambda_+^{k-1}) \end{bmatrix}, \quad \lambda_{\pm} = \frac{B_0 \pm \sqrt{\Delta}}{2}, \quad (4.3.27)$$

where $\Delta = B_0^2 - 4y$. After acting on the vector of initial conditions (4.3.26) the result simplifies to

$$R_a = (\lambda_+^a - \lambda_-^a)/\sqrt{\Delta}, \quad T_a = -yR_{a-1}, \quad (4.3.28)$$

with $a = k + 2$.

Just like the A-polynomial for the reciprocal quiver (4.1.18) factorizes when $x_1 = x_2 = x$, this A-polynomial does too, in the form

$$A(x, y) = A_1(x, y) \cdot A_2(x, y)^2, \quad (4.3.29)$$

where the blue factor reads as

$$A_1(x, y) = \begin{cases} (xy^n - 1)^2 - y = 0, & \text{for } a = 2n, \\ (xy^n - 1)^2 y - 1 = 0, & \text{for } a = 2n + 1, \end{cases} \quad (4.3.30)$$

whereas the red factor for the first few values of a looks as

$$A_2(x, y)|_{a=2} = xy + 1, \quad (4.3.31a)$$

$$A_2(x, y)|_{a=3} = x^2 y^3 + xy^2 - 1, \quad (4.3.31b)$$

$$A_2(x, y)|_{a=4} = x^3 y^6 + x^2 y^4 - xy^3 - xy^2 - 1, \quad (4.3.31c)$$

$$A_2(x, y)|_{a=5} = x^4 y^{10} + x^3 y^8 - x^2 y^6 - 2x^2 y^5 - xy^4 - xy^3 + 1. \quad (4.3.31d)$$

The blue factor is the correct one describing the asymptotics of the quiver series, since is the one that has a unique solution with the feature $y(x=0) = 1$.

This factorization arises due to the symmetry $x_1 \leftrightarrow x_2$, which degenerates at the value $x_1 = x_2 = x$. The quantum A-polynomial also factorizes, we will show this explicitly in the case of $a = 2$. In general, the number of linearly independent solutions to the equation $\hat{A}(\hat{x}_1, \hat{x}_2, \hat{y}) \cdot P_C = 0$ is $\deg_{\hat{y}} \hat{A} = a^2$. Due to the factorization of the quantum A-polynomial, the \hat{y} degree decreases, implying that the dimension of the space of solutions is also reduced. This means that some of the solutions upon $x_1 = x_2 = x$ become identical and lead to the factorization.

These classical A-polynomials are also genus zero curves with a rational parametrization

$$x(t) = \frac{(t-1)(-t)^{a-1}(\lambda_1 t^{a-1} - \lambda_2)^{a-1}}{(\lambda_1 t^a - \lambda_2)^a}, \quad y(t) = \frac{(\lambda_1 t^a - \lambda_2)^2}{t(\lambda_1 t^{a-1} - \lambda_2)^2} \quad (4.3.32a)$$

$$x(t) = t(-t)^{a-1} \frac{[a-1]_t^{a-1}}{[a]_t^a}, \quad y(t) = \frac{[a]_t^2}{t[a-1]_t^2}, \quad \lambda_1 = \lambda_2 = 1, \quad (4.3.32b)$$

which after $x_1 = x_2 = x$ they parameterise the red factor $A_2(x, y)$. To obtain a rational parametrization for the blue factor $A_1(x, y)$ we perform the same transformation $t \rightarrow (\lambda_2 t - 1)/(\lambda_1 t - 1)$

$$x(t) = t \frac{[(\lambda_1 t - 1)(\lambda_2 t - 1)(-\Delta_{a-1}(t))]^{a-1}}{\Delta_a(t)^a}, \quad y(t) = \frac{\Delta_a(t)^2}{(\lambda_1 t - 1)(\lambda_2 t - 1)\Delta_{a-1}(t)^2}, \quad (4.3.33a)$$

$$x(t) = -t \frac{[(a-2)t+1]^{a-1}}{[(1-a)t-1]^a}, \quad y(t) = \left[\frac{(a-1)t+1}{(a-2)t+1} \right]^2, \quad \lambda_1 = \lambda_2 = 1, \quad (4.3.33b)$$

where Δ_a defined in (4.3.14c).

$\left[\begin{smallmatrix} 2 & 0 \\ 0 & 2 \end{smallmatrix} \right]$ The value $a = 2$ is the simplest nontrivial case in which we can observe the factorization at both quantum and classical levels. Let us write the quantum A-polynomial in a way which is easy to see the factorization feature

$$\widehat{A}(\widehat{x}_1, \widehat{x}_2, \widehat{y}) = (q^3 \widehat{x}_1 \widehat{x}_2 \widehat{y}^2 - 1)(q^2 \widehat{x}_1 \widehat{x}_2 \widehat{y}^2 - 1) - (q \widehat{x}_2 \widehat{y} + 1)(q \widehat{x}_1 \widehat{y} + 1) \widehat{y}, \quad (4.3.34a)$$

$$\widehat{A}(\widehat{x}, \widehat{x}, \widehat{y}) = [q \widehat{x} \widehat{y} + 1][(q \widehat{x} \widehat{y} - 1)(q^2 \widehat{x}^2 \widehat{y}^2 - 1) - (q \widehat{x} \widehat{y} + 1) \widehat{y}], \quad (4.3.34b)$$

and for the classical one

$$A(\lambda_1 x, \lambda_2 x, y) = (\lambda_1 \lambda_2 x^2 y^2 - 1)^2 - (\lambda_2 x y + 1)(\lambda_1 x y + 1) y \quad (4.3.35a)$$

$$A(x, x, y) = (x y + 1)^2 [(x y - 1)^2 - y]. \quad (4.3.35b)$$

We have for the first parametrization

$$x(t) = (t-1)(-t) \frac{(\lambda_1 t - \lambda_2)}{(\lambda_1 t^2 - \lambda_2)^2}, \quad y(t) = \frac{(\lambda_1 t^2 - \lambda_2)^2}{t(\lambda_1 t - \lambda_2)^2}, \quad (4.3.36a)$$

$$x(t) = \frac{-t}{(t+1)^2}, \quad y(t) = \frac{(t+1)^2}{t}, \quad \lambda_1 = \lambda_2 = 1, \quad (4.3.36b)$$

while for the second

$$x(t) = -t \frac{(\lambda_1 t - 1)(\lambda_2 t - 1)}{(\lambda_1 \lambda_2 t^2 - 1)^2}, \quad y(t) = \frac{(\lambda_1 \lambda_2 t^2 - 1)^2}{(\lambda_1 t - 1)(\lambda_2 t - 1)}, \quad (4.3.37a)$$

$$x(t) = -\frac{t}{(t+1)^2}, \quad y(t) = (t+1)^2, \quad \lambda_1 = \lambda_2 = 1. \quad (4.3.37b)$$

4.4 Higher genus quiver A-polynomials

Having exhausted all nonequivalent families of quivers yielding genus zero classical A-polynomials, we switch our attention to the higher genus ones. Here we also define equivalent families of quivers up to framing (4.1.14) and/or reciprocal (4.1.18) transformations. Furthermore, there are two more operations that preserve the genus of the classical A-polynomial, these are $C_{1,1} \rightarrow 1 - C_{1,1}$ and $C_{2,2} \rightarrow 1 - C_{2,2}$ (remembering that $C_{1,1} = a$ and $C_{2,2} = b$). This allows us to focus only on quivers with $a, b > 0$. Quite surprisingly, the number of nonequivalent quivers with a given genus $g > 0$, happens to be finite, contrary to the $g = 0$ case, where we have infinite families (previous section 4.3).

(a, b)	$A(x_1, x_2, y)$
(3,2)	$y^6 x_1^2 x_2^3 - 2y^4 x_1 x_2^2 - y^4 x_1 x_2 - 3y^3 x_1 x_2 - y^3 x_1 + y^2 x_2 + y - 1$
(4,2)	$y^8 x_1^2 x_2^4 - 3y^5 x_1 x_2^2 - y^5 x_1 x_2 - 2y^4 x_1 x_2^2 - 4y^4 x_1 x_2 - y^4 x_1 - y^2 x_2 - y + 1$
(-1,-2)	$y^6 - y^5 - y^4 x_1 + 3y^3 x_1 x_2 + 2y^2 x_1^2 x_2 - x_1^3 x_2^2 + y^3 x_2 + y^2 x_1 x_2$
(-1,-3)	$y^8 - y^7 - y^6 x_1 - 2y^4 x_1^2 x_2 - 4y^4 x_1 x_2 - 3y^3 x_1^2 x_2 + x_1^4 x_2^2 - y^4 x_2 - y^3 x_1 x_2$
(3,-1)	$y^6 x_1^2 - 2y^4 x_1 x_2 - y^4 x_1 + 3y^3 x_1 x_2 + y^3 x_1 + y^2 x_2^2 - y x_2^2 - x_2^3$
(4,-1)	$y^8 x_1^2 + 3y^5 x_1 x_2 - 2y^4 x_1 x_2^2 + y^5 x_1 - 4y^4 x_1 x_2 - y^4 x_1 - y^2 x_2^3 + y x_2^3 + x_2^4$
(2,-2)	$y^6 x_1^3 + y^5 x_1^2 - y^4 x_1^2 - 3y^3 x_1 x_2 - y^3 x_2 + 2y^2 x_1 x_2 + y^2 x_2 - x_2^2$
(2,-3)	$y^8 x_1^4 + y^7 x_1^3 - y^6 x_1^3 - 2y^4 x_1^2 x_2 - 4y^4 x_1 x_2 - y^4 x_2 + 3y^3 x_1 x_2 + y^3 x_2 + x_2^2$

Table 4.1: Complete list of nonequivalent two-node quivers A-polynomials with $g = 1$, upon setting $x_1 = \lambda_1 x$ and $x_2 = \lambda_2 x$.

For example, table 4.1 displays a list of diagonal quivers with A-polynomials of genus one:

On the other hand, table 4.2 provides a the exhaustive list of quiver A-polynomials of small genus.

$g = 1$	$g = 2$	$g = 3$
(2,3), (2,4)	(2,5), (2,6)	(2,7), (2,8)
	(3,4), (3,5), (3,6)	(3,7), (3,8), (3,9)
		(4,5), (4,6), (4,7), (4,8)

Table 4.2: All nonequivalent pairs (a, b) that yield an A-polynomial with genus $g = 1, 2, 3$.

Finally, based on these examples, we conjecture that the set of A-polynomials of genus g for nonequivalent two-node quivers follows the pattern

$$\begin{aligned}
& (2, 2g + 1), (2, 2g + 2) \\
& (3, 3g - 2), (3, 3g - 1), (3, 3g) \\
& (4, 4g - 7), (4, 4g - 6), (4, 4g - 5), (4, 4g - 4) \\
\text{genus} = g, (a, b) : & \quad \quad \quad \vdots \\
& \underbrace{(g + 1, g + 2), \dots, (g + 1, 2(g + 1))}_{g+1}
\end{aligned} \tag{4.4.1}$$

Chapter 5

Conclusions

In this thesis, we have uncovered a rich structure surrounding 3d $\mathcal{N} = 2$ gauge theory, Chern-Simons theory, topological strings, knot theory, and quiver representation theory. On the one hand, we accomplished this by finding new nontrivial symmetries in the partition function of 3d $\mathcal{N} = 2$ gauge theory and for colored superpolynomials. On the other hand, we found the quiver A-polynomial curves for various infinite families of couplings of the supersymmetric theory and began their classification according to their genus.

In chapter 3 we proved the existence of nontrivial symmetries of the quiver series under certain conditions. Then, we provide an extensive set of examples of these symmetries appearing when the 3d SUSY gauge theory may be associated to a given knot. This discovery enabled us to find a permutohedra graph representing an enormous number of equivalent couplings of the 3d gauge theory. Lastly, if the knots-quivers correspondence is proven to be true for all knots, our results provide strong evidence that permutohedra graphs could be seen as a new knot invariants.

A very promising research question will be to find an interpretation of the permutohedra graph directly from the BPS-spectra of supersymmetric gauge theory and the homology of knots. Another ambitious goal would be to find explicit formulas for the number of equivalent quivers for a given knot.

We continued to derive the quiver A-polynomial curves for 3d supersymmetric from the quantum Nahm equations of the quiver series. Using insights from operations on the A-polynomial from knots, we extended those notions to define equivalence classes of quiver A-polynomial curves of 3d SUSY theory. On the basis of the genus of the A-polynomial, we achieved a classification of all nonequivalent A-polynomials arising from two-node quivers. Additionally, in chapter 4, we came across two different types of factorization of the quiver A-polynomial curves and explained them thanks to the underlying symmetries of the 3d theory.

To gain more insight into the quiver A-polynomial curves of 3d theory, it would be worth to deduce explicit formulas for the A-polynomials for larger quivers (e.g. three-node quiver). To that end, it would be convenient to find a definition of the quiver A-polynomial directly from the quiver data, without having to use the elimination algorithm on a case-by-case basis. On top of that, it would be interesting to observe the effect of the factorization of the A-polynomial curve on the classical BPS spectrum of the 3d gauge theory.

These efforts are only the beginning of a more systematic program where we

gain new insights into physical theories from the study of the properties of quiver generating series. This is because these q -series are simpler objects that exhibit remarkable features with direct consequences for the BPS-spectra of 3d theory and knots.

Appendix A

Local symmetry graph algorithm

Here we deduce the algorithm we used to derive all equivalent quivers for a given knot K . For concreteness, we use the simplest nontrivial case, knot $K = 5_2$. It turns out that $K = 5_2$ already encodes all details we need to consider for the algorithm.

In short,

Input: Homological degrees a_i, q_i, t_i of a knot \mathcal{K} and the quiver matrix \mathbf{C} .

Output: The symmetry graph $G_s(K)$, the list of symmetries of K with their associated colors.

The vertices of the graph $G_s(k)$ represent the equivalent quiver matrices $C \simeq C'$. Meanwhile, the edges of the graph $G_s(k)$ represent the action of a symmetry transposition relating two quiver matrices $C \leftarrow \begin{pmatrix} a & b \\ c & d \end{pmatrix} \rightarrow C'$. Where for compactness, in the symmetry graph $G_s(k)$ each pairing has an associated color $\begin{pmatrix} a & b \\ c & d \end{pmatrix}$

What are the steps of our code?

A.1 Find all pairings

First, it takes the homological degrees of the knot (a_i, q_i) , for $i = 1, \dots, m$, as in figure 3.10 for 5_2 . Then, it finds all pairings $\begin{pmatrix} a & b \\ c & d \end{pmatrix}$ and makes a list of them $LP(K)$. In essence, it tests the center of mass condition (3.2.4a) for all combinations of four elements $(q_a, a_a), (q_b, a_b), (q_c, a_c)$ and (q_d, a_d) where $a, b, c, d = 1, \dots, m$ plus they are pairwise distinct ($a \neq b$ and $c \neq d$)¹

$$LP(K) = \left\{ \begin{pmatrix} a_1 & b_1 \\ c_1 & d_1 \end{pmatrix}, \begin{pmatrix} a_2 & b_2 \\ c_2 & d_2 \end{pmatrix}, \dots, \begin{pmatrix} a_{N_p} & b_{N_p} \\ c_{N_p} & d_{N_p} \end{pmatrix} \right\} \quad (\text{A.1.1})$$

where N_p is the number of pairings of a given knot K .

In the case of $K = 5_2$ we have

$$LP(5_2) = \left\{ \begin{pmatrix} 1 & 3 \\ 4 & 5 \end{pmatrix}, \begin{pmatrix} 1 & 6 \\ 2 & 5 \end{pmatrix}, \begin{pmatrix} 1 & 6 \\ 3 & 4 \end{pmatrix}, \begin{pmatrix} 1 & 7 \\ 3 & 5 \end{pmatrix}, \right. \\ \left. \begin{pmatrix} 2 & 3 \\ 4 & 6 \end{pmatrix}, \begin{pmatrix} 2 & 5 \\ 3 & 4 \end{pmatrix}, \begin{pmatrix} 2 & 7 \\ 3 & 6 \end{pmatrix}, \begin{pmatrix} 4 & 7 \\ 5 & 6 \end{pmatrix} \right\} \quad (\text{A.1.2})$$

¹We do not need to test the t_i degrees because we are working only with thin knots, which satisfy $\delta = a_i + q_i/2 - t_i$, for some δ which independent of i , this guarantees that they are automatically satisfied for t_i .

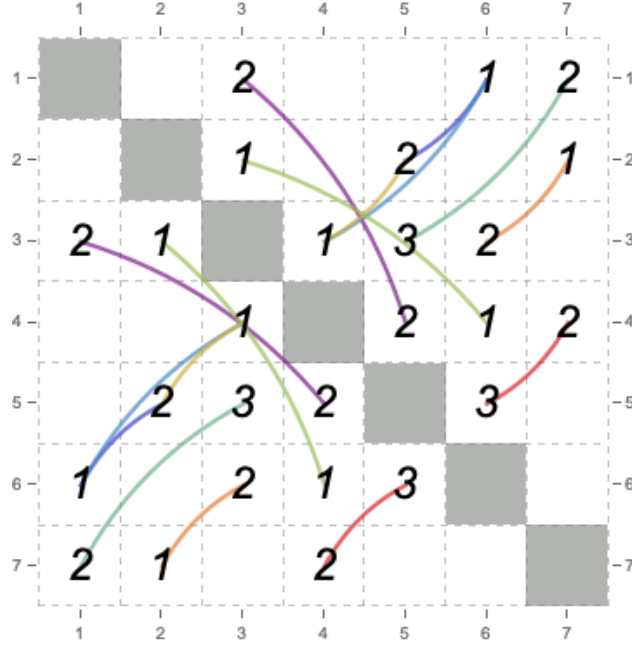


Figure A.1: Color legend of which entries are transposed on the quiver matrix.

A very clear and useful way to visualize the pairings $\begin{pmatrix} a & b \\ c & d \end{pmatrix}$ is by drawing a line between the entries $C_{a,b} \xleftrightarrow{\text{color}} C_{c,d}$ of the quiver matrix them on the quiver matrix as in figure A.1. There we have assigned a color to each pairing to keep track of it. These will be the same coloring of edges in $G_s(5_2)$, as seen in figure A.2 .

We have to remember that pairings $\begin{pmatrix} a & b \\ c & d \end{pmatrix}$ are not necessarily symmetries. For example, figure A.1 the two pairings $\begin{pmatrix} 1 & 3 \\ 4 & 5 \end{pmatrix}$ and $\begin{pmatrix} 2 & 3 \\ 4 & 6 \end{pmatrix}$ lead to trivial transpositions. Moreover, they do not satisfy the constraints (3.2.4b) from the local equivalence theorem 2. That is why they do not appear in $G_s(5_2)$ in figure A.2.

When looking for symmetries under transposition of elements of the quiver matrix $C_{a,b} \xleftrightarrow{\text{color}} C_{c,d}$, in principle, we would need to check the constraints (3.2.4) on all possible combinations. However, thanks to the fact that only pairings may be symmetries, we only need to test those in $LP(5_2)$. This is a drastic simplification. In spite of that reduction, for a general case, we have to test possible trivial pairings for every equivalent quiver matrix. The reason is that in general, pairings that might be trivial alone, like $\begin{pmatrix} 1 & 6 \\ 3 & 4 \end{pmatrix}$ might later combine into a non-trivial cycle $C_{1,6} \xleftrightarrow{\text{color}_i} C_{2,5} \xleftrightarrow{\text{color}_j} C_{3,4}$.

A.2 First generation of equivalent quivers

The following step is to take each pairing $\begin{pmatrix} a & b \\ c & d \end{pmatrix}$ from $LP(K)$ (A.1.1) and apply one-by-one all the transpositions of the off-diagonal entries of the quiver matrix $C_{a,b} \xleftrightarrow{\text{color}} C_{c,d}$. For every transposition, we verify if it satisfies the constraints (3.2.4b) from the local equivalence theorem 2, if they do we call them a *down-right symmetry*. We will explain what do we mean by "down-right" in a moment.

In the explicit example of $K = 5_2$, that $C(5_2)$ has the following three symmetries

$$C(5_2) = M_{0,1} = \begin{bmatrix} 2 & 1 & 2 & 1 & 2 & 1 & 2 \\ 1 & 0 & 1 & 0 & 2 & 0 & 1 \\ 2 & 1 & 3 & 1 & 3 & 2 & 3 \\ 1 & 0 & 1 & 1 & 2 & 1 & 2 \\ 2 & 2 & 3 & 2 & 4 & 3 & 4 \\ 1 & 0 & 2 & 1 & 3 & 2 & 3 \\ 2 & 1 & 3 & 2 & 4 & 3 & 5 \end{bmatrix}$$

$$\begin{matrix} M_{1,1} \swarrow \left(\begin{smallmatrix} 1 & 6 \\ 2 & 5 \end{smallmatrix}\right) \\ \begin{bmatrix} 2 & 1 & 2 & 1 & 2 & 2 & 2 \\ 1 & 0 & 1 & 0 & 1 & 0 & 1 \\ 2 & 1 & 3 & 1 & 3 & 2 & 3 \\ 1 & 0 & 1 & 1 & 2 & 1 & 2 \\ 2 & 1 & 3 & 2 & 4 & 3 & 4 \\ 2 & 0 & 2 & 1 & 3 & 2 & 3 \\ 2 & 1 & 3 & 2 & 4 & 3 & 5 \end{bmatrix} \end{matrix}$$

$$\begin{matrix} M_{1,2} \downarrow \left(\begin{smallmatrix} 2 & 5 \\ 3 & 4 \end{smallmatrix}\right) \\ \begin{bmatrix} 2 & 1 & 2 & 1 & 2 & 1 & 2 \\ 1 & 0 & 1 & 0 & 1 & 0 & 1 \\ 2 & 1 & 3 & 2 & 3 & 2 & 3 \\ 1 & 0 & 2 & 1 & 2 & 1 & 2 \\ 2 & 1 & 3 & 2 & 4 & 3 & 4 \\ 1 & 0 & 2 & 1 & 3 & 2 & 3 \\ 2 & 1 & 3 & 2 & 4 & 3 & 5 \end{bmatrix} \end{matrix}$$

$$\begin{matrix} M_{1,3} \searrow \left(\begin{smallmatrix} 2 & 7 \\ 3 & 6 \end{smallmatrix}\right) \\ \begin{bmatrix} 2 & 1 & 2 & 1 & 2 & 1 & 2 \\ 1 & 0 & 1 & 0 & 2 & 0 & 2 \\ 2 & 1 & 3 & 1 & 3 & 1 & 3 \\ 1 & 0 & 1 & 1 & 2 & 1 & 2 \\ 2 & 2 & 3 & 2 & 4 & 3 & 4 \\ 1 & 0 & 1 & 1 & 3 & 2 & 3 \\ 2 & 2 & 3 & 2 & 4 & 3 & 5 \end{bmatrix} \end{matrix}$$

where $M_{1,1} = C_{1,6} \leftrightarrow C_{2,5}$, $M_{1,2} = C_{2,6} \leftrightarrow C_{2,5}$ and $M_{1,3} = C_{2,7} \leftrightarrow C_{3,6}$.

In the above expression, we can appreciate that if we think of $C(5_2)$ as the initial matrix, the equivalent quiver matrices $M_{1,1}$, $M_{1,2}$ and $M_{1,3}$ as descendants and the transpositions as arrows pointing downwards. This is the reason behind the "down-" part of down-right symmetry. Then, set

$$DRS(C) = \left\{ \begin{pmatrix} 1 & 6 \\ 2 & 5 \end{pmatrix}, \begin{pmatrix} 2 & 5 \\ 3 & 4 \end{pmatrix}, \begin{pmatrix} 2 & 7 \\ 3 & 6 \end{pmatrix} \right\} \quad (\text{A.2.1})$$

is the set of down-right symmetries of C . The "-right" part will become apparent in the next subsection.

The above are the first vertices and edges of our symmetry graph $G_s(5_2)$. The list of edges reads

$$LE(G_s(5_2)) = \left\{ M_{0,1} \leftarrow \begin{pmatrix} 1 & 6 \\ 2 & 5 \end{pmatrix} \rightarrow M_{1,1}, M_{0,1} \leftarrow \begin{pmatrix} 2 & 5 \\ 3 & 4 \end{pmatrix} \rightarrow M_{1,2}, \right. \\ \left. M_{0,1} \leftarrow \begin{pmatrix} 2 & 7 \\ 3 & 6 \end{pmatrix} \rightarrow M_{1,3} \right\} \quad (\text{A.2.2})$$

In general, we would have: $C(K) = M_{0,1} \xleftrightarrow{\text{color}} M_{1,\nu}$ the starting vertex $M_{0,1}$ shares an edge with the equivalent matrix $M_{1,\nu}$, where $\nu = 1, \dots, N_s(C)$ and $N_s(C) = DRS(C)$, with $0 \leq N_s(C) \leq N_p$ (number of down-right symmetries of C). We also give the annotation that the edge should be colored with the color corresponding to the pairing $\begin{pmatrix} a & b \\ c & d \end{pmatrix}$.

To understand the subindices notation, it helps to think of the equivalent matrices as vertices of a rooted tree graph² like in figure A.2. There we can see that the initial quiver matrix $C = M_{0,1}$ is the root vertex and the equivalent matrices $M_{1,1}$, $M_{1,2}$ and $M_{1,3}$ correspond to the first generation arising from $M_{0,1}$.

In short, the first subindex g in $M_{g,\nu}$ specifies in which generation is the matrix, or how many transpositions it is away from $M_{0,1}$. Whereas, the second subindex ν indicates which matrix in the g -generation we are referring to.

²Although the graph, it is not even a tree graph, this is just a layout.

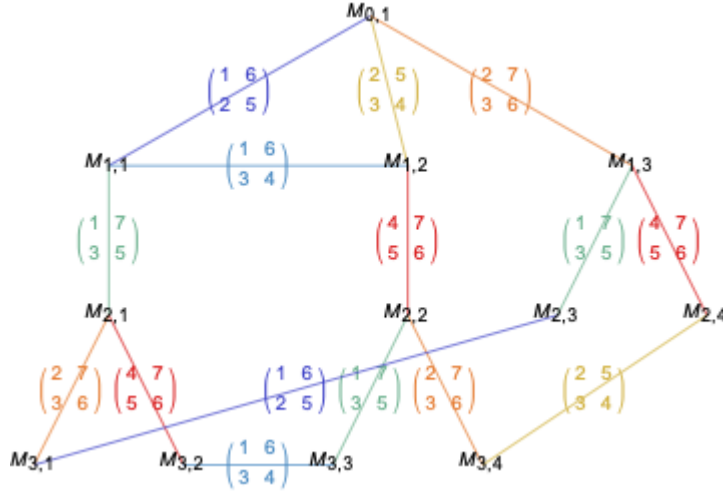


Figure A.2: A tree graph version of the symmetry graph of 5_2

A.3 From the second to the last generation of equivalent quivers

Now we are ready to look for the second generation of equivalent quiver matrices. As before, we perform every transposition from our list of pairings (A.1.1) on $M_{1,\nu}$ and test the constraints. However, we already know that $M_{1,\nu}$ has a symmetry, the one that leads us back to $M_{0,1}$. Hence, when testing on $M_{1,\nu}$ all transpositions from the list of pairings, we make sure to exclude that one. That symmetry will belong to what we will call, the *up-left symmetries*, which we will explain in breve why "up-left".

Coming back to our explicit example of 5_2 , we test the pairings (A.1.1) on $M_{1,1}$, we see that $M_{1,1}$ has two down-right symmetries³, $DRS(M_{1,1}) = \{(\frac{1}{3} \frac{6}{4}), (\frac{1}{3} \frac{7}{5})\}$.

After we apply the first symmetry transposition, we find $M_{1,1} \leftarrow (\frac{1}{3} \frac{6}{4}) \rightarrow M_{1,2}$. This is the horizontal edge in figure A.2. We call such symmetries horizontal symmetries. Moreover, since $M_{1,2}$ is on the r.h.s. of $M_{1,1}$, this explains the the "-right" in down-right symmetries. This also means that, in contrast to $M_{0,1}$ where all its symmetries lead to new equivalent quivers, now we may have symmetries that lead to known equivalent quivers.

This is why, in general, after applying each symmetry transposition to $M_{1,\nu}$ we need to compare the resulting equivalent quiver matrix $\tilde{M}_{1,\nu}$ with all known equivalent quiver matrices. This will determine if $\tilde{M}_{1,\nu}$ is really a new equivalent matrix. Later we will see there is a clever argument to simplify the task of comparing matrices⁴. Next, we apply the transposition corresponding to the second symmetry of $M_{1,1}$. The result, is a new equivalent quiver matrix, $M_{1,1} \leftarrow (\frac{1}{3} \frac{7}{5}) \rightarrow M_{2,1}$.

In regard to $M_{1,2}$, there are two pairings we do not need to test,

$$ULS(M_{1,2}) = \{(\frac{2}{3} \frac{5}{4}), (\frac{1}{3} \frac{6}{4})\} \quad (\text{A.3.1})$$

³Excluding $(\frac{1}{2} \frac{6}{5})$ because it leads back to $M_{0,1}$.

⁴In principle, if we keep track of the elements that we have transposed we could deduce if the resulting matrix is a new matrix, without having to compare it with others. However, in practice the number of equivalent matrices grows exponentially, so it is not efficient to keep track of all the sequences of transpositions.

because we know, they are already symmetries. We refer to them as *up-left symmetries*. When looking at the diagram A.2, it is pretty clear that $\begin{pmatrix} 2 & 5 \\ 3 & 4 \end{pmatrix}$ takes $M_{1,2}$ up to the generation above. Whereas $\begin{pmatrix} 1 & 6 \\ 3 & 4 \end{pmatrix}$ takes $M_{1,2}$ to the left, with a known equivalent quiver matrix.

When we test the other pairings from (A.1.1) on $M_{1,2}$ we find that it has another symmetry $DRS(M_{1,2}) = \{(\frac{4}{5} \frac{7}{6})\}$ where $M_{1,1} \leftrightarrow M_{1,2}$. Therefore, in our code we need to keep track of those symmetry to exclude them from the testing list.

We see $M_{1,2}$ has a new symmetry beside the aforementioned symmetry, namely $(\frac{4}{5} \frac{7}{6})$. Then, after applying $M_{1,2} \leftarrow (\frac{4}{5} \frac{7}{6}) \rightarrow \tilde{M}_{1,2}$ we need to compare $\tilde{M}_{1,2}$ with $M_{1,3}$. We easily see that it does not match. Still, we can not guarantee that it does not match $M_{2,1}$. Thus, we need to compare it with $M_{2,1}$ too. After checking that $\tilde{M}_{1,2}$ and $M_{2,1}$ are different, we can assign a new edge $M_{1,2} \leftarrow (\frac{4}{5} \frac{7}{6}) \rightarrow \tilde{M}_{2,2}$ connecting to a new vertex $M_{2,2}$.

To finish deriving the whole second generation, we repeat the same procedure with $M_{1,3}$. We find $DRS(M_{1,3}) = \{(\frac{1}{3} \frac{7}{5}), (\frac{4}{5} \frac{7}{6})\}$. The nice observation is that, after we apply the transpositions, we do not need to compare the resulting matrices with $M_{1,1}$ nor $M_{1,2}$. Why? Because if those symmetries would lead to either $M_{1,1}$ or $M_{1,2}$ we would already have found them when we compared the symmetries of $M_{1,1}$ nor $M_{1,2}$ with $M_{1,3}$.

Hence, it only remains for us to compare the resulting matrices with $M_{2,1}$ and $M_{2,2}$. After a quick check, we make sure that those are new equivalent matrices, so we assign them their respective new vertices $M_{1,3} \leftarrow (\frac{1}{3} \frac{7}{5}) \rightarrow M_{2,3}$ and $M_{2,4}$ along with their edges joining it with $M_{1,3} \leftarrow (\frac{1}{5} \frac{7}{6}) \rightarrow M_{2,4}$.

We repeat the same process for the third generation $M_{3,\nu}$ out of $M_{2,\nu}$. Here we see that for the down-right symmetries of $M_{2,3}$ and $M_{2,4}$ lead to $M_{3,1}$ and $M_{3,4}$, respectively, which were found before from $M_{2,1}$ and $M_{2,2}$, see A.2. This is why it is important to compare a potentially new equivalent quiver matrix $M_{g,\nu} \leftarrow \begin{pmatrix} a & b \\ c & d \end{pmatrix} \rightarrow \tilde{M}_{g,\nu}$ also with the equivalent quiver matrices from the next generation $M_{g+1,\nu'}$.

Lastly, we see that when repeating the process, the third generation does not produce any new equivalent quiver matrices. Hence, this means we have finished and we have found all equivalent quiver matrices and their symmetries.

An important observation for producing a memory efficient algorithm is that we do not need the equivalent matrices from the first generation $M_{1,\nu}$ anymore to construct the third or further generations $M_{g,\nu}$, with $g \geq 3$. Thanks to that, we can erase $M_{1,\nu}$ RAM memory space for future generations. Every time after we construct a generation $M_{g+1,\nu}$ we no longer need the matrices can always erase the previous generation $M_{g,\nu}$. This will

To construct the third generation, we just need to repeat the process we just explained. However, how do we know that the program will stop? Simply, the size of the quiver matrix is finite. Hence, there is only a finite number of possible transpositions. When do we know that we reached the last generation? When all symmetries of the whole latest generation lead to no new equivalent quivers.

A.4 The algorithm

Here are three useful observations that will help us code an efficient program for constructing the graph of symmetries of the knot $G_s(K)$:

1. We mentioned that every time we apply a down-right symmetry $M_{g,\nu} \leftarrow \begin{pmatrix} a & b \\ c & d \end{pmatrix} \rightarrow \tilde{M}_{g,\nu}$, in principle, we need to compare it with all the other known equivalent quivers to determine if it is indeed a new equivalent quiver matrix. This would be very time consuming for a computer. In practice we compare $\tilde{M}_{g,\nu}$ only with $M_{g,\nu' > \nu}$ (to the right of $M_{g,\nu}$ in the diagram) and $M_{g+1,\nu''}$ (below $M_{g,\nu}$ in the diagram).

We do not need to compare $\tilde{M}_{g,\nu}$ to any equivalent quiver from previous generations $M_{g' < g, \nu'}$. This is because we excluded the up-left symmetries, so it can not be a symmetry that takes $M_{g,\nu}$ to $M_{g-1,\nu''}$. It can not be a symmetry connecting with generations further up $M_{g'' < g-1, \nu}$, because that would imply $M_{g=g''+1, \nu}$ which is a contradiction. Similarly, since $\begin{pmatrix} a & b \\ c & d \end{pmatrix}$ is not an up-left symmetry, we do not need to compare $\tilde{M}_{g,\mu'}$ with any $M_{g,\nu' < \nu}$.

2. Thanks to the above conclusion, after we derived $M_{g+1,\nu'}$ from $M_{g,\nu}$ we do not no longer need $M_{g,\nu}$. Therefore, to clear the space in the RAM, every time we find the whole new generation, we delete the matrices from the previous one.
3. *How do we know that the program will stop?* Simply, because the size of the quiver matrix is finite. Hence, there is only a finite amount of possible transpositions. *When do we know that we reached the last generation?* When none of the symmetries of the latest generation lead to new equivalent quivers.

The following two functions can be used to effectively construct the $G_s(K)$.

First function obtains a list of all possible pairings.

Second function constructs $G_s(K)$.

Algorithm 1 Auxiliar functions

```
1: function search4pairings(a,q,m = dim q)
2:    $LP(K) \leftarrow \{\}$  ▷ List of pairings  $\begin{pmatrix} a & b \\ c & d \end{pmatrix}$  as in (A.1.1)
3:   for  $i = 1 \dots m$  do
4:     for  $j = i + 1 \dots m$  do
5:       for  $k = 1 \dots m \ \& \ k \neq j$  do
6:         for  $l = k + 1 \dots m \ \& \ l \neq j$  do
7:           if  $a_i + a_j = a_k + a_l \ \& \ q_i + q_j = q_k + q_l$  then
8:              $LP(K) \leftarrow LP(K) \cup \begin{pmatrix} i & j \\ k & l \end{pmatrix}$ 
9:   return  $LP(K)$ 
10:
11: function testconstraints(mat,  $\begin{pmatrix} a & b \\ c & d \end{pmatrix}$ ,  $m = \sqrt{\dim \text{mat}}$ ) ▷ mat is a matrix.
12:   test  $\leftarrow 0$ 
13:   if  $|\text{mat}_{a,b} - \text{mat}_{c,d}| = 1$  then ▷  $\text{mat}_{a,b}$  are elements of mat.
14:     if  $\text{mat}_{a,b} > \text{mat}_{c,d}$  then
15:       for  $p = 1 \dots m$  do
16:         if  $\text{mat}_{p,a} + \text{mat}_{p,b} - \delta_{p,a} - \delta_{p,b} = \text{mat}_{p,c} + \text{mat}_{p,d}$  then
17:           test  $\leftarrow \text{test} + 1$ 
18:         else
19:           Break
20:     else
21:       for  $p = 1 \dots m$  do
22:         if  $\text{mat}_{p,a} + \text{mat}_{p,b} = \text{mat}_{p,c} + \text{mat}_{p,d} - \delta_{p,c} - \delta_{p,d}$  then
23:           test  $\leftarrow \text{test} + 1$ 
24:         else
25:           Break
26:     if test =  $m$  then return True
27:     else
28:       return False
29:   else
30:     return False
31:
32: function search4symms( $M_{g,\nu}$ ,  $m = \sqrt{\dim M_{g,\nu}}$ ,  $LP(K) \setminus ULS(M_{g,\nu})$ )
33:   ▷  $ULS(M_{g,\nu})$  as in (A.3.1) ◁
34:    $DRS(M_{g,\nu}) \leftarrow \{\}$  ▷  $DRS(M_{g,\nu})$  as in (A.2.1)
35:   for  $\sigma = 1, \dots, \#(LP(K) \setminus ULS(M_{g,\nu}))$  do
36:     if testconstraints( $M_{g,\nu}$ ,  $m$ ,  $\begin{pmatrix} i_\sigma & j_\sigma \\ k_\sigma & l_\sigma \end{pmatrix}$ ) = true then
37:        $DRS(M_{g,\nu}) \leftarrow DRS(M_{g,\nu}) \cup \left\{ \begin{pmatrix} i_\sigma & j_\sigma \\ k_\sigma & l_\sigma \end{pmatrix} \right\}$ 
38:   return  $DRS(M_{g,\nu})$ 
```

Algorithm 2 Constructing $G_s(K)$, first part

```

1: function constructgraph( $M_{g=0,\nu=1} = C, \mathbf{a}, \mathbf{q}, m = \dim \mathbf{a}$ )
2:    $\triangleright$  Variables  $\triangleleft$ 
3:    $G_s(K) \leftarrow \{\}$   $\triangleright$  The graph of symmetries for the knot  $K$ 
4:   totalsymms  $\leftarrow \{\}$   $\triangleright$  A list with all the symmetries.
5:    $g \leftarrow 0$   $\triangleright$  Generation in the tree graph, as in A.2
6:   testsymms  $\leftarrow 0$   $\triangleright$  Counter ...

7:    $\triangleright$  Operations  $\triangleleft$ 
8:    $\triangleright$  Searching for the first generation  $g = 1$   $\triangleleft$ 
9:    $LP(K) \leftarrow \text{search4pairings}(\mathbf{a}, \mathbf{q}, m)$   $\triangleright$  As in (A.1.1)
10:   $DRS(M_{0,1}) \leftarrow \text{search4symms}(M_{0,1}, m, LP(K))$   $\triangleright$  As in (A.2.1)
11:  totalsymms  $\leftarrow$  totalsymms  $\cup$   $DRS(M_{0,1})$ 
12:  for  $\nu = 1 \dots \#(DRS(M_{0,1}))$  do
13:   $ULS(M_{g+1,\nu}) \leftarrow \left\{ \begin{pmatrix} i_\nu & j_\nu \\ k_\nu & l_\nu \end{pmatrix} \right\}$ 
14:   $M_{g+1,\nu} \leftarrow M_{g,1}(i_\nu, j_\nu) \leftrightarrow M_{g,1}(k_\nu, l_\nu)$   $\triangleright$   $M_{g+1,\nu}$  is the resulting matrix after applying the transposition of entries  $(i_\nu, j_\nu)$  and  $(k_\nu, l_\nu)$  to  $M_{g,1}$ .
15:   $G_s(K) \leftarrow G_s(K) \cup \{M_{g,1} \leftarrow \begin{pmatrix} i_\nu & j_\nu \\ k_\nu & l_\nu \end{pmatrix} \rightarrow M_{g+1,\nu}\}$ 
16:   $N_{g+1} \leftarrow \#(DRS(M_{g,1}))$   $\triangleright$  Number of equivalent quivers in generation  $g$ .
17:  Clear( $M_{g,1}, DRS(M_{g,1})$ )  $\triangleright$  Freeing RAM space.

```

Algorithm 3 Constructing $G_s(K)$, second part

```

18:   $\triangleright$  Searching for the second til the last generation  $g \geq 2$   $\triangleleft$ 
19:  while  $N_{g+1} > 0$  do  $\triangleright$  Until there are no new equivalent quiver matrices.
20:     $g \leftarrow g + 1$ 
21:     $N_{g+1} \leftarrow 0$ 
22:    for  $\nu = 1 \dots N_g$  do
23:       $DRS(M_{g,\nu}) \leftarrow \text{search4symms}(M_{g,\nu}, m, LP(K) \setminus ULS(M_{g,\nu}))$ 
24:       $\text{totalsymms} \leftarrow \text{totalsymms} \sqcup DRS(M_{g,\nu})$ 
25:      for  $\sigma = 1 \dots \#(DRS(M_{g,\nu}))$  do
26:         $\tilde{M}_{g,\nu}(\sigma) \leftarrow M_{g,\nu}(i_\sigma, j_\sigma) \leftrightarrow M_{g,\nu}(k_\sigma, l_\sigma)$ 
27:        for  $\mu = \nu + 1 \dots N_g$  do
28:          if  $\tilde{M}_{g,\nu}(\sigma) = M_{g,\mu}$  then
29:             $ULS(M_{g,\mu}) \leftarrow ULS(M_{g,\mu}) \cup \left\{ \begin{pmatrix} i_\sigma & j_\sigma \\ k_\sigma & l_\sigma \end{pmatrix} \right\}$ 
30:             $G_s(K) \leftarrow G_s(K) \cup \left\{ M_{g,\nu} \leftarrow \begin{pmatrix} i_\sigma & j_\sigma \\ k_\sigma & l_\sigma \end{pmatrix} \rightarrow M_{g,\mu} \right\}$ 
31:            Break
32:          else
33:             $\text{testsymms} \leftarrow \text{testsymms} + 1$ 
34:          if  $\text{testsymms} = N_g - \nu$  then
35:            for  $\rho = 1, \dots, N_{g+1}$  do
36:              if  $\tilde{M}_{g,\nu}(\sigma) = M_{g+1,\rho}$  then
37:                 $ULS(M_{g+1,\rho}) \leftarrow ULS(M_{g+1,\rho}) \cup \left\{ \begin{pmatrix} i_\sigma & j_\sigma \\ k_\sigma & l_\sigma \end{pmatrix} \right\}$ 
38:                 $G_s(K) \leftarrow G_s(K) \cup \left\{ M_{g,\nu} \leftarrow \begin{pmatrix} i_\sigma & j_\sigma \\ k_\sigma & l_\sigma \end{pmatrix} \rightarrow M_{g+1,\rho} \right\}$ 
39:                Break
40:              else
41:                 $\text{testsymms} \leftarrow \text{testsymms} + 1$ 
42:            if  $\text{testsymms} = N_g - \nu + N_{g+1}$  then
43:               $N_{g+1} \leftarrow N_{g+1} + 1$ 
44:               $M_{g+1,N_{g+1}} \leftarrow \tilde{M}_{g,\nu}(\sigma)$ 
45:               $ULS(M_{g+1,N_{g+1}}) \leftarrow ULS(M_{g+1,N_{g+1}}) \cup \left\{ \begin{pmatrix} i_\sigma & j_\sigma \\ k_\sigma & l_\sigma \end{pmatrix} \right\}$ 
46:               $G_s(K) \leftarrow G_s(K) \cup \left\{ M_{g,\nu} \leftarrow \begin{pmatrix} i_\sigma & j_\sigma \\ k_\sigma & l_\sigma \end{pmatrix} \rightarrow M_{g+1,N_{g+1}} \right\}$ 
47:               $\text{Clear}(M_{g,\nu}, \tilde{M}_{g,\nu}(\forall \sigma), ULS(M_{g,\nu}), DRS(M_{g,\nu}))$ 
48:
49:   $\triangleright$  Results  $\triangleleft$ 
50:  if  $N_{g=1} > 0$  then
51:    return  $\{G_s(k), \text{totalsymms}, LP(K)\}$ 
52:  else
53:    return This knot has no symmetries.

```

References

- [1] Cyril Closset and Heeyeon Kim. “Three-dimensional $\mathcal{N} = 2$ supersymmetric gauge theories and partition functions on Seifert manifolds: A review”. In: *Int. J. Mod. Phys. A* 34.23 (2019), p. 1930011. DOI: [10.1142/S0217751X19300114](https://doi.org/10.1142/S0217751X19300114).
- [2] Sergey Shadchin. “On F-term contribution to effective action”. In: *J. High Energy Phys.* 2007.08 (2007), p. 052. DOI: [10.1088/1126-6708/2007/08/052](https://doi.org/10.1088/1126-6708/2007/08/052).
- [3] Sara Pasquetti. “Factorisation of $\mathcal{N} = 2$ theories on the squashed 3-sphere”. In: *J. High Energy Phys.* 2012.4 (2012), p. 120. DOI: [10.1007/JHEP04\(2012\)120](https://doi.org/10.1007/JHEP04(2012)120).
- [4] Chiung Hwang, Hee-Cheol Kim, and Jaemo Park. “Factorization of the 3d superconformal index”. In: *arXiv:1211.6023 [hep-th]* (2013).
- [5] Marcos Marino. *Chern-Simons theory, matrix models, and topological strings*. International series of monographs on physics 131. Clarendon Press, 2005. ISBN: 978-0-19-856849-0.
- [6] Enore Guadagnini. *The Link Invariants of the Chern-Simons Field Theory.pdf*. Expositions in Mathematics. 1993. ISBN: 3-11-014028-4.
- [7] David Tong. *Lectures on Gauge Theory*. 2018. URL: <https://www.damtp.cam.ac.uk/user/tong/gaugetheory/gt.pdf>.
- [8] Hiroshi Ooguri and Cumrun Vafa. “Knot Invariants and Topological Strings”. In: *Nuclear Physics B* 577.3 (2000), pp. 419–438. DOI: [10.1016/S0550-3213\(00\)00118-8](https://doi.org/10.1016/S0550-3213(00)00118-8).
- [9] Tudor Dimofte, Davide Gaiotto, and Sergei Gukov. “3-Manifolds and 3d Indices”. In: *arXiv:1112.5179 [hep-th]* (2011).
- [10] Tudor Dimofte, Davide Gaiotto, and Sergei Gukov. “Gauge Theories Labelled by Three-Manifolds”. In: *arXiv:1108.4389 [hep-th]* (2011).
- [11] Christopher Beem, Tudor Dimofte, and Sara Pasquetti. “Holomorphic blocks in three dimensions”. In: *J. High Energy Phys.* 2014.12 (2014), p. 177. DOI: [10.1007/JHEP12\(2014\)177](https://doi.org/10.1007/JHEP12(2014)177).
- [12] Piotr Kucharski. “Quivers for 3-manifolds: the correspondence, BPS states, and 3d $\mathcal{N}=2$ theories”. In: *arXiv:2005.13394 [hep-th, physics:math-ph]* (2020).
- [13] Tobias Ekholm et al. “ \widehat{Z} at large N : from curve counts to quantum modularity”. In: *arXiv:2005.13349 [hep-th]* (2020).
- [14] Tobias Ekholm et al. “Branches, quivers, and ideals for knot complements”. In: *arXiv:2110.13768 [hep-th]* (2021).
- [15] Edward Witten. “Quantum field theory and the Jones polynomial”. In: *Communications in Mathematical Physics* 121.3 (1989), pp. 351–399. DOI: [10.1007/BF01217730](https://doi.org/10.1007/BF01217730).

- [16] Vaughan F. R. Jones. “A polynomial invariant for knots via von Neumann algebras”. In: *Bull. Amer. Math. Soc.* 12.1 (1985), pp. 103–111. DOI: [10.1090/S0273-0979-1985-15304-2](https://doi.org/10.1090/S0273-0979-1985-15304-2).
- [17] P. Freyd et al. “A new polynomial invariant of knots and links”. In: *Bull. Amer. Math. Soc.* 12.2 (1985), pp. 239–246. DOI: [10.1090/S0273-0979-1985-15361-3](https://doi.org/10.1090/S0273-0979-1985-15361-3).
- [18] Jozef H. Przytycki and Pawel Traczyk. “Invariants of links of Conway type”. In: *arXiv:1610.06679 [math]* (2016).
- [19] Sergei Gukov and Marko Stosic. “Homological algebra of knots and BPS states”. In: *arXiv:1112.0030 [hep-th]* (2013), pp. 309–367. DOI: [10.2140/gtm.2012.18.309](https://doi.org/10.2140/gtm.2012.18.309).
- [20] N. Seiberg and E. Witten. “Electric-magnetic duality, monopole condensation, and confinement in $N=2$ supersymmetric Yang-Mills theory”. In: *Nuclear Physics B* 426.1 (1994), pp. 19–52. DOI: [10.1016/0550-3213\(94\)90124-4](https://doi.org/10.1016/0550-3213(94)90124-4).
- [21] N. Seiberg and E. Witten. “Monopoles, duality and chiral symmetry breaking in $N = 2$ supersymmetric QCD”. In: *Nuclear Physics B* 431.3 (1994), pp. 484–550. DOI: [10.1016/0550-3213\(94\)90214-3](https://doi.org/10.1016/0550-3213(94)90214-3).
- [22] Sergei Gukov. “Three-Dimensional Quantum Gravity, Chern-Simons Theory, and the A-Polynomial”. In: *Commun. Math. Phys.* 255.3 (2005), pp. 577–627. DOI: [10.1007/s00220-005-1312-y](https://doi.org/10.1007/s00220-005-1312-y).
- [23] Stavros Garoufalidis. “On the characteristic and deformation varieties of a knot”. In: *Proceedings of the Casson Fest.* Mathematical Sciences Publishers, 2004, pp. 291–309. DOI: [10.2140/gtm.2004.7.291](https://doi.org/10.2140/gtm.2004.7.291).
- [24] Stavros Garoufalidis and Thang T Q Le. “The colored Jones function is q-holonomic”. In: *Geom. Topol.* 9.3 (2005), pp. 1253–1293. DOI: [10.2140/gt.2005.9.1253](https://doi.org/10.2140/gt.2005.9.1253).
- [25] D. Cooper et al. “Plane curves associated to character varieties of 3-manifolds”. In: *Invent Math* 118.1 (1994), pp. 47–84. DOI: [10.1007/BF01231526](https://doi.org/10.1007/BF01231526).
- [26] Mina Aganagic and Cumrun Vafa. “Large N Duality, Mirror Symmetry, and a Q -deformed A -polynomial for Knots”. In: *arXiv:1204.4709 [hep-th]* (2012).
- [27] Hiroyuki Fuji, Sergei Gukov, and Piotr Sułkowski. “Super- A -polynomial for knots and BPS states”. In: *Nuclear Physics B* 867.2 (2013), pp. 506–546. DOI: [10.1016/j.nuclphysb.2012.10.005](https://doi.org/10.1016/j.nuclphysb.2012.10.005).
- [28] Hitoshi Murakami and Yoshiyuki Yokota. *Volume Conjecture for Knots*. Vol. 30. SpringerBriefs in Mathematical Physics. Springer Singapore, 2018. ISBN: 978-9-811-31149-9. DOI: [10.1007/978-981-13-1150-5](https://doi.org/10.1007/978-981-13-1150-5).
- [29] Jessica S. Purcell. “Hyperbolic Knot Theory”. In: *arXiv:2002.12652 [math]* (2020).
- [30] Piotr Kucharski et al. “BPS states, knots, and quivers”. In: *Phys. Rev. D* 96.12 (2017), p. 121902. DOI: [10.1103/PhysRevD.96.121902](https://doi.org/10.1103/PhysRevD.96.121902).
- [31] Piotr Kucharski et al. “Knots-quivers correspondence”. In: *Adv. Theor. Math. Phys.* 23.7 (2019), pp. 1849–1902. DOI: [10.4310/ATMP.2019.v23.n7.a4](https://doi.org/10.4310/ATMP.2019.v23.n7.a4).
- [32] Geir T. Helleloid and Fernando Rodriguez-Villegas. “Counting quiver representations over finite fields via graph enumeration”. In: *Journal of Algebra* 322.5 (2009), pp. 1689–1704. DOI: [10.1016/j.jalgebra.2009.04.032](https://doi.org/10.1016/j.jalgebra.2009.04.032).

- [33] Tom Bridgeland. “Quantum groups via Hall algebras of complexes”. In: *Ann. Math.* 177.2 (2013), pp. 739–759. DOI: [10.4007/annals.2013.177.2.9](https://doi.org/10.4007/annals.2013.177.2.9).
- [34] Christof Geiß. “Introduction to moduli spaces associated to quivers”. In: *Contemporary Mathematics*. Vol. 406. American Mathematical Society, 2006, pp. 31–50. ISBN: 978-0-8218-3818-1. DOI: [10.1090/conm/406/07652](https://doi.org/10.1090/conm/406/07652).
- [35] Ralf Schiffler. *Quiver Representations*. CMS Books in Mathematics. Springer International Publishing, 2014. ISBN: 978-3-319-09203-4. DOI: [10.1007/978-3-319-09204-1](https://doi.org/10.1007/978-3-319-09204-1).
- [36] Maxim Kontsevich and Yan Soibelman. “Cohomological Hall algebra, exponential Hodge structures and motivic Donaldson–Thomas invariants”. In: *Commun. Number Theory Phys.* 5.2 (2011), pp. 231–252. DOI: [10.4310/CNTP.2011.v5.n2.a1](https://doi.org/10.4310/CNTP.2011.v5.n2.a1).
- [37] Alexander I. Efimov. “Cohomological Hall algebra of a symmetric quiver”. In: *Compositio Mathematica* 148.4 (2012), pp. 1133–1146. DOI: [10.1112/S0010437X12000152](https://doi.org/10.1112/S0010437X12000152).
- [38] Tobias Ekholm, Piotr Kucharski, and Pietro Longhi. “Physics and geometry of knots-quivers correspondence”. In: *arXiv:1811.03110 [hep-th]* (2020).
- [39] Tobias Ekholm, Piotr Kucharski, and Pietro Longhi. “Multi-cover skeins, quivers, and 3d $\mathcal{N} = 2$ dualities”. In: *J. High Energy Phys.* 2020.2 (2020), p. 18. DOI: [10.1007/JHEP02\(2020\)018](https://doi.org/10.1007/JHEP02(2020)018).
- [40] Miłosz Panfil and Piotr Sułkowski. “Topological strings, strips and quivers”. In: *J. High Energy Phys.* 2019.1 (2019), p. 124. DOI: [10.1007/JHEP01\(2019\)124](https://doi.org/10.1007/JHEP01(2019)124).
- [41] Taro Kimura et al. “Branes, quivers and wave-functions”. In: *arXiv:2011.06783 [hep-th, physics:math-ph]* (2020).
- [42] Jakub Jankowski et al. “Permutohedra for knots and quivers”. In: *Phys. Rev. D* 104.8 (2021), p. 086017. DOI: [10.1103/PhysRevD.104.086017](https://doi.org/10.1103/PhysRevD.104.086017).
- [43] Günter M. Ziegler. *Lectures on Polytopes*. Vol. 152. Graduate Texts in Mathematics. Springer New York, 1995. ISBN: 978-0-387-94365-7. DOI: [10.1007/978-1-4613-8431-1](https://doi.org/10.1007/978-1-4613-8431-1).
- [44] Hélder Larraguível et al. “Nahm sums, quiver A-polynomials and topological recursion”. In: *Journal of High Energy Physics* 2020.7 (2020), p. 151. DOI: [10.1007/JHEP07\(2020\)151](https://doi.org/10.1007/JHEP07(2020)151).
- [45] Claude Itzykson and Jean Bernard Zuber. *Quantum field theory*. International series in pure and applied physics. McGraw-Hill International Book Co, 1980. ISBN: 978-0-07-032071-0.
- [46] H Larraguível, G V Lopez, and J A Nieto. “Nambu-Goto action and classical rebits in any signature and in higher dimensions”. In: *Rev. Mex. Fis.* (2017), p. 4.
- [47] O. Aharony et al. “Aspects of N=2 Supersymmetric Gauge Theories in Three Dimensions”. In: *Nuclear Physics B* 499.1-2 (1997), pp. 67–99. DOI: [10.1016/S0550-3213\(97\)00323-4](https://doi.org/10.1016/S0550-3213(97)00323-4).
- [48] Nick Dorey and David Tong. “Mirror Symmetry and Toric Geometry in Three-Dimensional Gauge Theories”. In: *J. High Energy Phys.* 2000.05 (2000), p. 018. DOI: [10.1088/1126-6708/2000/05/018](https://doi.org/10.1088/1126-6708/2000/05/018).

- [49] Dongmin Gang, Nakwoo Kim, and Sangmin Lee. “Holography of 3d-3d correspondence at Large N ”. In: *arXiv:1409.6206 [hep-th]* (2014). DOI: [10.1007/JHEP04\(2015\)091](https://doi.org/10.1007/JHEP04(2015)091).
- [50] Dongmin Gang and Nakwoo Kim. “Large \mathcal{N} twisted partition functions in 3d-3d correspondence and Holography”. In: *arXiv:1808.02797 [hep-th]* (2018). DOI: [10.1103/PhysRevD.99.021901](https://doi.org/10.1103/PhysRevD.99.021901).
- [51] Dongmin Gang, Nakwoo Kim, and Leopoldo A. Pando Zayas. “Precision Microstate Counting for the Entropy of Wrapped M5-branes”. In: *J. High Energy Phys.* 2020.3 (2020), p. 164. DOI: [10.1007/JHEP03\(2020\)164](https://doi.org/10.1007/JHEP03(2020)164).
- [52] Miłosz Panfil, Marko Stošić, and Piotr Sułkowski. “Donaldson-Thomas invariants, torus knots, and lattice paths”. In: *Phys. Rev. D* 98.2 (2018), p. 026022. DOI: [10.1103/PhysRevD.98.026022](https://doi.org/10.1103/PhysRevD.98.026022).
- [53] Horatiu Nastase. *Classical Field Theory*. Cambridge University Press, 2019. ISBN: 978-1-108-56939-2.
- [54] Steven Weinberg. *The quantum theory of fields 1, 1*, Cambridge University Press, 2013. ISBN: 978-1-139-64416-7.
- [55] Francesco Benini and Wolfer Peelaers. “Higgs branch localization in three dimensions”. In: *J. High Energy Phys.* 2014.5 (2014), p. 30. DOI: [10.1007/JHEP05\(2014\)030](https://doi.org/10.1007/JHEP05(2014)030).
- [56] Yosuke Imamura and Shuichi Yokoyama. “Index for three dimensional superconformal field theories with general R-charge assignments”. In: *J. High Energy Phys.* 2011.4 (2011), p. 7. DOI: [10.1007/JHEP04\(2011\)007](https://doi.org/10.1007/JHEP04(2011)007).
- [57] Abhijit Gadde. “Lectures on the Superconformal Index”. In: *arXiv:2006.13630 [hep-th]* (2020).
- [58] Werner Nahm. “Conformal Field Theory and Torsion Elements of the Bloch Group”. In: *Frontiers in Number Theory, Physics, and Geometry II: On Conformal Field Theories, Discrete Groups and Renormalization*. Springer, 2007, pp. 67–132. ISBN: 978-3-540-30308-4. DOI: [10.1007/978-3-540-30308-4_2](https://doi.org/10.1007/978-3-540-30308-4_2).
- [59] Stavros Garoufalidis and Don Zagier. “Asymptotics of Nahm sums at roots of unity”. In: *arXiv:1812.07690 [hep-th]* (2018).
- [60] Masha Vlasenko and Sander Zwegers. “Nahm’s Conjecture: Asymptotic Computations and Counterexamples”. In: *arXiv:1104.4008 [math]* (2011).
- [61] Yong-Shi Wu. “Statistical Distribution for Generalized Ideal Gas of Fractional-Statistics Particles”. In: *Phys. Rev. Lett.* 73.7 (1994), pp. 922–925. DOI: [10.1103/PhysRevLett.73.922](https://doi.org/10.1103/PhysRevLett.73.922).
- [62] Kazumoto Iguchi. “Generalized Lagrange theorem and thermodynamics of a multispecies quasiparticle gas with mutual fractional exclusion statistics”. In: *Phys. Rev. B* 58.11 (1998), pp. 6892–6911. DOI: [10.1103/PhysRevB.58.6892](https://doi.org/10.1103/PhysRevB.58.6892).
- [63] W. Nahm, A. Recknagel, and M. Terhoeven. “Dilogarithm identities in conformal field theory”. In: *Mod. Phys. Lett. A* 08.19 (1993), pp. 1835–1847. DOI: [10.1142/S0217732393001562](https://doi.org/10.1142/S0217732393001562).
- [64] Stavros Garoufalidis and Thang TQ Lê. “Nahm sums, stability and the colored Jones polynomial”. In: *Res Math Sci* 2.1 (2015), p. 1. DOI: [10.1186/2197-9847-2-1](https://doi.org/10.1186/2197-9847-2-1).

- [65] Jiannis K. Pachos. *Introduction to Topological Quantum Computation*. Cambridge University Press, 2012. ISBN: 978-0-511-79290-8. DOI: [10.1017/CBO9780511792908](https://doi.org/10.1017/CBO9780511792908).
- [66] Colin Adams. *The knot book: an elementary introduction to the mathematical theory of knots*. American Mathematical Society, 2004. ISBN: 978-0-8218-3678-1.
- [67] Dror Bar-Natan. “On Khovanov’s categorification of the Jones polynomial”. In: *Algebr. Geom. Topol.* 2.1 (2002), pp. 337–370. DOI: [10.2140/agt.2002.2.337](https://doi.org/10.2140/agt.2002.2.337).
- [68] Jacob Rasmussen. “Knots, Polynomials, and Categorification”. In: (2019), p. 94. URL: <https://www.dpmms.cam.ac.uk/~jar60/PCMINotes.pdf>.
- [69] Mikhail Khovanov. “A categorification of the Jones polynomial”. In: *arXiv:math/9908171* (1999).
- [70] Mikhail Khovanov. “A functor-valued invariant of tangles”. In: *Algebr. Geom. Topol.* 2.2 (2002), pp. 665–741. DOI: [10.2140/agt.2002.2.665](https://doi.org/10.2140/agt.2002.2.665).
- [71] Marko Petkovšek, Herbert S. Wilf, and Doron Zeilberger. *A=B*. A K Peters, 1996. ISBN: 978-1-56881-063-8.
- [72] Manuel Kauers and Peter Paule. *The concrete tetrahedron: symbolic sums, recurrence equations, generating functions, asymptotic estimates*. Texts and monographs in symbolic computation. SpringerWienNewYork, 2011. ISBN: 978-3-7091-0444-6.
- [73] Sergei Gukov and Piotr Sulkowski. “A-polynomial, B-model, and quantization”. In: *J. High Energ. Phys.* 2012.2 (2012), p. 70. DOI: [10.1007/JHEP02\(2012\)070](https://doi.org/10.1007/JHEP02(2012)070).
- [74] Satoshi Nawata et al. “Super-A-polynomials for twist knots”. In: *J. High Energ. Phys.* 2012.11 (2012), p. 157. DOI: [10.1007/JHEP11\(2012\)157](https://doi.org/10.1007/JHEP11(2012)157).
- [75] *Physics and mathematics of link homology*. Contemporary mathematics volume 680. American Mathematical Society, 2016. ISBN: 978-1-4704-1459-7.
- [76] Micheal Atiyah and Raul Bott. “The Yang-Mills equations over Riemann surfaces”. In: *Phil. Trans. R. Soc. Lond. A* 308.1505 (1983), pp. 523–615. DOI: [10.1098/rsta.1983.0017](https://doi.org/10.1098/rsta.1983.0017).
- [77] Stavros Garoufalidis, Aaron D. Lauda, and Thang T. Q. Lê. “The colored HOMFLYPT function is q -holonomic”. In: *Duke Math. J.* 167.3 (2018). DOI: [10.1215/00127094-2017-0030](https://doi.org/10.1215/00127094-2017-0030).
- [78] S. B. Arthamonov, A. D. Mironov, and A. Yu. Morozov. “Differential hierarchy and additional grading of knot polynomials”. In: *Theor Math Phys* 179.2 (2014), pp. 509–542. DOI: [10.1007/s11232-014-0159-9](https://doi.org/10.1007/s11232-014-0159-9).
- [79] S. Arthamonov et al. “Link polynomial calculus and the AENV conjecture”. In: *J. High Energ. Phys.* 2014.4 (2014), p. 156. DOI: [10.1007/JHEP04\(2014\)156](https://doi.org/10.1007/JHEP04(2014)156).
- [80] Marko Stosic and Paul Wedrich. “Rational links and DT invariants of quivers”. In: *International Mathematics Research Notices* 2021.6 (2021), pp. 4169–4210. DOI: [10.1093/imrn/rny289](https://doi.org/10.1093/imrn/rny289).
- [81] Marko Stosic and Paul Wedrich. “Tangle addition and the knots-quivers correspondence”. In: *arXiv:2004.10837 [hep-th]* (2020).

- [82] Nathan M. Dunfield, Sergei Gukov, and Jacob Rasmussen. “The Superpolynomial for Knot Homologies”. In: *arXiv:math/0505662* (2005).
- [83] Satoshi Nawata and Alexei Oblomkov. “Lectures on knot homology”. In: *arXiv:1510.01795 [hep-th, physics:math-ph]* (2018).
- [84] Marcelo Aguiar and Federico Ardila. “Hopf monoids and generalized permutahedra”. In: *arXiv:1709.07504 [math]* (2017).
- [85] Hiroyuki Fuji, Sergei Gukov, and Piotr Sułkowski. “Volume Conjecture: Refined and Categorized”. In: *Advances in Theoretical and Mathematical Physics* 16.6 (2012), pp. 1669–1777. DOI: [10.4310/ATMP.2012.v16.n6.a3](https://doi.org/10.4310/ATMP.2012.v16.n6.a3).
- [86] Hiroyuki Fuji et al. “3d analogs of Argyres-Douglas theories and knot homologies”. In: *J. High Energ. Phys.* 2013.1 (2013), p. 175. DOI: [10.1007/JHEP01\(2013\)175](https://doi.org/10.1007/JHEP01(2013)175).